The 2006 Eruption of Augustine Volcano, Alaska
Power, J.A., Coombs, M.L., and Freymueller, J.T., editors
U.S. Geological Survey Professional Paper 1769

Chapter 16

Augustine Volcano—The Influence of Volatile Components in Magmas Erupted A.D. 2006 to 2,100 Years Before Present

By James D. Webster[1], Charles W. Mandeville[1], Beth Goldoff[1], Michelle L. Coombs[2], and Christine Tappen[3]

Abstract

The petrology and geochemistry of 2006 eruptive products of Augustine Volcano, Alaska, have been investigated through analyses of whole-rock samples, phenocrysts, silicate melt inclusions, and matrix glasses to constrain processes of magma evolution, eruption, and degassing. Particular attention was directed toward the concentrations and geochemical relationships involving the magmatic volatile components H_2O, CO_2, S, and Cl. The analytical results for 2006 samples have been integrated with data for samples of Pleistocene basalt, prehistoric andesites, and 1986 andesites from Augustine to provide a broad view of volatile behavior in Augustine magmas. The observation of generally similar geochemical features for this range of eruptions indicates that magmatic and volatile degassing processes have been relatively consistent during the past 2,100 years.

Augustine andesites range from low-silica to high-silica compositions and contain phenocrysts of plagioclase, orthopyroxene, and clinopyroxene, with lesser olivine, amphiboles, iron-titanium oxides, and apatite. The groundmass varies from strongly crystallized and/or oxidized to comparatively clear, microlite-poor vesicular glass. Coexisting iron-titanium oxides of 2006 rock samples, which are generally consistent with those of prior eruptive materials, indicate f_{O_2} values of approximately NNO+1.5 to NNO+2.5 and oxide crystallization temperatures of 835 to 1,052°C.

The compositions of matrix and melt-inclusion glasses range from rhyodacite to rhyolite and show relationships that reflect magma evolution involving fractional crystallization and multiple stages of mingling and/or mixing. In particular, melt inclusions of low-silica andesites express mixing of magmas with more widely varying compositions, than do melt inclusions of high-silica andesites and dacites. The melt inclusions of 2006, 1986, and prehistoric andesites contain moderate to high concentrations of H_2O and Cl and lesser CO_2 and SO_2. Comparing the abundances of H_2O, CO_2, and Cl in these melt inclusions with experimentally established volatile solubilities for felsic melts indicates that the 2006 and prehistoric samples are most consistent with the ascent of fluid-saturated magmas containing 1 weight percent of H_2O-enriched vapor under closed-system conditions and that pressures of volatile phase exsolution range from 150 to less than 20 MPa. This closed-system behavior was maintained to quite shallow depths prior to eruption, and this pressure range is consistent with constraints derived from 2006 geodetic measurements indicating magma storage and crystallization at 4 to 6 km and upwards to near-surface depths. The magmatic fluids were relatively oxidizing and included H_2O-enriched and HCl-, H_2S-, S_2-, and $SO_2 \pm CO_2$-bearing vapors; hydrosaline aqueous liquids largely enriched in Cl^-, SO_4^{2-}, alkalis, and H_2O; and moderately saline, H_2O-poor liquids containing Cl^-, SO_4^{2-}, and alkali elements.

Introduction

The diverse 2006 eruptive activities of Augustine Volcano, Alaska, included pyroclastic flows; explosive injection of glassy juvenile ash, rock fragments, and gases into the troposphere and lower stratosphere; and lahars, lava flows, dome-forming extrusions, associated block-and-ash flows, and small phreatic explosions (Power and others, 2006; Vallance and others, this volume; McGee and others, this volume; and other contributions to this volume). The estimated total volume of 2006 eruptive materials is approximately 73 million

[1]Department of Earth and Planetary Sciences, American Museum of Natural History, Central Park West at 79th St., New York, NY 10024-5192.

[2]Alaska Volcano Observatory, U.S. Geological Survey, 4200 University Drive, Anchorage, AK 99508.

[3]251 Pleasant Street, New London, NH 03257.

m^3 (dense-rock equivalent, or DRE; Coombs and others, this volume). The compositions of the erupted magmas, based on whole-rock data, range from basaltic andesite to dacite, though high- through low-silica andesitic magmas were dominant (Larsen and others, this volume; Vallance and others, this volume). Analyses of groundmass glasses establish the maximum in the range in silica content of the most chemically evolved melts as >79 weight percent (Izbekov and others, 2006; Larsen and others, this volume).

Knowledge of the silica content of the eruptive products is important, because the concentration of SiO_2 controls the physical properties of magma, through melt polymerization, which exerts a strong control on eruptive behavior of volcanoes. In this regard, the 2006 Augustine magma compositions changed from (1) dominantly low-SiO_2 andesitic scoria during the January explosive phase, to (2) dominantly high-SiO_2 andesite during a continuous phase of rapid lava effusion in late January and early February, to (3) dense low- and intermediate-SiO_2 andesites during the final, effusive phase in March (Coombs and others, this volume; Vallance and others, this volume; Larsen and others, this volume). Concurrently, the phases of eruptive activities ranged from (1) a series of Vulcanian explosions that produced ash plumes and pyroclastic flows, lahars, and mixed snow and rock avalanches during the explosive phase, to (2) continuous eruption of ash plumes and pyroclastic flows, to (3) an intervening eruptive pause, to (4) late-stage, dome growth and emission of lava flows during the effusive phase.

Magmatic volatile components also control eruptive activities and magmatic processes because they influence: melt viscosity and magma rheology, rates of component diffusion through melts, the thermal stability of aluminosilicate melts and minerals, and the exsolution of fluids. The manner of fluid exsolution exerts a strong control on styles of volcanic eruption and on the compositions and textures of eruptive materials. Thus, it is important to establish the compositions of melt and coexisting magmatic fluids during magma evolution, pre- and syn-eruptive fluid exsolution, and subsequent post-eruptive degassing at Augustine Volcano.

During volcanic activity preceding 2006, Augustine erupted magmas that were variably enriched in the magmatic volatile components H_2O, CO_2, S, and Cl. This observation is well demonstrated from extensive investigations of the 1976 and 1986 eruptions. Johnston's (1978, 1979) analyses of materials erupted in 1976, for example, measured elevated Cl concentrations (0.3 to 0.6 weight percent) in silicate melt inclusions and estimated preeruptive H_2O concentrations to have averaged 6.5 ± 1.5 weight percent. The former study also concluded that some melts erupted in 1976 were saturated in a Cl- and H_2O-rich fluid. Roman and others (2006) studied 1986 eruptive materials, and measured the abundances of H_2O, CO_2, Cl, and SO_3 in melt inclusions. This study also determined that magma mixing processes continued during magma ascent, based on relationships involving H_2O, K_2O, and SiO_2 in the melt-inclusion data. Recent research on materials erupted in prehistoric time has determined highly variable enrichments of magmatic H_2O and Cl (Tappen and others, 2009) and evidence of preeruptive volatile phase saturation of some fractions of these ancient magmas (Webster and others, 2006).

The objectives of this investigation are to determine the petrologic characteristics, major-element compositions, and abundance of volatile components of silicate melt inclusions and matrix glasses representing magmas erupted in A.D. 2006 and those erupted in prehistoric time (for example, 2,100, 1,700, 1,400, and 1,000 years before present) and more recently (A.D. 1986). The petrology and geochemistry of 2006 eruptive products are addressed in more detail by Larsen and others (this volume). We have integrated compositional data for 238 melt inclusions and 42 analyses of matrix glasses to illuminate relationships between the volatile components and processes of magma evolution, magmatic volatile phase exsolution, and ensuing processes of volcanic eruption at Augustine Volcano.

We refer to fluids and/or volatile phases, in this chapter, to include all noncrystalline, polycomponent phases, but this terminology does not bear on silicate melts that also are fluids by this definition. Relatively low-density, volatile component-enriched phases are denoted vapor, and higher density phases are referred to as liquid. The low-density phases are commonly dominated by H_2O and/or CO_2, and higher-density liquids are most commonly enriched in H_2O and electrolytes and may also involve molten sulfides. We refer to electrolyte-enriched fluids as saline, and the relatively dense fluids that are dominated by aluminosilicate constituents are addressed as melts.

Samples Investigated

This investigation reports petrologic and petrographic descriptions and compositional data for nine rock samples collected from 2006 tephra, dome, pyroclastic-flow, and lahar units (collected in February and August of 2006); a pumice sample from a 1986 pyroclastic-flow deposit; and a sample of Pleistocene basalt (table 1; appendix I). The 2006 samples include high- and low-silica andesites representing magma erupted during the three phases of the 2006 eruption: the explosive, continuous, and concluding effusive phase.

Our 1986 sample (AVO 208) was collected from a broad pyroclastic-flow deposit on the north flank of the volcano during the summer of 2003 (table 1). The porphyritic olivine basalt (RBW91A137) was found as a juvenile clast in the mid-section of a 10-m thick hyaloclastite outcrop on the volcano's south flank, and was collected there in 1991 by Dr. Richard B. Waitt (U.S. Geological Survey). This singular basalt outcrop contains ≤18 cm-wide, rounded to subangular, porphyritic olivine basalt clasts in a palagonite matrix and is presumably Pleistocene in age (Waitt and Begét, 2009).

The data resulting from the investigation of these samples are compared with results from Tappen and others (2009) of similar research on five samples of prehistoric fall deposits (tephra units C1 (AVO 201), C2 (AVO 202), H (AVO 204),

Table 1. Descriptions and collection localities for rock samples from Augustine Volcano, Alaska.

Rock Sample	Unit	Age of Eruption	Sample Type	Sample Location
RBW91A137	Juvenile clast-bearing hyaloclastite	Pleistocene[1]	Porphyritic olivine basalt	South flank of volcano
AVO 201	Lower C1 tephra	≈ 1,000 yr B.P.	Light-gray pumiceous tephra	Near South Point
AVO 202	Lower C2 tephra	≈ 1,000 yr B.P.	Light-gray pumiceous tephra	Near South Point
AVO 203	Tephra I	≈ 1,700 yr B.P.	Light-gray pumiceous tephra	Yellow Cliffs
AVO 204	Tephra H	≈ 1,400 yr B.P.	Light-gray pumiceous tephra	Between SE Point and East Point
AVO 205	Tephra G	≈ 2,100 yr B.P.	Light-gray pumiceous tephra	Near NE Point
AVO 208	Pyroclastic flow	A.D. 1986	Pumiceous tephra	North slope of volcano
06AUMC010.p1	Pyroclastic flow	A.D. 2006	High-silica andesite	NNE of crater
06AUMC008B.p1A	Lahar	A.D. 2006	Low-silica andesite scoria; banded	SSE coast of island
06AUMC005c.p5A	Lahar	A.D. 2006	Low-silica andesite scoria	SSW coast of island
06AUCWM007	Pyroclastic flow	A.D. 2006	Low-silica andesite scoria	N slope near crater rim
06AUCWM012	Block and ash flow	A.D. 2006	High-silica andesite	N slope near crater rim
06AUCWM014	Block and ash flow	A.D. 2006	Dense low-silica andesite	N slope near crater rim
06AUJW001	Dome extrusion	A.D. 2006	Oxidized, dense low-silica andesite	Crater rim
06AUJW004	Pyroclastic flow	A.D. 2006	Dense low-silica andesite	N slope near crater rim
06AUJW010	Block and ash flow	A.D. 2006	Dense low-silica andesite	N slope near crater rim

[1]Basalt estimated to have formed during Pleistocene eruption (Waitt and Begét, 2009).

I (AVO 203), G (AVO 205), using the nomenclature of Waitt and Begét, 2009), and with samples from the 1986 eruption studied by Roman and others (2006). Details on sample localities, petrology, and geochemistry for the prehistoric tephra samples are included therein.

Methods

Sample Preparation

Phenocrysts, silicate melt inclusions, and matrix glasses were analyzed in polished thin sections and in grain mounts prepared by gently crushing the rocks, picking individual phases, and mounting these phases on glass slides with epoxy. Three to five polished thin sections were prepared from each of the 2006 samples and studied petrographically.

The great majority of silicate melt inclusions in these samples are, as described below, vitreous and free of daughter crystals, but most melt inclusions hosted by clinopyroxene of the basalt sample (RBW91A137) are partially crystallized so they were re-fused to glass by heating mineral separates of melt inclusion-bearing, clinopyroxene phenocrysts at 1,100 to 1,150°C for 4 to 6 hours in open crucibles at one atmosphere.

Electron Microprobe Analysis

Electron microprobe analyses (EPMA) of glass and minerals were conducted with a Cameca SX-100 at the American Museum of Natural History (AMNH). Pyroxene, amphibole, and plagioclase phenocrysts, as well as glass in melt inclusions and in groundmass were analyzed for SiO_2, Al_2O_3, Na_2O, K_2O, CaO, FeO, MnO, TiO_2, MgO, F, P_2O_5, Cl, and S using wavelength-dispersive techniques at 15 KeV. We used a 2-nA beam current to analyze Na_2O, K_2O, FeO, SiO_2, and F, and a 10-nA beam current to analyze all other elements. The peak counting times for Na_2O, K_2O, SiO_2, and F were 20 seconds; for FeO were 20 to 30 seconds; for Al_2O_3, CaO, MnO, TiO_2, and MgO were 30 seconds; and for P_2O_5, Cl, and S were 40 to 60 seconds. Standards for S, Cl, and F were $BaSO_4$, scapolite, and synthetic MgF_2, respectively. The major- and trace-element concentrations of internal "standard" glasses (a felsic peralkaline obsidian and a natural topaz rhyolite reference glass that

are generally similar in composition to that of the glasses of this study) were also determined to monitor analytical accuracy and instrumental drift. The 1-σ analytical precision for the glass analyses has been estimated from 26 analyses of the obsidian (conducted during five analytical sessions spanning a one-year period and given here in relative percent): 0.7 for SiO_2, 1 for Al_2O_3, 3 for K_2O, 4 for Cl, 5 for Na_2O, 8 for CaO, 10 for FeO, 30 for F and TiO_2, and 60 for MnO. The abundances of MgO, S, and P_2O_5 are <0.005 weight percent in this obsidian and hence unrepresentative of the melt-inclusion compositions, so their 1-σ precisions were estimated from melt-inclusion data from individual samples to be ≤8, 25, and 25 relative percent, respectively.

To minimize Na and K migration during glass analyses, these constituents were analyzed with a 2-nA beam current during the first pass and the melt inclusions and areas of matrix glass were moved constantly under a defocused beam. We also used a subcounting (time zero intercept) routine for some Na analyses in melt inclusions from low-silica andesite. The stability of the Na and K signals for glass analyses reported in this study was confirmed by conducting 3 successive analyses on the same area of glass of randomly selected samples. Most melt-inclusion and matrix-glass analyses utilized an 8-µm electron-beam diameter, but a 4-µm beam diameter was required for some analyses of matrix glasses to avoid vesicles and microlites. Additionally, the small size and paucity of crystal-free melt inclusions in sample 06AUJW001 demanded the use of a 2-µm beam diameter for analysis on a stationary point on the melt inclusion, but the glass was moved under the beam during analysis.

Pairs of adjoining titanomagnetite and ilmenite grains were analyzed for Al_2O_3, FeO, MnO, TiO_2, and MgO with the electron beam set at 40 nA, 15-Kev, and with a 1-µm beam diameter. All elements were counted for 30 seconds at the peak position. Major- and trace-element concentrations of minerals were verified on magnetite and ilmenite standards.

Infrared Spectroscopic Analyses of Glasses

Dissolved H_2O and CO_2 concentrations in the glass of melt inclusions were measured by Fourier Transform Infrared (FTIR) spectroscopy utilizing techniques described by Newman and others (1986) and Mandeville and others (2002) that are summarized here. Room-temperature infrared (IR) spectroscopic measurements on melt inclusions of prehistoric and 1986 samples were conducted in transmittance mode using a Nicolet 20SXB FTIR spectrometer attached to a Spectra Tech IR Plan microscope at the AMNH. IR spectra were collected over the mid-IR to near-IR regions using a KBr beam splitter, MCT/A detector, globar source, and 1,000 scans with a spectral resolution of 4 cm^{-1}. More recent transmission FTIR analyses of melt inclusions in 2006 samples were performed with a Thermo Electron Nexus 670 spectrometer interfaced with a Continuum IR microscope at the AMNH utilizing a KBr beam splitter, MCT/A detector, globar source, and 200 to 400 scans with 4 cm^{-1} spectral resolution. For all analyses, the IR objective and spectrometer were purged with dry nitrogen at a rate of 15 liters/minute.

The melt inclusion and matrix glasses were analyzed 3 to 4 times each, and the total dissolved H_2O and CO_2 concentrations in these glasses were determined from the intensity of IR bands at 4,500 cm^{-1} (hydroxyl OH^-) and 5,200 cm^{-1} (molecular H_2O) and 2,350 cm^{-1} (CO_2). The reported H_2O concentrations refer to total H_2O. The thicknesses of the doubly polished, melt inclusion-bearing phenocryst wafers were measured 8 to 10 times using a Mitutoyo digimatic indicator which has a precision of ±2 µm. The 1-σ precision for H_2O and CO_2 analyses of these glasses is estimated as 0.1 and 0.02 weight percent, respectively.

Results

Description of the Rock Samples

All of the prehistoric tephra, 1986, and 2006 rock samples are porphyritic and contain phenocrysts of plagioclase, orthopyroxene, and clinopyroxene with plagioclase dominant; the abundance of orthopyroxene is subequal to or exceeds that of clinopyroxene. Most samples also contain minor to trace phenocrystic olivine and amphibole, and the accessory phases include apatite and Fe-Ti oxides. Larsen and others (this volume) report that all 2006 rocks that they examined contain 36 to 44 volume percent phenocrysts, and Tappen and others (2009) observed 30 to 40 volume percent phenocrysts in the prehistoric tephra. The groundmass materials are vesicular and vitreous to strongly devitrified. All rocks contain trace to abundant microlites. The Pleistocene olivine basalt (RBW91A137) is porphyritic and contains 0.2 to 11 volume percent plagioclase (An_{74-91}), 12.2 to 14.2 volume percent clinopyroxene ($Wo_{35-42}En_{48-53}Fs_{5-11}$) 3.5 to 6.5 volume percent olivine ($Fa_{13-22}Fo_{77-88}$), 1.7 volume percent amphibole (Mg numbers of 63-73), and trace amounts of orthopyroxene ($Wo_2En_{66}Fs_{32}$) (Daley, 1986; C. Tappen, unpublished data). Additional petrographic details for all samples are provided in the appendix and by Tappen and others (2009).

The whole-rock compositions for three of these samples were determined and are reported in table 2. The other six samples were not analyzed, but given their textural and mineral-chemical characteristics that are described below, we determine that most are low- to high-silica andesites on the basis of comparisons with sample descriptions and analyses from Larsen and others (this volume).

Phenocrysts

Plagioclase

Plagioclase occurs as phenocrysts and microphenocrysts, and individual crystals appear twinned, broken, rounded,

Table 2. Bulk compositions of whole-rock samples, Augustine Volcano, Alaska

[Major to trace elements (including Ni-Zn) measured by X-ray fluorescence and all other trace elements by inductively coupled plasma mass spectroscopy at Washington State University]

Rock Sample	06AUMC005c.p5	06AUMC008b.p1	06AUMC010.p1
(wt percent)			
SiO_2	57.42	57.35	62.61
Al_2O_3	17.67	17.52	16.81
TiO_2	0.72	0.72	0.56
MgO	4.61	4.75	3.36
CaO	8.51	8.46	6.64
MnO	0.14	0.14	0.13
FeO[1]	6.58	6.73	5.36
Na_2O	3.48	3.46	3.81
K_2O	0.74	0.74	0.98
P_2O_5	0.13	0.13	0.14
TOTAL	99.61	99.11	98.87
(ppm)			
Ni	28	28	24
Cr	56	60	43
V	195	195	130
Ga	17	17	17
Cu	36	36	20
Zn	61	63	57
La	8.21	8.21	10.36
Ce	17.22	17.28	20.98
Pr	2.28	2.31	2.66
Nd	10.55	10.76	11.77
Sm	3.05	3.08	3.13
Eu	1.02	1.00	0.97
Gd	3.32	3.30	3.24
Tb	0.57	0.58	0.56
Dy	3.61	6.71	3.51
Ho	0.78	0.79	0.76
Er	2.15	2.25	2.19
Tm	0.33	0.33	0.33
Yb	2.11	2.16	2.19
Lu	0.34	0.35	0.36
Ba	314	313	427
Th	1.46	1.49	2.12
Nb	2.26	2.21	2.83
Y	20.84	21.38	21.39
Hf	2.43	2.51	2.98
Ta	0.16	0.16	0.20
U	0.55	0.58	0.81
Pb	2.15	1.94	2.50
Rb	13.0	13.0	18.2
Cs	0.30	0.29	0.40
Sr	319	320	312
Sc	24.9	26.1	20.3
Zr	83	83	104

[1]All iron reported as FeO.

or euhedral. Plagioclase is also a dominant component of glomeroporphyritic aggregates containing orthopyroxene and clinopyroxene ± Fe-Ti oxides. These multiphase clots have been observed previously in the products of other eruptions by Johnson (1986) and Tappen and others (2009) and may represent breakdown of amphibole and pyroxene or remobilized phenocrysts from earlier magmas. Most plagioclase crystals range from 0.05 to 3.5 mm in length, but a few rare phenocrysts are as large as 4.8 mm in length. Plagioclase phenocrysts exhibit a variety of internal textural features including: simple normal and reverse zoning, simple oscillatory zoning, oscillatory zoning with complex internal resorption-growth boundaries and/or as rims, and other oscillatory zoned phenocrysts contain coarse sieve textures in cores. Although most are characterized by simple oscillatory zoning; more rarely, plagioclase phenocrysts are composed of coarsely sieved cores surrounded by growth boundaries that are both oscillatory in composition and appear complexly resorbed. Melt inclusions, inclusions of orthopyroxene microlites, and oxide inclusions occur within these compositional resorption-growth boundaries. Other growth zones contain dusty material that is texturally reminiscent of crystallized groundmass.

Plagioclase phenocrysts and microphenocrysts from seven 2006 samples range from andesine to bytownite (An_{36-82}; table 3). Larsen and others (this volume) provide a detailed analysis of plagioclase petrography, geochemistry, and crystallization history for 2006 samples.

Pyroxenes

Orthopyroxene is more abundant than clinopyroxene in most samples. Pyroxenes typically have subhedral to euhedral crystal morphologies, but some grains are distinctly rounded. Most pyroxene phenocrysts are not zoned.

Orthopyroxene phenocrysts are typically larger than clinopyroxene phenocrysts. The former exhibit lengths as large as 1.8 mm while most are <1.2 mm in length. Orthopyroxene phenocrysts in three 2006 samples are hypersthene with $Wo_{1-3}En_{64-76}Fs_{21-33}$ and Mg numbers of 66-78 (table 4). Clinopyroxene occurs as subhedral to euhedral crystals with most phenocrysts ranging from 0.05 to 1 mm in length. A few rare phenocrysts are up to 2 mm in length. Clinopyroxene phenocrysts in three 2006 samples are augitic with $Wo_{44-45}En_{41-47}Fs_{7-14}$ and Mg numbers of 74 to 87. Most phenocrysts contain ≤2 weight percent Al_2O_3, but some contain nearly 5 weight percent Al_2O_3.

Iron-titanium oxides

Ilmenite and titanomagnetite occur as phenocrysts, microphenocrysts, and microlites in the groundmass, and as inclusions in other phenocrysts of these samples. The oxides are subhedral to anhedral, and some are as large as 0.5 mm in length although most are ≤0.3 mm long. All but two of the samples contain both oxides in physical contact with one another, and most exhibit little to no visible evidence of exsolution.

The composition of ilmenite in four 2006 samples ranges from X_{ilm} 0.50 to 0.72 and the corresponding titanomagnetite compositions range from X_{usp} 0.21 to 0.48 (calculated with QUILF of Andersen and others, 1993, and evaluated by Bacon and Hirshmann, 1988). Estimated equilibration temperatures and oxygen fugacities (f_{O_2}), based on the compositions of coexisting oxide minerals, are reported in table 5. We note that because of the elevated f_{O_2} of these magmas, which are outside of the acceptable calibration range for the QUILF algorithm (Evans and others, 2006; Lattard and others, 2005), we reduced the temperatures determined with QUILF and reported in the figures and tables by 30°C (Rutherford and Devine, 1996). This approach is consistent with that of Larsen and others (this volume).

Amphibole

Approximately one-half of the 2006 samples studied contain rare amphibole, and sample 06AUJW001 contains several volume percent amphibole. Most of the rare amphibole phenocrysts are subhedral and rounded, and some crystals are embayed. Of the amphiboles observed in these samples, roughly half of the crystals show either reaction rims or rim alteration, and the other half are devoid of evidence of mineral replacement of amphibole rims. Some amphibole occurs as inclusions in other silicate minerals.

Analyzed amphiboles contain from 45.4 to 49.4 weight percent SiO_2, 6.2 to 9.4 weight percent Al_2O_3, 14.8 to 15.9 weight percent MgO, and 11.4 to 13.0 weight percent FeO (table 6). The TiO_2 content ranges from 1.0 to 2.4 weight percent, and total alkalis vary from 1.3 to 2.3 weight percent. Na_2O and K_2O exhibit negative correlations with the SiO_2 contents of amphibole (table 6). All 2006 amphiboles analyzed in this study are identified as magnesio-hornblende based on the classification of Leake (1997) and Hawthorne and Oberti (2007). Chlorine concentrations range from 0.06 to 0.09 weight percent with the highest value occurring in the core of an iron-rich crystal that is zoned with respect to Mg, Ti, Ca, F and Cl (table 6). Fluorine concentrations in 2006 amphiboles vary widely from below detection (<0.02 weight percent) to 0.47 weight percent in the rim of this zoned crystal (table 6). One amphibole from a dense, intermediate-silica andesite scoria clast (06AUJFL001b; Larsen and others, this volume, their table 8) erupted during the continuous phase (January 28 to February 10, 2006) contains 42.8 weight percent SiO_2, 14.9 weight percent MgO, 10.96 weight percent FeO, 2.3 weight percent Na_2O, 9.9 weight percent CaO, and 0.05 weight percent Cl as well as elevated Al_2O_3 (for example, 11.4 weight percent) slightly extending the range of compositions determined for 2006 samples.

Olivine

Olivine is a very minor phase in most of the 2006 rocks studied. It typically occurs as small rounded, subhedral, embayed, and altered grains generally <0.6 mm in diameter. The typical form of alteration involves oxidation along rims

Table 3. Compositions of plagioclase in 2006 rock samples of Augustine Volcano, Alaska.

[Electron microprobe analyses (wt percent) of representative plagioclase phenocrysts from seven rock samples]

Rock Sample	06AU JW004	06AU JW004	06AU JW010	06AU JW010	06AU CWM007	06AU CWM007	06AU CWM012	06AU CWM012	06AU MC005	06AU MC005	06AU MC008	06AU MC008	06AU MC010	06AU MC010
Composition	Anorthitic	Albitic	Anorthitic	Albitic	Anorthitic	Albitic	Anorthitic	Subequal An-Ab	Anorthitic	Subequal An-Ab	Anorthitic	Albitic	Anorthitic	Albitic
SiO_2	48.20	55.02	51.16	57.50	51.55	58.36	47.64	54.26	52.48	56.69	48.84	60.86	54.12	56.60
Al_2O_3	33.28	29.50	31.74	26.95	30.59	26.89	33.63	28.52	30.62	27.80	31.49	23.88	29.91	27.28
TiO_2	0.01	0.00	0.00	0.01	0.03	0.07	0.04	0.03	0.00	0.05	0.00	0.03	0.02	0.00
MgO	0.04	0.02	0.03	0.08	0.04	0.03	0.02	0.04	0.01	0.00	0.06	0.04	0.02	0.03
CaO	16.38	9.77	14.30	8.99	13.48	9.00	16.80	10.93	13.21	10.33	16.24	7.20	12.70	9.62
MnO	0.02	0.00	0.03	0.00	0.00	0.00	0.04	0.00	0.07	0.00	0.03	0.00	0.05	0.00
FeO	0.47	0.23	0.40	0.38	0.52	0.29	0.41	0.49	0.38	0.05	0.79	0.87	0.33	0.29
Na_2O	2.33	7.07	3.50	5.57	3.54	5.86	1.99	5.99	3.90	5.68	2.42	6.93	4.04	6.20
K_2O	0.02	0.12	0.05	0.18	0.10	0.15	0.07	0.11	0.08	0.14	0.06	0.42	0.07	0.19
TOTAL	100.75	101.73	101.21	99.66	99.85	100.64	100.63	100.37	100.74	100.74	99.93	100.23	101.26	100.21
Chemical Formula														
Si	2.20	2.45	2.30	2.58	2.35	2.59	2.18	2.45	2.37	2.52	2.25	2.71	2.42	2.54
Al	1.79	1.55	1.69	1.43	1.64	1.41	1.81	1.52	1.63	1.46	1.71	1.25	1.57	1.44
Ti	0.00	0.00	0.00	0.00	0.00	0.00	0.00	0.00	0.00	0.00	0.00	0.00	0.00	0.00
Mg	0.00	0.00	0.00	0.01	0.00	0.00	0.00	0.00	0.00	0.00	0.00	0.00	0.00	0.00
Ca	0.08	0.47	0.69	0.43	0.66	0.43	0.82	0.53	0.64	0.49	0.80	0.34	0.61	0.46
Mn	0.00	0.00	0.00	0.00	0.00	0.00	0.00	0.00	0.00	0.00	0.00	0.00	0.00	0.00
Fe	0.02	0.01	0.02	0.01	0.02	0.01	0.02	0.02	0.01	0.02	0.03	0.03	0.01	0.01
Na	0.21	0.61	0.31	0.48	0.31	0.50	0.18	0.52	0.34	0.49	0.22	0.60	0.35	0.54
K	0.00	0.01	0.00	0.01	0.01	0.01	0.00	0.01	0.00	0.01	0.00	0.02	0.00	0.01
End Members														
An	79.44	43.03	69.11	46.62	67.39	45.50	82.02	49.91	64.88	49.73	78.49	35.58	63.21	45.67
Ab	20.45	56.34	30.60	52.26	32.02	53.60	17.58	49.49	34.65	49.47	21.16	61.95	36.38	53.26
Or	0.12	0.63	0.29	1.11	0.60	0.90	0.41	0.60	0.47	0.80	0.35	2.47	0.41	1.07

[1]FeO represents all iron.

Table 4. Compositions of pyroxenes in 2006 rock samples of Augustine Volcano, Alaska.

[Electron microprobe analyses (wt. percent) of representative orthopyroxene (opx) and clinopyroxene (cpx) phenocrysts from three rock samples. Original iron analysis was determined as FeO and is reported herein separately as Fe_2O_3 and FeO. Chemical formula and end members computed with PRBDATNT (Harlow and others, 2006)]

Rock Sample	06AUM C008b.p1a	06AUM C008b. p1a	06AUM-C008b.p1a	06AUM-C008b.p1a	06AUJ W001	06AUJ W001	06AUJ W001	06AUJ W001	06AUC WM012	06AUC-WM012	06AUC-WM012	06AUC WM012
Mineral	Opx	Opx	Cpx	Cpx	Opx	Opx	Cpx	Cpx	Opx	Cpx	Cpx	Cpx
SiO_2	52.75	53.66	50.02	51.08	53.21	53.57	52.31	52.83	53.23	53.00	52.84	52.37
TiO_2	0.24	0.32	0.08	0.43	0.20	0.17	0.24	0.32	0.05	0.34	0.31	0.25
Al_2O_3	0.83	1.44	4.85	2.16	1.14	0.82	1.29	1.49	0.62	1.59	1.54	1.28
Fe_2O_3	0.81	4.54	2.31	2.32	0.17	0.00	1.86	0.95	0.00	2.23	0.33	0.70
FeO	20.15	12.38	4.14	7.25	18.73	20.71	6.93	8.62	19.65	6.80	8.60	7.36
MnO	0.75	0.49	0.18	0.39	0.57	0.74	0.34	0.33	1.08	0.35	0.30	0.31
MgO	22.63	25.66	15.80	14.10	24.16	23.13	14.58	14.36	23.02	14.46	14.43	14.91
CaO	1.70	1.39	20.95	21.16	1.13	1.10	21.51	21.19	0.89	21.17	21.22	21.26
Na_2O	0.01	0.07	0.26	0.34	0.00	0.03	0.42	0.36	0.07	0.78	0.35	0.29
K_2O	0.00	0.04	0.01	0.00	0.00	0.00	0.02	0.04	0.01	0.00	0.02	0.00
TOTAL	99.87	99.99	98.60	99.23	99.31	100.27	99.50	100.49	98.62	100.72	99.94	98.73
Chemical Formula												
Si	1.96	1.94	1.85	1.92	1.97	1.98	1.95	1.96	1.99	1.95	1.97	1.97
Al_{IV}[1]	0.04	0.06	0.15	0.08	0.03	0.02	0.05	0.04	0.01	0.05	0.03	0.03
Al	0.00		0.06	0.02	0.02	0.01	0.01	0.02	0.02	0.02	0.03	0.02
Ti	0.01	0.01	0.02	0.01	0.01	0.01	0.01	0.01	0.00	0.01	0.01	0.01
Fe^{3+}	0.02	0.12	0.06	0.07	0.01	0.00	0.05	0.03	0.00	0.06	0.01	0.02
Fe^{2+}	0.63	0.37	0.13	0.23	0.58	0.64	0.22	0.27	0.62	0.21	0.27	0.23
Mn	0.02	0.02	0.01	0.01	0.02	0.02	0.01	0.01	0.03	0.01	0.01	0.01
Mg	1.26	1.38	0.87	0.79	1.33	1.27	0.81	0.79	1.28	0.79	0.80	0.83
Ca	0.07	0.05	0.83	0.85	0.05	0.04	0.86	0.84	0.04	0.84	0.85	0.86
Na	0.00	0.01	0.02	0.03	0.00	0.00	0.03	0.03	0.01	0.06	0.03	0.02
K	0.00	0.002	0.00	0.00	0.00	0.00	0.00	0.00	0.00	0.00	0.00	0.00
Mg numbers[2]	66	78	87	77	69	66	78	74	66	78	74	78
End Members												
En	64.39	76.35	47.62	42.25	68.08	65.06	43.01	41.72	66.36	43.15	41.80	43.44
Fs	32.12	20.66	7.00	12.19	29.62	32.69	11.44	14.03	31.78	11.41	14.00	12.03
Wo	3.49	2.98	45.38	45.56	2.30	2.25	45.55	44.25	1.86	45.43	44.20	44.53

[1] Tetrahedrally coordinated aluminum.
[2] Mg numbers = 100x(cations Mg/(cations Mg + cations Fe^{2+})). Data are based on analyses of 4 orthopyroxene and 5 clinopyroxene phenocrysts from sample 06AUMC008b.p1a, 4 orthopyroxene and 4 clinopyroxene phenocrysts from sample 06AUJW001, and 6 orthopyroxene and 5 clinopyroxene phenocrysts from sample 06AUCWM012.

Table 5. Compositions of iron-titanium oxide minerals in 2006 samples of Augustine Volcano, Alaska.

[Electron microprobe analyses (wt percent) of representative ilmenite (ilm) and titanomagnetite (usp = ulvospinel) grains. FeO represents all iron]

Rock Sample	06AUM C008	06AUM C008	06AUC WM007	06AUC-WM007	06AUC WM012	06AUC-WM012	06AU JW004	06AUJ W004
Mineral	Ilm	Usp	Ilm	Usp	Ilm	Usp	Ilm	Usp
Oxide (wt percent)								
TiO_2	33.28	12.00	33.69	12.84	35.41	7.99	36.12	9.29
Al_2O_3	0.61	2.92	0.37	1.67	0.41	2.01	0.44	1.98
FeO	58.99	76.74	57.03	78.03	61.86	85.24	61.26	83.69
MnO	0.17	0.35	0.26	0.44	0.32	0.47	0.29	0.44
MgO	2.64	3.23	1.96	2.14	1.88	1.74	1.95	1.94
TOTAL	95.79	95.58	93.45	95.46	100.03	97.83	100.18	97.70
X_{usp}[1]	-	0.376	-	0.374	-	0.221	-	0.258
X_{ilm}[1]	0.642	-	0.619	-	0.627	-	0.627	-
Av. T (°C)[2]	960±55		977±39		845±7		875±29	
Log fo_2[3]	-9.01±0.8		-8.75±0.6		-10.47±0.1		-10.05±.04	
DFMQ[4]	2.0±0.1		2.0±0.3		2.5±0.1		2.3±0.1	
No. of pairs analyzed	10		8		7		8	

[1] Cation assignment based on Stormer (1983). Ulvospinel = usp.

[2] Av. T (°C) = average temperature in °C calculated with QUILF from Andersen and others (1993); data also evaluated using methods of Bacon and Hirshmann (1988), and corrected by reducing temperatures by 30°C given that the range in fo_2 exceeds that of the useful range for QUILF; see text for discussion.

[3] Log fo_2 calculated with QUILF from Andersen and others (1993).

[4] DFMQ = number of log units from the fayalite-magnetite-quartz buffer based on Chou (1978).

and along internal cracks. Representative compositions of olivine phenocrysts in 2006 rocks are reported in table 7 of Larsen and others (this volume).

Groundmass

The groundmass of these samples varies from strongly crystallized and/or oxidized to comparatively clear, microlite-poor vesicular glass. Typically, the high-silica rocks contain trace microlites in the groundmass. For example, samples 06AUJW001, 06AUMC008, 06AUCWM007, and 06AUCWM014 contain relatively fresh matrix glass. Conversely, the low-silica rock samples contain a felty, microlite-rich groundmass. The matrix glasses of these samples are dacitic to rhyolitic in bulk composition. The matrix glasses from these samples also contain a range of volatile component abundances; H_2O varies from 0.09 to 0.12 weight percent, and CO_2 is not observed at the 30-ppm limit of detection. The compositions of the matrix glasses are generally consistent with those of the corresponding melt inclusions except that the former generally contain less H_2O, Cl, and S (table 7).

Description of the Melt Inclusions of the 2006, 1986, and Pleistocene Basalt Samples

Silicate Melt Inclusions in the 2006 Samples

Melt inclusions occur in plagioclase, orthopyroxene, clinopyroxene, amphibole, and apatite. Most of these inclusions contain one or more vapor and/or glass-contraction bubbles and are partially crystallized to completely vitreous; the glass appears colorless to light pink or brown in color. The melt inclusions range from <1 to >100 microns in diameter, but most are <50 microns in size.

We focused our investigation on melt inclusions in plagioclase and pyroxene phenocrysts. The 131 melt inclusions in 2006 samples analyzed for this study were unheated

Table 6. Compositions of amphiboles in 2006 rock samples of Augustine Volcano, Alaska.

[Electron microprobe analyses (wt percent) of representative amphibole phenocrysts in two rock samples. Amphiboles not zoned chemically]

Rock Sample	06AUMC008	06AUMC008	06AUMC008	06AUMC008	06AUMC008	06AUMC008	06AUJW001	06AUJW001	06AUJW001	06AUJW001
SiO_2	45.36	47.23	46.84	46.97	47.55	48.08	48.44	47.84	47.09	49.44
TiO_2	2.43	1.63	1.53	1.51	1.62	1.49	1.53	1.30	0.97	1.36
Al_2O_3	9.45	7.69	7.12	7.07	7.12	7.11	6.86	7.31	8.41	6.22
FeO[1]	12.08	11.37	12.21	11.97	11.67	12.08	11.49	12.66	12.99	11.95
MnO	0.22	0.32	0.35	0.35	0.37	0.32	0.37	0.54	0.59	0.39
MgO	15.08	15.38	15.65	15.50	15.55	15.65	15.75	15.25	14.77	15.93
CaO	11.38	11.09	11.19	11.20	11.17	11.15	11.19	10.87	10.01	11.18
Na_2O	2.10	1.49	1.50	1.39	1.50	1.48	1.31	1.22	1.41	1.29
K_2O	0.23	0.13	0.10	0.11	0.16	0.11	0.09	0.08	0.11	0.11
S	b.d.	0.01	0.01	0.01	0.01	b.d.[2]	0.01	b.d.	b.d.	b.d.
F	0.07	0.17	b.d.	b.d.	0.23	b.d.	0.04	0.47	0.07	0.17
Cl	0.07	0.06	0.06	0.07	0.07	0.08	0.06	0.06	0.09	0.08
O=F,Cl	0.05	0.09	0.02	0.02	0.12	0.02	0.03	0.23	0.05	0.10
TOTAL	98.49	96.60	96.56	96.17	97.05	97.58	97.16	97.59	96.55	98.13
					Chemical Formula					
T-Site Si^{+4}	6.58	6.93	6.84	6.89	6.97	6.98	7.05	6.96	6.94	7.14
T-Site $^{V}Al^{+3}$	1.42	1.07	1.16	1.11	1.03	1.02	0.95	1.05	1.06	0.86
C-Site $^{I}Al^{+3}$	0.20	0.26	0.06	0.11	0.20	0.20	0.22	0.21	0.40	0.20
C-Site Ti^{+4}	0.27	0.18	0.17	0.17	0.18	0.16	0.17	0.14	0.11	0.15
C-Site Fe^{+3}	0.09	0.02	0.47	0.37	0.03	0.09	0.02	0.29	0.03	0.01
C-Site Fe^{+2}	1.38	1.37	1.02	1.10	1.41	1.38	1.38	1.25	1.57	1.43
C-Site Mn^{+2}	0.03	0.04	0.04	0.04	0.05	0.04	0.05	0.07	0.07	0.05
C-Site Mg^{+2}	3.26	3.37	3.41	3.39	3.40	3.39	3.42	3.31	3.24	3.43
B-Site Ca^{+2}	1.77	1.74	1.75	1.76	1.75	1.73	1.75	1.69	1.58	1.73
B-Site Na^{+}	0.01	0.01	0.08	0.06	0.00	0.02	0.00	0.05	0.00	0.01
A-Site Na^{+}	0.58	0.41	0.35	0.33	0.43	0.40	0.37	0.30	0.40	0.35
A-Site K^{+}	0.04	0.03	0.02	0.02	0.03	0.02	0.02	0.01	0.02	0.02
TOTAL	15.62	15.44	15.37	15.36	15.46	15.42	15.38	15.31	15.42	15.37
Mineral	mghb[3]	mghb	mghb	mghb	mghb	mghb	mghb	mghb	mghb	mghb

and naturally vitreous. We strove to locate and analyze melt inclusions in the periphery of plagioclase and pyroxene phenocrysts, as they are more likely to represent newer (that is, 2006) magma, but we also studied randomly located melt inclusions in these phenocrysts. Melt inclusions are most abundant in plagioclase, and some of the plagioclase-hosted inclusions occur in compositionally zoned boundary layers that are aligned parallel to the crystallographic growth planes of the host mineral; these boundary layers appear mottled when viewed petrographically with crossed nichols in transmitted light. Prior research has suggested that such patchy or sieve-textured zones form during heating and resorption events (Bacon and others, 1992; Lowenstern, 1995; Browne and others, 2006; Blundy and Cashman, 2001, 2005; Tappen and others, 2009). A small number of the melt inclusions analyzed were located in these resorption-growth boundary

Table 6. Compositions of amphiboles in 2006 rock samples of Augustine Volcano, Alaska. —Continued

[Electron microprobe analyses (wt percent) of representative amphibole phenocrysts in two rock samples. Amphiboles not zoned chemically]

Rock Sample	06AUJW001	06AUJW001	06AUJW001	06AUJW001	06AUJW001	06AUJW001	06AUJW001	06AUJW001	06AUJW001
SiO_2	49.35	48.50	48.51	46.94	46.18	47.22	48.78	48.44	49.11
TiO_2	1.35	1.35	1.23	1.01	1.07	1.15	1.14	1.23	1.36
Al_2O_3	7.28	7.20	7.16	8.52	8.90	8.55	7.00	7.13	6.18
FeO[1]	13.12	12.77	12.52	13.51	13.58	13.05	12.78	12.88	11.88
MnO	0.47	0.52	0.51	0.55	0.52	0.58	0.54	0.52	0.43
MgO	14.92	15.13	15.16	14.71	14.57	14.63	15.41	15.18	15.75
CaO	10.49	10.74	10.65	10.19	9.89	10.20	10.62	10.60	11.02
Na_2O	1.48	1.25	1.14	1.47	1.40	1.32	1.31	1.35	1.12
K_2O	0.11	0.11	0.13	0.12	0.12	0.10	0.09	0.18	0.11
S	0.01	b.d.	b.d.	b.d.	0.01	b.d.	b.d.	0.01	0.01
F	0.23	0.40	0.26	b.d.	0.20	0.06	0.26	0.11	0.15
Cl	0.06	0.07	0.07	0.05	0.07	0.07	0.07	0.07	0.06
O=F,Cl	0.12	0.20	0.14	0.01	0.11	0.04	0.14	0.07	0.08
TOTAL	98.89	98.06	97.36	97.07	96.50	96.95	98.04	97.73	97.18
				Chemical Formula					
T-Site Si^{+4}	7.09	7.05	7.08	6.86	6.80	6.92	7.08	7.05	7.15
T-Site $^{V}Al^{+3}$	0.91	0.95	0.92	1.14	1.20	1.08	0.92	0.95	0.85
C-Site $^{I}Al^{+3}$	0.33	0.28	0.31	0.33	0.34	0.40	0.27	0.28	0.21
C-Site Ti^{+4}	0.15	0.15	0.14	0.11	0.12	0.13	0.12	0.14	0.15
C-Site Fe^{+3}	0.01	0.01	0.01	0.22	0.03	0.06	0.02	0.01	0.02
C-Site Fe^{+2}	1.57	1.55	1.52	1.44	1.37	1.55	1.54	1.56	1.43
C-Site Mn^{+2}	0.06	0.06	0.06	0.07	0.07	0.07	0.07	0.07	0.05
C-Site Mg^{+2}	3.20	3.28	3.30	3.21	3.20	3.20	3.33	3.30	3.42
B-Site Ca^{+2}	1.62	1.67	1.67	1.60	1.56	1.60	1.65	1.65	1.72
B-Site Na^{+}	0.08	0.00	0.01	0.04	0.05	0.01	0.00	0.01	0.01
A-Site Na^{+}	0.34	0.35	0.32	0.38	0.35	0.37	0.37	0.37	0.31
A-Site K^{+}	0.02	0.02	0.03	0.02	0.02	0.02	0.02	0.03	0.02
TOTAL	15.35	15.37	15.34	15.40	15.37	15.39	15.39	15.40	15.33
Mineral	mghb	mghb	mghb	mghb	mghb	mghb	mghb	mghb	mghb

[1]FeO represents all iron. [2]Below detection limit = b.d. [3]Mghb=magnesiohornblende.

layers, but the compositions of these inclusions show no systematic differences with those trapped in other portions of plagioclase. We avoided analysis of melt inclusions located in the patchy-mottled sieve-textured cores of plagioclase phenocrysts. Melt inclusions in pyroxene do not typically occur within compositional boundaries, because most pyroxene phenocrysts are more homogeneous than the corresponding plagioclase phenocrysts for individual samples. We also avoided melt inclusions that contain crystals, lay along cracks, or those that contain multiple or excessively large vapor and/or glass-contraction bubbles that are indicative of leakage after entrapment.

The silicate melt inclusions of these samples are dacitic to rhyolitic in bulk composition (table 7). Melt inclusions from 2006 samples contain 0.4 to 6 weight percent CaO, 0.8 to 5 weight percent FeO, and 0.2 to 2.0 weight percent MgO.

Table 7. Average compositions of silicate melt inclusions and matrix glass of rock samples from Augustine Volcano, Alaska.

[Major to trace elements in matrix glass (mat gl) and representative melt inclusions (MI) hosted by plagioclase (plag), clinopyroxene (cpx), or orthopyroxene (opx) determined by electron microprobe; H_2O and CO_2 measured by fourier-transform infrared spectroscopy]

Rock Sample	06AUMC 005c.p5 plag MI	06AUM-C008b. p1 plag MI	06AUM-C008b. p1 mat gl	06AUM C010. p1 plag MI	06AUJ W001 mat gl	06AU JW004 plag MI	06AUJ W004 mat gl	06AUC-WM007 plag MI	06AUC-WM007 mat gl	06AUJ W010 plag MI	06AUC-WM012 plag MI	06AUC-WM014 mat gl	AVO208 (1986) plag MI[1]	1986 plag and cpx MI[2]	Prehistoric MI[3]	Prehistoric mat gl[3]	RB-W91A137 cpx MI
(wt. percent)																	
SiO_2	70.17± 2.23	69.90± 2.56	71.19± 3.18	72.17± 1.91	73.76± 1.04	72.56± 1.52	74.30± 2.04	73.44± 1.89	75.86± 2.69	75.69± 0.86	73.26± 1.25	65.34± 3.43	71.86± 1.45	72.96± 1.25	72.63± 1.56	75.39± 2.20	54.92± 1.54
Al_2O_3	13.54± 1.21	13.69± 1.52	13.26± 2.67	12.13± 0.70	12.61± 0.23	12.26± 0.46	12.14± 0.72	12.04± 0.55	13.10± 3.44	11.77± 0.67	11.50± 0.57	15.68± 1.38	12.19± 0.19	12.57± 0.42	12.38± 0.61	12.93± 0.48	14.61± 0.73
TiO_2	0.39± 0.28	0.40± 0.24	0.59± 0.42	0.26± 0.10	0.36± 0.04	0.29± 0.16	0.39± 0.14	0.30± 0.20	0.43± 0.17	0.27± 0.15	0.37± 0.09	0.96± 0.10	0.35± 0.11	0.26± 0.08	0.19± 0.08	0.33± 0.07	0.62± 0.11
MgO	0.54± 0.34	0.72± 0.35	0.51± 0.26	0.35± 0.15	0.36± 0.05	0.52± 0.16	0.24± 0.13	0.41± 0.24	0.25± 0.20	0.44± 0.09	0.60± 0.11	0.46± 0.12	0.47± 0.08	0.17± 0.05	0.36± 0.12	0.49± 0.14	5.89± 0.91
CaO	2.81± 0.84	3.21± 0.95	2.99± 1.46	1.79± 0.45	1.93± 0.14	1.87± 0.24	1.69± 0.99	1.81± 0.32	1.71± 1.40	1.78± 0.20	1.70± 0.30	1.85± 0.55	1.92± 0.12	2.11± 0.14	2.04± 0.25	2.38± 0.44	10.33± 1.59
MnO	0.09± 0.04	0.08± 0.05	0.09± 0.09	0.11± 0.09	0.05± 0.02	0.08± 0.06	0.04± 0.02	0.04± 0.06	0.05± 0.07	0.09± 0.06	0.06± 0.06	0.06± 0.02	0.06± 0.03	n.a.[5]	0.06± 0.03	0.06± 0.03	0.16± 0.03
FeO[4]	2.85± 1.43	2.97± 1.02	3.95± 2.11	1.59± 0.27	1.68± 0.26	2.07± 0.61	1.92± 0.64	1.84± 0.87	1.52± 0.40	1.85± 0.50	2.47± 0.30	4.77± 0.93	2.00± 0.33	1.84± 0.32	1.59± 0.52	1.82± 0.29	6.86± 1.13
Na_2O	4.56± 0.51	4.55± 0.83	4.09± 2.05	3.86± 0.42	4.39± 0.11	4.85± 0.93	4.24± 0.24	5.50± 0.87	4.28± 0.91	5.21± 0.45	3.91± 0.59	04.43± 0.18	3.80± 0.31	3.82± 0.28	4.10± 0.33	4.23± 0.27	2.04± 0.50
K_2O	1.72± 0.16	1.82± 0.27	2.26± 0.38	2.14± 0.56	2.19± 0.08	2.23± 0.20	2.62± 0.37	2.20± 0.30	2.72± 0.62	2.52± 0.28	2.27± 0.25	1.48± 0.18	2.03± 0.06	1.80± 0.21	1.61± 0.27	1.84± 0.21	0.61± 0.12
P_2O_5	0.11± 0.11	0.10± 0.08	0.14± 0.15	0.05± 0.02	0.05± 0.01	0.05± 0.03	0.07± 0.01	0.08± 0.06	0.07± 0.02	0.06± 0.04	0.07± 0.03	0.30± 0.06	0.07± 0.03	n.a.	0.05± 0.02	0.06± 0.03	0.15± 0.03
S	0.02± 0.01	0.02± 0.02	0.01± 0.01	0.02± 0.01	0.01± 0.01	0.02± 0.03	0.00± 0.01	0.02± 0.01	0.01± 0.01	0.01± 0.01	0.02± 0.01	b.d.[6]	0.02± 0.01	0.02± 0.01	0.02± 0.01	0.01± 0.01	0.23± 0.11
Cl	0.36± 0.03	0.38± 0.12	0.33± 0.24	0.44± 0.13	0.23± 0.02	0.45± 0.14	0.26± 0.08	0.41± 0.12	0.20± 0.05	0.43± 0.06	0.56± 0.15	0.35± 0.02	0.44± 0.07	0.29± 0.06	0.31± 0.06	0.32± 0.03	0.30± 0.04
F	0.02± 0.02	0.03± 0.03	0.03± 0.04	0.03± 0.06	0.03± 0.04	0.03± 0.06	0.03± 0.03	0.06± 0.09	0.15± 0.02	0.03± 0.03	0.06± 0.08	0.02± 0.02	0.03± 0.04	n.a.	0.02± 0.03	0.03± 0.05	0.03± 0.04
TOTAL	97.18	97.88	100.63	94.76	98.68	97.00	97.94	97.96	101.00	100.15	96.91	95.76	95.30	96.02	95.38	99.88	97.26
Number of analyses	13	54	6	23	9	14	6	8	6	6	13	3	14	8	79	18	6
CO_2	<0.003	n.a.	n.a.	<0.003	<0.003	<0.003	n.a.	n.a.	n.a.	n.a.	<0.003	n.a.	n.a.	0.011± 0.007	0.009± 0.033	n.a.	n.a.
H_2O	4.1 ± 0.01	n.a.	n.a.	3.08 ± 1.30	0.01	1.70 ± 0.56	n.a.	n.a.	n.a.	n.a.	3.16 ± 0.14	n.a.	2.58 ± 0.98	3.46 ± 1.92	4.19 ± 1.82	n.a.	n.a.

[1]Data of this study. [2]Data of Roman and others (2006). [3]Data of Tappen and others (2009) for melt inclusions hosted by plagioclase, pyroxene, and amphibole. [4]All iron reported as FeO. [5]Constituent not analyzed. [6]Constituent below detection limit; matrix glass analyses for 06AUCWM014 may have included iron-titanium oxides in groundmass glass.

Silicate Melt Inclusions in the 1986 Sample

The silicate melt inclusions from sample AVO 208 are rhyolitic in composition and are somewhat more chemically evolved than some melt inclusions of the 2006 samples. The melt inclusions contain less cafemic constituents than those in 2006 rocks; the concentrations of CaO, FeO, and MgO in the former range from 1.8 to 2.1, 1.5 to 2.4, and 0.3 to 0.6 weight percent, respectively. Water was measured in several of these melt inclusions, and the average concentration is 2.6 weight percent. Sulfur varies from 0.02 to 0.04 weight percent and Cl from 0.38 to 0.51 weight percent, respectively.

Silicate Melt Inclusions in the Basalt

The clinopyroxene-hosted silicate melt inclusions in the basalt sample (RBW91A137) are basaltic-andesite to andesitic in composition. Water was not measured directly in these melt inclusions, but the apparent H_2O concentration of most of these reheated melt inclusions varies from 2 to 4 weight percent using the volatile-by-difference method. These estimated H_2O concentrations could be lower than those in the melt at the time of entrapment due to diffusive loss of H_2 and H_2O out the melt inclusions during reheating and refusion. Sulfur varies from 0.08 to 0.36 and Cl from 0.27 to 0.37 weight percent, respectively.

What do the Melt Inclusion Compositions Represent?

Some silicate melt inclusions are influenced by syn- and post-entrapment processes that modify their compositions and render them nonrepresentative of the bulk melt at the time of entrapment (Lowenstern, 1995; Danyushevsky and others, 2000; Anderson, 2003, Bodnar and Student, 2006). Melt-inclusion compositions may be modified, for example, by host crystallization after entrapment, because post-entrapment crystallization of plagioclase on melt inclusion-host wall contacts increases the SiO_2, FeO, MgO, and K_2O contents and simultaneously reduces the abundances of Al_2O_3, CaO, and Na_2O in the residual melt of the inclusion. Neither the plagioclase- or pyroxene-hosted melt inclusions of this study exhibit trends indicative of this process.

Melt-inclusion glass may also be modified by leakage or post-entrapment diffusive re-equilibration. Consequently, we analyzed no melt inclusions on cracks and the felsic melt inclusions did not require re-fusion to glass prior to analysis, so we consider the abundances of volatile components to represent those of the local melt at the time or entrapment. It is conceivable that H_2O was partially exchanged between bulk magma and entrapped melt after entrapment, through the diffusion of H_2 through the host phenocrysts (Roedder, 1984; Massare and others, 2002), but we cannot constrain the potential consequences of this process. As noted previously, however, the pyroxene-hosted basaltic-andesite melt inclusions were refused and quenched to glass prior to analysis, and their compositions are likely to reflect some diffusive loss of H_2O.

The average compositions of the felsic melt inclusions of 2006 high-silica andesites are equivalent, at the 1-σ level of confidence, with their corresponding areas of matrix glass except for differences in the volatile-components H_2O, S, and Cl. This observation is important as it indicates that the compositions of the late-stage aliquots of melt that quenched to form matrix glass and melt entrapped in growing plagioclase and pyroxene were alike, and, thus, the melt inclusions are compositionally representative of the late-stage melts of 2006 magmas.

Compositional Relationships Involving Melt Inclusions in the Basalt, 1986, and 2006 Samples

The integration of these melt inclusion data sets provides important insights into the evolution of 2006 and earlier Augustine magmas. The differentiation of relatively primitive to residual rhyolitic melts caused the alkalis to increase in abundance and to exhibit increased dispersion in the highly felsic melts. For example, the melt inclusions in 2006 eruptive materials that were analyzed contain higher alkali contents than the melt inclusions from prehistoric tephra. The whole-rock data detail the overall trend.

Before proceeding, we note that detailed analysis and interpretation of the Pleistocene basalts (Larsen and others, this volume) show them to be geochemically distinct from all younger, historic eruptive materials of Augustine Volcano; the geochemical trends characterizing Pleistocene basalts are inconsistent with those of younger volcanic rocks. The former rocks exhibit trends that are lower in K_2O and related large-ion lithophile trace elements; rare-earth elements (REE); and the high-field strength elements Zr, Hf, Nb, and Ta than those of rocks representing historic eruptions. Therefore, in the figures (fig. 1) and discussion that follow, we include data from whole-rock samples and melt inclusions of the Pleistocene basalts in order to provide some constraints on the geochemistry of relatively primitive Augustine magmas, even though the compositions of these older basaltic magmas may be geochemically distinct from the younger basaltic magmas that are not yet well constrained.

The compositions of melt inclusions and matrix glasses exhibit geochemical trends that reflect processes of magma evolution. Magmatic differentiation, for example, is accompanied by decreasing concentrations of alkaline earth elements and increasing abundances of alkali elements in residual fractions of melt. Plots of CaO and MgO versus Na_2O and K_2O in the integrated data sets for Augustine rocks show two distinct relationships (fig. 2). One correlation (that is, mixing trend 1) involves the melt inclusions, groundmass glasses, and some whole-rock data of predominantly low-silica rock samples that is best fit with a linear trend expressing the consequences of magma evolution dominated by hybridization. Although the melt inclusions of the Pleistocene basalt (RBW91A137) may be geochemically distinct from

younger basaltic magmas of Augustine Volcano, we interpret the mixing line to be directed toward their compositions because (1) this trend is consistent with the abundances of nonvolatile components in whole-rock samples, and (2) we have no other constraints at this time.

The second correlation (that is, mixing trend 2, fig. 2) is also best fit with a linear curve, but in this case the trend involves either small reductions in alkaline earth concentrations with increasing alkali abundances or no statistically significant change in CaO and MgO (figs. 2*A*, 2*B*, 2*C*). Many of the melt inclusions that contain less K_2O and Na_2O, represented by the second trend, also contain lower FeO and TiO_2 concentrations. This second trend characterizes the geochemistry of melt-inclusion and matrix glasses from dacitic and high-silica andesitic rock samples of prehistoric, 1986, and 2006 eruptions, and it includes glasses from some 2006 low-silica andesites. Given its linear nature, we interpret it to reflect magma evolution also dominated by magma mixing and/or mingling, but of two relatively silicic end members.

The chemical evolution of magmas can be expressed with the Larsen Index ([(SiO_2x0.333)+(K_2O)]-(CaO+FeO+Mg)) on a weight percent basis; Carmichael and others, 1974). We have applied this index to the Augustine melt-inclusion data in order to interpret the behavior of P, S, and Cl. Phosphorus, for example, shows significant dispersion in the integrated data sets (fig. 3*A*). The highest P values occur in dacitic to rhyodacitic melt inclusions. In addition, the P concentrations of all of these relatively felsic melt inclusions decrease from values as high as 0.35 weight percent to values near zero as their compositions vary from dacite to rhyolite. Relative to P, the S concentrations of all dacitic to rhyolitic melt inclusions show somewhat less dispersion and range from 100 to 700 ppm (fig. 3*B*), and this range is similar to that determined for felsic melt inclusions in 1976 magmas (100 to 500 ppm S; Johnston, 1978). Chlorine also exhibits significant dispersion in the dacitic to rhyodacitic melt inclusions, as it varies from 0.1 to nearly 0.8 weight percent (fig. 3C). This range is consistent with the 0.3 to 0.6 weight percent Cl determined in melt inclusions of 1976 rocks by Johnston (1978) and the 0.22 to 0.37 weight percent Cl in 1986 melt inclusions studied by Roman and others (2006).

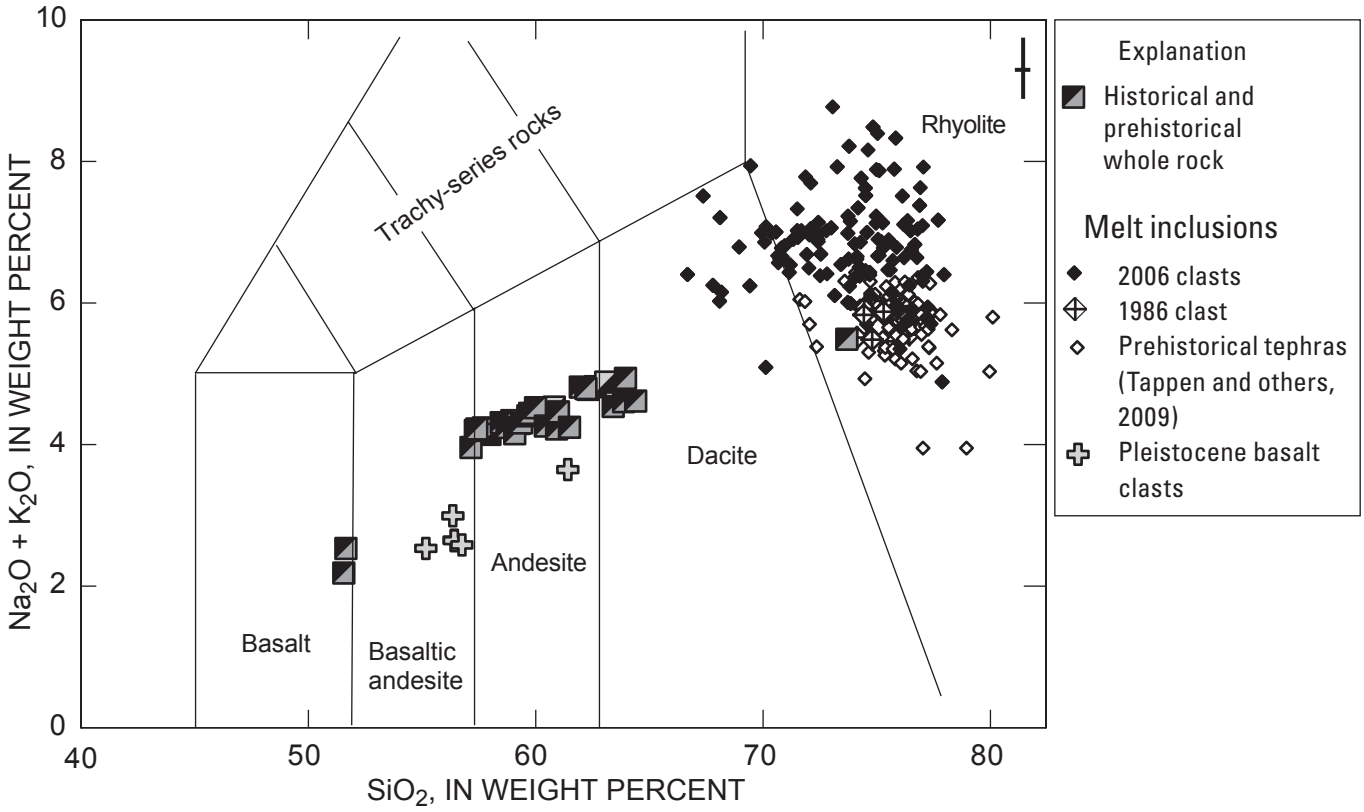

Figure 1. Plot of the relation between concentrations of total alkali elements and silica in Augustine Volcano whole-rock samples (Keinle and Forbes, 1976; Daley, 1986; Larsen and others, this volume) (black and gray squares) and silicate melt inclusions from 2006 rock samples (see text and appendix for descriptions) (black diamonds), prehistoric tephra (open diamonds), 1986 tephra (gridded diamonds), and reheated andesitic melt inclusions from Pleistocene basalt (filled crosses). Data reflect magma evolution and are reported on an anhydrous basis with analytical totals normalized to 100 weight percent. Representative and relative 1-σ precision for melt-inclusion analyses shown in upper right corner. Rock fields after Le Bas and others (1986).

It is noteworthy that the S contents of all felsic melt inclusions are distinctly less than those of the basaltic-andesite melt inclusions of the Pleistocene basalt. Moreover, the presence of 0.08 to 0.36 weight percent S and 0.27 to 0.37 weight percent Cl in these basaltic-andesite melt inclusions (from sample RBW91A137) is consistent with those of basaltic melt inclusions hosted by Fo_{80-85} olivine phenocrysts of Augustine basalt (Johnston, 1978; Zimmer and others, 2004). The latter inclusions contain 0.24 to 0.45 weight percent S and 0.3 to 0.6 weight percent Cl, as well as H_2O concentrations approaching 5 weight percent. Interestingly, these abundances of volatile components in mafic to intermediate-silica content melt inclusions are also consistent with observations made from other mafic, subduction-related magmas. Wade and others (2006), for example, determined that high-Al basaltic liquids from Arenal Volcano contained up to 4 weight percent H_2O, >0.2 weight percent S, and approximately 0.15 weight percent Cl. Straub and Layne (2003) measured 0.7 to 0.9 weight percent Cl and also estimated up to 10 weight percent H_2O in andesitic melt inclusions of volcanic rocks from the Izu arc. Gurenko and others (2005) found 0.04 to 0.29 weight percent S in basaltic-andesite melt inclusions from Chikurachki volcano, Russia. Moreover, Anderson (1982) reports that up to 0.33 weight percent S occurs in rehomogenized melt inclusions of such magmas on a world-wide basis; just as Wallace (2005) notes that these volatile abundances are consistent with those recorded for other subduction-related volcanic systems.

The integrated 2006-, 1986-, and prehistoric-sample melt-inclusion data exhibit no distinct relationships involving CO_2 and magma differentiation, because the CO_2 abundances of most melt inclusions are below the limit of detection. The inclusions do, however, contain widely ranging abundances of H_2O (fig. 4). The H_2O concentrations of the melt inclusions from 2006 samples range from 1.2 to 4.7 weight percent, range from approximately 2 to 6 weight percent for the 1986 samples (that is, ours and those of Roman and others, 2006), and range from approximately 2 to 8 weight percent for melt inclusions of prehistoric samples. These data have been plotted, for comparison, relative to the computed H_2O and CO_2 concentrations of vapor-saturated rhyolitic melt at pressures of 20 to 400 MPa (200 to 4,000 bars) and temperatures of 900 to 1,000°C. Plots like these provide key constraints on pressures of melt and magmatic fluid equilibration as addressed below.

Discussion

Magma Evolution at Augustine During the Past 2,100 Years

Outcrops at Augustine are dominated by andesite and dacite (Waitt and Begét, 2009); basaltic and basaltic-andesite rocks are rare at the surface. This skewed compositional distribution of volcanic rocks indicates that the more primitive mafic magmas feeding this volcano differentiate significantly before eruption. Prior research concluded that magma mixing/mingling is crucial to the evolution of Augustine magmas and that the geochemical features of this process are overprinted by crystal fractionation, assimilation, and fluid exsolution. Johnston (1978) was one of the first to articulate this after systematic analysis of 1976 eruptive products. He surmised that fluid-saturated, residual dacitic melt mixed with fluid-undersaturated basaltic melt, and that extensive crystallization occurred afterward within the resulting mixed products. In a recent study of the compositionally heterogeneous materials of the 1986 eruption, Roman and others (2006) determined that some batches of erupted magma reflect mixing in the shallow crust of newly arrived, comparatively mafic magma with compositionally evolved magma that was residual from the 1976 eruption. They also concluded that some 1986 material represents juvenile magma that evolved without mixing. More complex mixing processes for 1986 magmas were called upon by Harris (1994) and Johnson and others (1996). In this three-component scenario, relatively new magma mixed with magma residual from the 1976 eruption and with partially crystallized residual "rind" material that was low in K_2O and very low in related incompatible elements (Larsen and others, this volume).

Other research has interpreted evidence of a stronger role of fractional crystallization. Daley (1986) argued from analyses of prehistoric, 1935, 1963–64, and 1976 eruptive materials, that andesitic magmas formed by crystal fractionation of parental basaltic magmas at comparatively high pressures, and this process was followed by subsequent fractionation of andesitic liquid to dacitic compositions by low-pressure crystallization. To Daley (1986), magma mixing had only minor effects on magma evolution. Moreover, Johnson and others (1996) concluded that closed-system crystal fractionation was the dominant evolutionary process for some 1976 magmas, even though their interpretation of oxygen isotopic characteristics of whole-rock data was consistent with magma mixing. More recent research (Tappen and others, 2009) on tephra from 4 prehistoric eruptions reveals that crystal fractionation was dominant even though the phenocrysts also provide ample evidence of mixed and/or mingled magmas. Given the extent of prior research on processes of magma differentiation in 1986 and older magmas, we focus herein on processes reflected in 2006 rocks in the following discussion, but we also compare these results with those bearing on prior eruptions to provide a broad context for processes of magma evolution at Augustine Volcano (fig. 5).

Mixing and/or Mingling in 2006 Magmas

The 2006 eruptive materials afford ample evidence of magma hybridization. During our field work and that of others in the summer of 2006 (Vallance and others, this volume; Larsen and others, this volume; Tilman, 2008), a large variety of banded rocks, that are definitive evidence of incomplete mixing of magmas of differing compositions, was observed (fig. 6). In addition, hand sample 06AUMC008B.p1A exhibits light- and intermediate-gray banding on a smaller scale. The

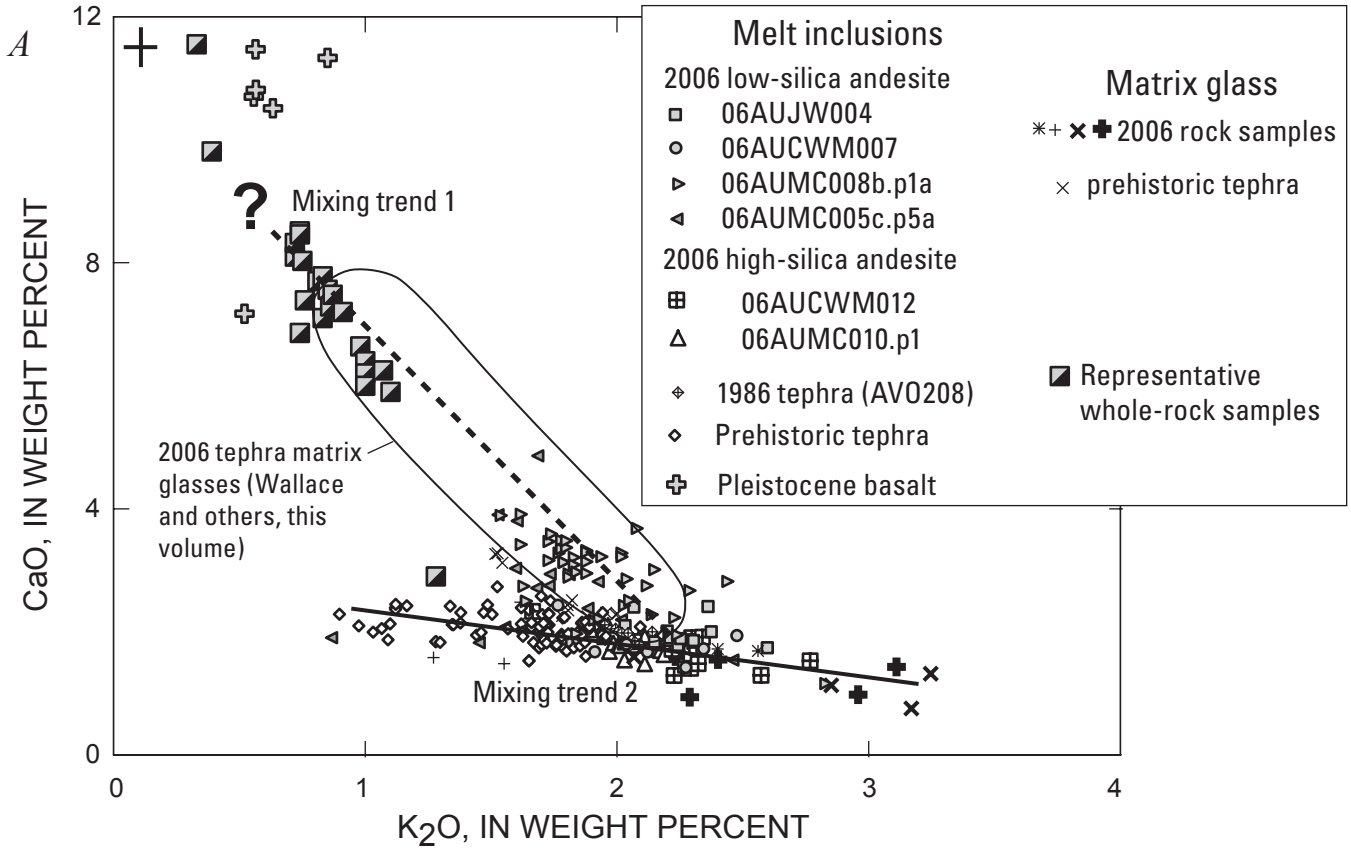
A
Melt inclusions
2006 low-silica andesite
06AUJW004
06AUCWM007
06AUMC008b.p1a
06AUMC005c.p5a
2006 high-silica andesite
06AUCWM012
06AUMC010.p1
1986 tephra (AVO208)
Prehistoric tephra
Pleistocene basalt
Matrix glass
2006 rock samples
prehistoric tephra
Representative whole-rock samples
Mixing trend 1
Mixing trend 2
2006 tephra matrix glasses (Wallace and others, this volume)
CaO, IN WEIGHT PERCENT
K2O, IN WEIGHT PERCENT
0
4
8
12
0
1
2
3
4

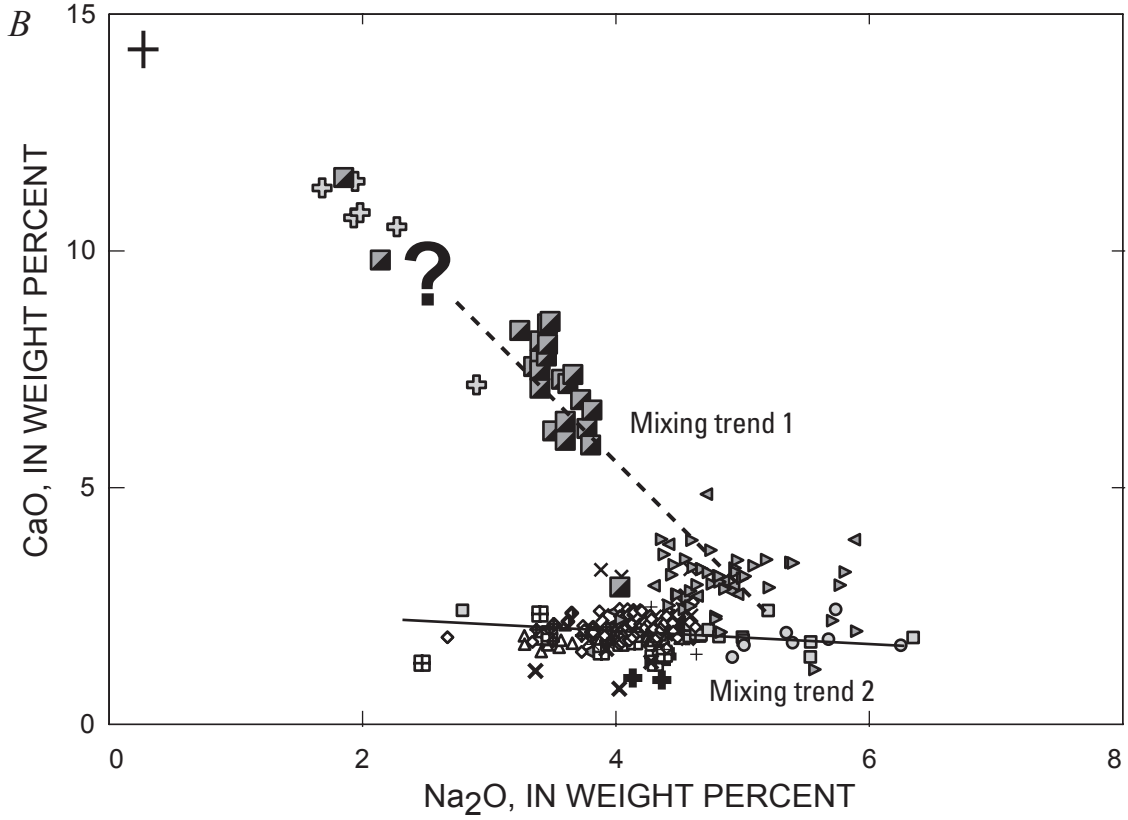
B
Mixing trend 1
Mixing trend 2
CaO, IN WEIGHT PERCENT
Na2O, IN WEIGHT PERCENT
0
5
10
15
0
2
4
6
8

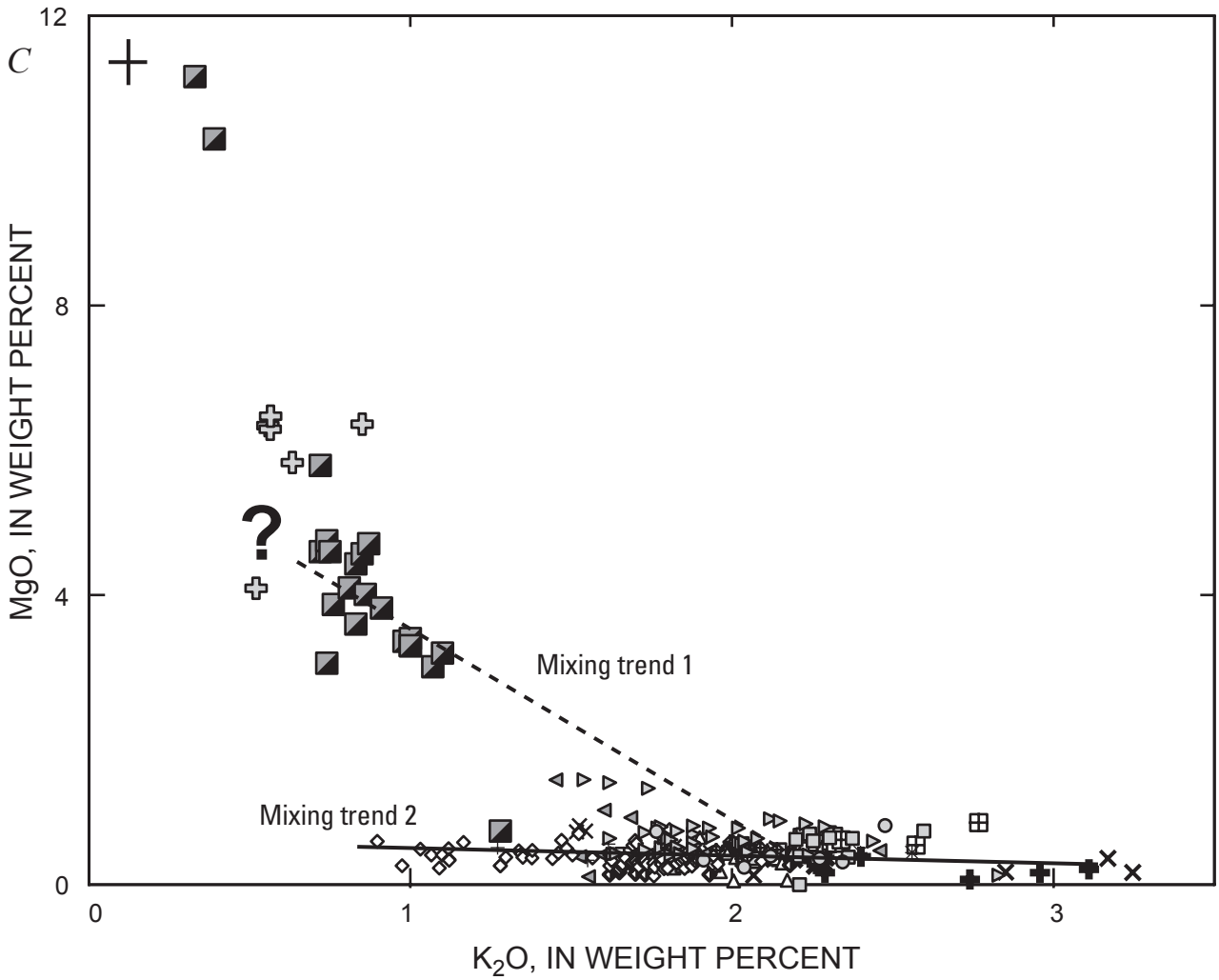

Figure 2. Plots of the relations between the concentrations of CaO and K_2O (*A*), CaO and Na_2O (*B*), and MgO and K_2O (*C*) for Augustine Volcano melt inclusions, matrix glasses, and whole-rock samples; the curves are schematic. Felsic melt inclusions from low-silica andesitic 2006 rock samples are shown with small gray-filled symbols and include 06AUJW004 (squares), 06AUCWM007 (circles), 06AUMC008b.p1A (right-pointing triangles), and 06AUMC005c.p5A (left-pointing triangles). Reheated melt inclusions from Pleistocene basalt sample (RBW91A137) represented by large filled crosses. Felsic melt inclusions from high-silica andesitic 2006 rock samples are shown with small clear-filled symbols and include 06AUCWM012 (gridded squares) and 06AUMC010.p1 (upward-pointing triangles). Other felsic melt inclusions from high-silica andesitic to dacitic rock samples are shown with small clear-filled symbols and include prehistoric tephra (open diamonds) (Tappen and others, 2009), our 1986 ignimbrite sample AVO 208 (gridded diamonds), other 1986 tephra (diamonds clear on one side and filled on right-hand side; sample 86E-63-2 of Roman and others, 2006). Our matrix glass analyses include samples 06AUCWM007 (bold X's), 06AUCMW014 (faint crosses), 06AUJW004 (bold crosses), 06AUJW001 (bold asterisks), 06AUMC008b.p1A (faint asterisks), and prehistoric tephra (faint X's). Elliptical field represents approximate range in CaO and K_2O for hundreds of matrix glass analyses from 2006 tephra (Wallace and others, this volume). Representative whole-rock samples shown as large, variably filled squares (Tappen and others, 2009; Keinle and Forbes, 1976; Daley, 1986; Harris, 1994). The data acquired from low-silica rock samples are consistent with upper curve (dashed line of mixing trend 1) and reflect consequences of magma mixing/mingling and other processes. Large question mark reflects unknown compositional characteristics of the basaltic mixing end member. Data from dominantly high-silica rock samples are consistent with the lower curve (solid line of mixing trend 2). This trend also reflects melt evolution dominated by magma mixing/mingling that apparently involved two high-silica magmas with varying K_2O and Na_2O concentrations and marginally varying CaO and SiO_2 concentrations. The silica content of nearly all of the latter melt inclusions, normalized to an H_2O-free basis, ranges from 71 to 78 weight percent. Representative and relative 1-σ precision for glass analyses is shown as cross in upper left corner. See text for discussion.

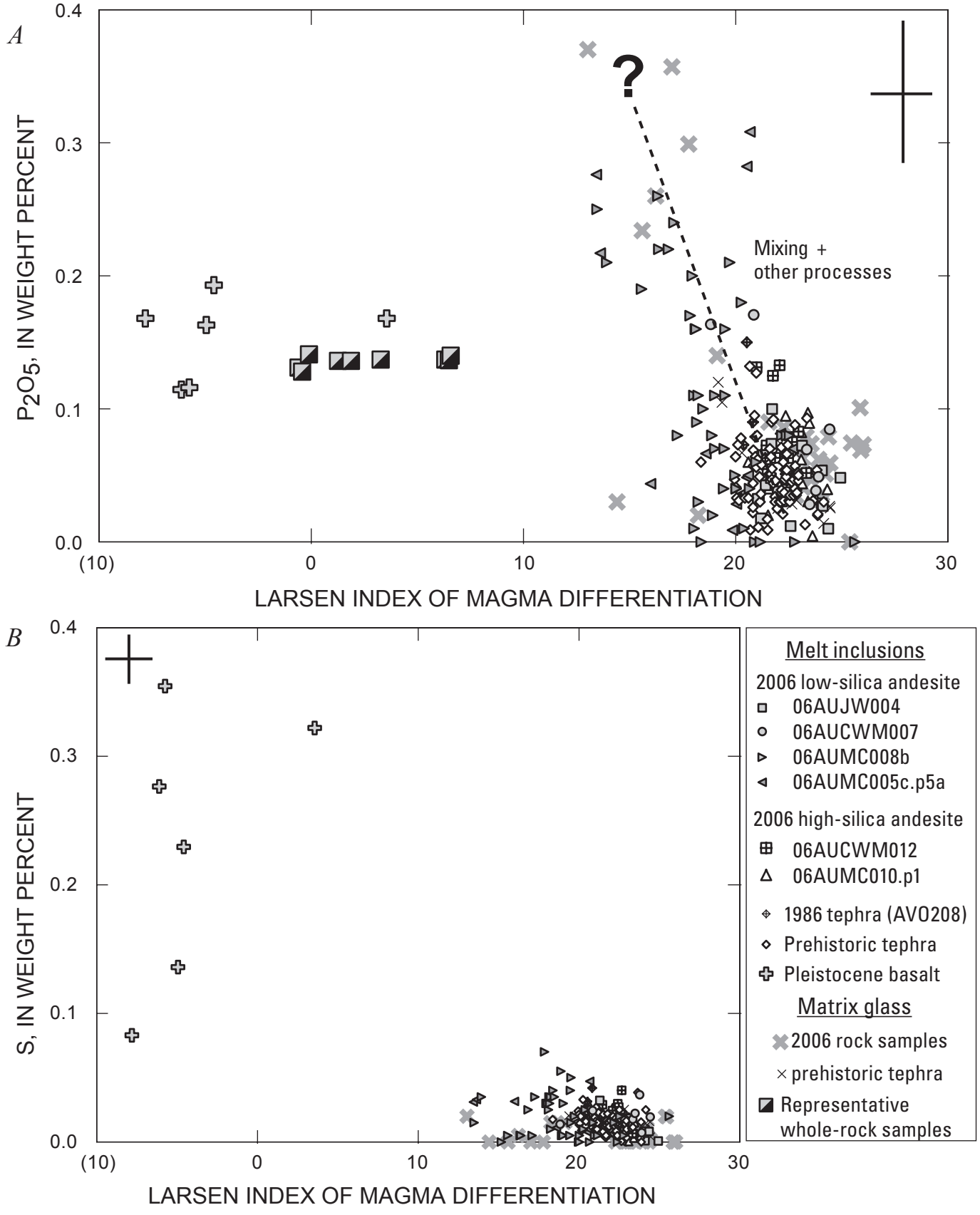
A
0.4
0.3
0.2
0.1
0.0
P_2O_5, IN WEIGHT PERCENT
?
Mixing +
other processes
(10)
0
10
20
30
LARSEN INDEX OF MAGMA DIFFERENTIATION
B
0.4
0.3
0.2
0.1
0.0
S, IN WEIGHT PERCENT
(10)
0
10
20
30
LARSEN INDEX OF MAGMA DIFFERENTIATION
Melt inclusions
2006 low-silica andesite
06AUJW004
06AUCWM007
06AUMC008b
06AUMC005c.p5a
2006 high-silica andesite
06AUCWM012
06AUMC010.p1
1986 tephra (AVO208)
Prehistoric tephra
Pleistocene basalt
Matrix glass
2006 rock samples
prehistoric tephra
Representative
whole-rock samples

mixing-based origin of these macroscopic features is further supported by microscopic-scale textural features in 2006 samples. These observations include the presence of numerous reversely zoned plagioclase phenocrysts, resorption-growth features in plagioclase, and partially resorbed and orthopyroxene-rimmed olivine phenocrysts. Moreover, the temperatures recorded by coexisting iron-titanium oxide minerals contained in the groundmass of 2006 rock samples (for example, 835 to 1,052°C) vary significantly (fig. 7), and they are consistent with the temperature ranges estimated for 2006 magmas by Larsen and others (this volume) and for temperature estimates of older Augustine magmas (Johnston, 1978; Johnson, 1986; Roman and others, 2006, Tappen and others, 2009). This observed dispersion in temperature for oxides within individual samples is a consequence of mixing processes (fig. 7). In fact, many of the plagioclase-hosted inclusions that occur within distinct resorption-growth zones are a result of and an indication of the interaction of extant plagioclase phenocrysts with younger aliquots of magma that were hotter and more H_2O enriched, and, therefore, they reflect the interaction of younger magma with phenocrysts of an older magma. The apparent method of entrapment of these inclusions (that is, heating through magma mixing) is consistent with their geochemical characteristics further supporting the occurrence of magma mingling and/or mixing.

The variety of mixing processes involving materials erupted in 2006 is complex; Larsen and others (this volume), for example, call for two stages of hybridization. In their model, the initial two-component mixing event involved a juvenile batch of hot, relatively volatile-rich, mafic magma that combined with cooler, crystal-rich, high-silica andesitic magma (that was likely residual from 1986 or older eruptive

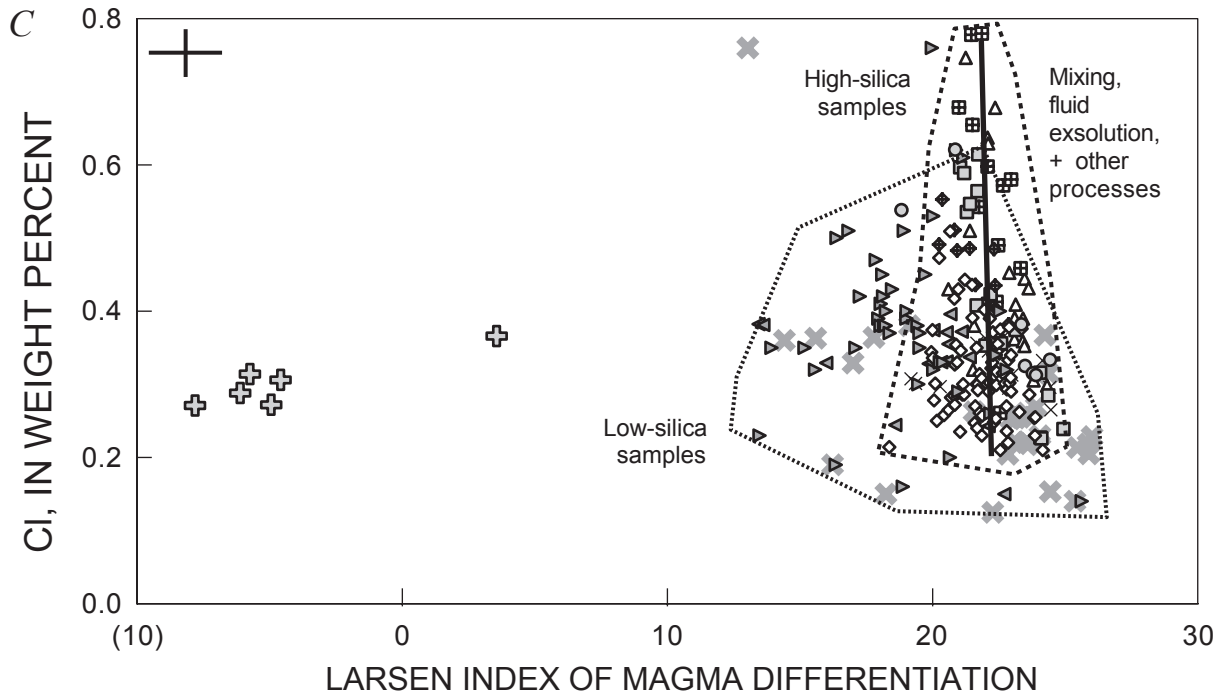

Figure 3. Plots of the relation between the concentrations of P_2O_5 (*A*), S (*B*), and Cl (*C*) and the Larsen differentiation index (for example, [[SiO_2x0.333] + K_2O] versus [CaO + MgO + FeO]] on a wt. percent basis) for melt inclusions and matrix glasses of Augustine Volcano rock samples; samples and symbols same as in figure 2, except all 2006 matrix glasses are shown as gray X's and those of prehistoric tephra shown as faint X's. Data express the changes in volatile- and fluxing-component concentrations in residual melt with progressive magma evolution assuming that basaltic-andesite melt inclusions (filled crosses) are geochemically representative of magmas parental to prehistoric, 1986, and 2006 magmas. *A*, Phosphorus concentrations generally decrease from Pleistocene andesitic melt inclusions and all whole rocks to that of the felsic melt inclusions from 2006, 1986, and prehistoric high-silica andesitic and dacitic rock samples and for most of the felsic melt inclusions of low-silica andesites of same eruptive units. However, the P_2O_5 contents of some felsic melt inclusions of low-silica andesites evolved to higher abundances with magma evolution. *B*, Sulfur concentrations of felsic melt inclusions of all Augustine rock samples are very low and reflect sulfide crystallization and/or exsolution of magmatic fluid(s). *C*, Chlorine concentrations of melt inclusions are highly variable; fields for low-SiO_2 andesitic rocks (dotted envelope) and high-SiO_2 andesitic rocks (dashed envelope) shown for comparison. Chlorine data reflect magma mixing, fractional crystallization, and fluid(s) exsolution as described in text. Representative and relative 1-σ precision for glass analyses is shown as cross in upper corners.

activities) to form the 2006 low-silica andesitic magma. The second mixing event that they observe involved syneruptive hybridization of low-silica and high-silica andesitic magma to form intermediate-silica andesitic rocks.

Our mixing trend 1 (fig. 2) is consistent with the first two-component mixing process of Larsen and others (this volume) that involved the combination of an unidentified mafic magma with older crystal-rich, high-silica andesitic residual magma. Interestingly, our analyses of glass compositions (figs. 2 and 3) allow us to provide some constraints on the composition of the melt in the high-silica andesitic magma that was involved in the mixing. Based on the curves shown in these figures, this melt contained ≤2 weight percent CaO, ≤1 weight percent MgO, ≥2.2 weight percent K_2O, ≥5 weight percent Na_2O, ≤0.05 weight percent P_2O_5, and ≤0.2 weight percent Cl. Close inspection of the most alkali-enriched melt inclusions of figures 2*A* and 2*B* also shows several data points representing more highly evolved glasses from the low-silica andesite samples, and it is important to note that these glass compositions are not compatible with the mixing trend 1 line because they imply a break-in-slope of the trend. These highly evolved samples of glass contain 3 or more weight percent K_2O and nearly 6 weight percent Na_2O, and we interpret them to reflect the consequences of fractional crystallization

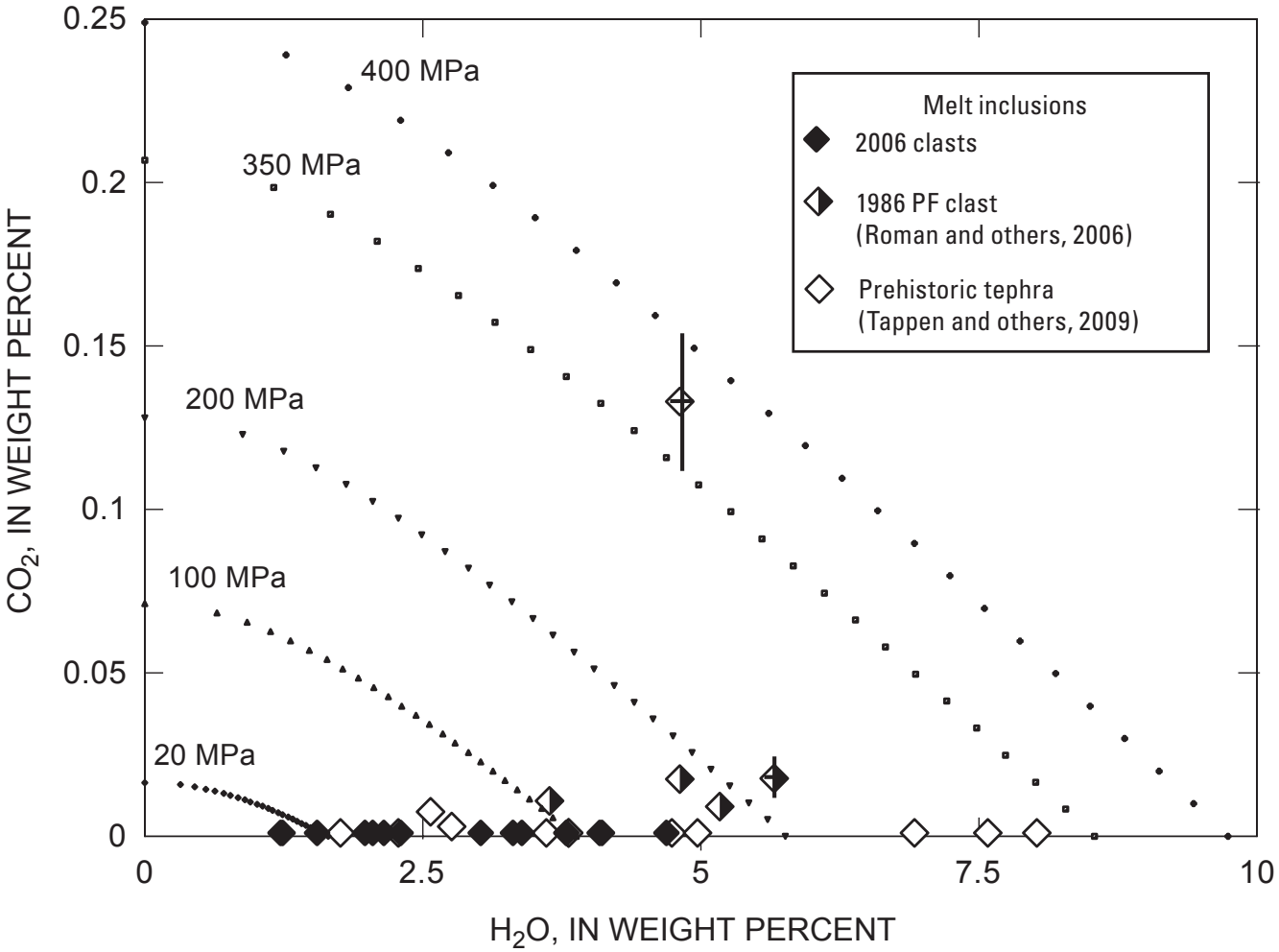

Figure 4. Plots of the relation between CO_2 and H_2O in 28 silicate melt inclusions from Augustine Volcano rock samples including prehistoric rocks (open diamonds; Tappen and others, 2009), 1986 tephra (diamonds filled on right side; sample 86E-63-2 of Roman and others, 2006), and our 2006 samples (filled diamonds). Data are plotted in reference to isobaric curves for rhyolitic melt saturated in CO_2- and H_2O-dominated fluid(s) using model of Newman and Lowenstern (2002). Melt inclusions in this plot reflect either minimum trapping pressure (given independent evidence that a melt inclusion represents fluid-saturated melt) or pressures at which a fluid-phase would have exsolved (if no such evidence is available). Prehistoric melt inclusions represent trapping or fluid-exsolution pressures ranging from 20 to >350 MPa, melt inclusions from 1986 samples represent trapping or fluid-exsolution pressures of about 10 to 220 MPa, and melt inclusions from 2006 samples reflect trapping or fluid-exsolution pressures of about 20 to 160 MPa. Estimated values for 1-σ precision for CO_2 and H_2O in glasses are shown as vertical and horizontal lines for two representative high- and low-CO_2 melt inclusions. See text for discussion.

of low-silica andesitic magma that occurred subsequent to mixing. Relatively late-stage fractionation, like this, is consistent with the presence of microlite-enriched groundmass in the low-silica andesitic rocks (Larsen and others, this volume).

Our mixing trend 2 is based on glass compositions, and it is inconsistent with the second hybridization process recognized by Larsen and others (this volume). Through their analysis of whole-rock data, Larsen and others described mixing of low- and high-silica andesitic magmas to generate hybrid andesitic magmas with intermediate silica contents. Compared with this second mixing trend of Larsen and others (this volume), our mixing trend 2 involves highly variable K_2O abundances that are not compatible with the bulk geochemistry of most of the andesites studied by Larsen and others (this volume). The origin of the felsic, low K_2O-end member is discussed in more detail below.

Fractional Crystallization in Magmas Erupted from Augustine in 2006

The 2006 rock samples contain normally zoned plagioclase and pyroxene phenocrysts, as well as highly evolved rhyolitic matrix glasses and silicate melt inclusions contained within andesitic to dacitic whole rocks. These features are normal products of fractional crystallization. The effects of fractional crystallization are also seen in the presence of fine-grained gabbroic inclusions, erupted in 2006, that are low in incompatible elements. These geochemical characteristics led Larsen and others (this volume) to interpret the gabbro to represent accumulated residual crystals. It is also noteworthy that the groundmass of the 2006 low-silica andesitic rocks contains abundant microlites and exhibits a felty texture; whereas, the matrix of high-silica andesitic rocks are microlite-poor and

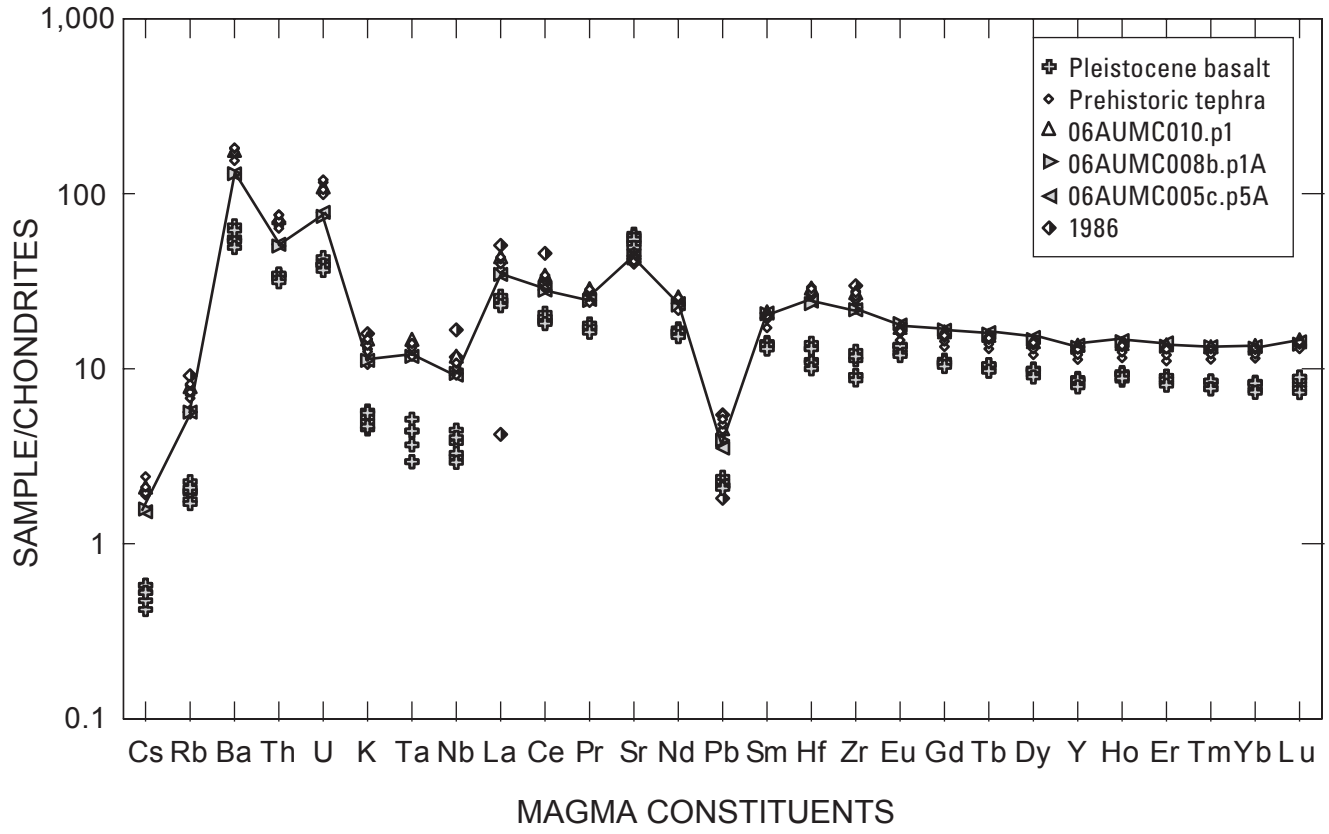

Figure 5. Plot of potassium and trace-element concentrations of Augustine Volcano whole-rock samples normalized to chondritic values (Sun and McDonough, 1995) for five prehistoric tephra (diamonds; from Tappen and others, 2009), six Pleistocene basalts (open crosses; Larsen and others, this volume), 06AUMC010.p1 (open upward-pointing triangles), 06AUMC008b.p1A (gray-filled right-pointing triangles), and 06AUMC005c.p5A (gray-filled left-pointing triangles), and 1986 tephra. Drawn line fitted to normalized data of sample 06AUMC005c.p5A as an example of 2006 eruptive materials relative to older eruptive materials. See text for discussion.

Figure 6. Photograph of large banded boulder within 2006 Augustine pyroclastic-flow deposit showing textural evidence of magma mingling. Bolder located on north slope of Augustine Volcano. One-half meter long rock hammer shown for scale.

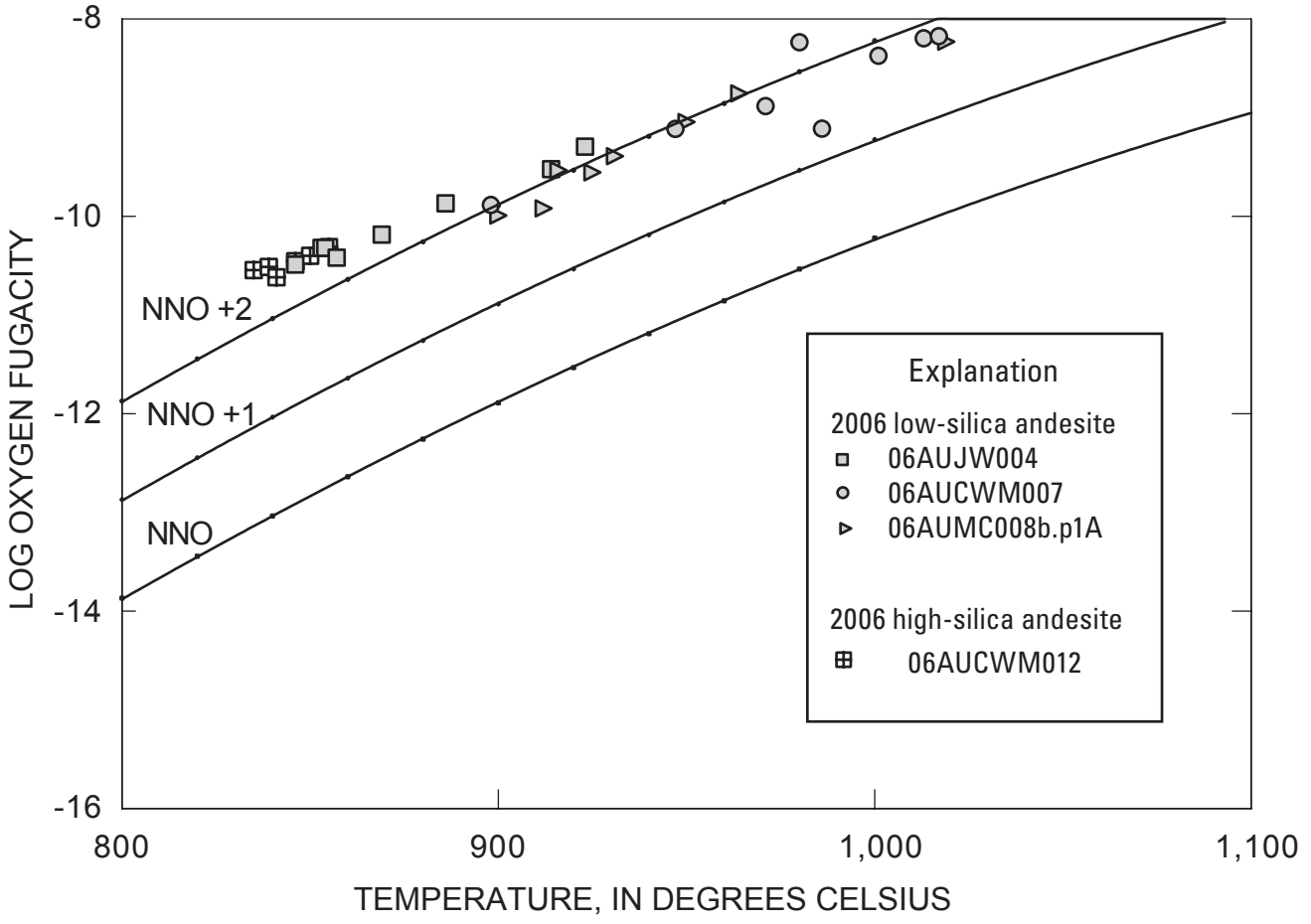

Figure 7. Plot of calculated equilibration temperature (°C) and log of oxygen fugacity (relative to nickel-nickel oxygen buffer = NNO) for coexisting (and "touching") pairs of ilmenite and titanomagnetite. Iron-titanium oxide minerals in 2006 rock samples: 06AUJW004 (gray-filled squares), 06AUCWM007 (gray-filled circles), 06AUCWM012 (gridded squares), and 06AUMC008b.p1A (gray-filled triangles). Data calculated using techniques of Andersen and others (1993) and evaluated using the method of Bacon and Hirshmann (1988), and corrected by reducing temperatures 30°C because these algorithms are not directly applicable to these oxide minerals at such elevated oxygen fugacities. See text for discussion of these methods.

contain glass suitable for microbeam analysis. This indicates that post-mixing, late-stage crystallization of magma forming the low-silica andesites influenced the composition of their near-final and final melts. As explained below and by Larsen and others (this volume), this stage of crystallization may have been facilitated by shallow magma ascent and decompression- and degassing-related processes.

A detailed trace-element analysis of whole-rock samples by Larsen and others (this volume), however, indicates that the high-silica andesites are not fractional crystallization-derived differentiates of the low-silica andesitic magmas that formed by magma mixing. In particular, the abundances of Cr and Ni of the high-silica andesites are too enriched and the concentrations of large-ion lithophile and some high-field strength elements are not sufficiently enriched to reflect an origin based solely on fractional crystallization.

The Behavior of Volatile Components in Evolving Augustine Magmas During the Previous 2,100 Years

Prior research indicates that some fractions of 1976, 1986, and 2006 magmas were fluid saturated during ascent (Johnston, 1978; Roman and others, 2006; Webster and others, 2006), so it is pertinent to consider the evidence and consequences of fluid exsolution on magma differentiation at Augustine. The analysis of volatile-component and fluid behavior in the most recently erupted Augustine magmas is challenging, however, due to the complex histories involving magma mixing, mingling, and fractional crystallization.

In discussion that follows, the compositions of silicate melt inclusions from our prehistoric, 1986, and 2006 eruptive materials are shown to provide distinct geochemical evidence of preeruptive fluids in some fractions of the corresponding magmas. Interpretation of the melt-inclusion data further suggests that initial volatile phase exsolution occurred prior to the entrapment of many of the melt inclusions. Specifically, the melt-inclusion data are compared with experimentally determined solubilities of volatile components in coexisting melt and fluid(s), but this approach can be problematic. Augustine magmas exsolve volatile phases that are variably enriched in the four principal volatile components H_2O, CO_2, S, and Cl (Symonds and others, 1990; McGee and others, this volume), and the sum of their partial pressures ($p_{H_2O} + p_{CO_2} + p_{S_{species}} + p_{Cl_{species}}$) must equal the total pressure of a fluid-saturated magma. It follows that all four components must be considered simultaneously in data treatments like this. For example, the presence of elevated S and/or Cl in a fluid phase will dilute the H_2O and CO_2 concentrations and alter the activity-composition mixing relationships (Botcharnikov and others, 2004; Webster and others, 2005) and, hence, change the larger behavior of H_2O and CO_2 in such fluids. Unfortunately, most experimental data are limited at present to pseudo-ternary systems including silicate melt-H_2O-CO_2, melt-H_2O-Cl, or melt-H_2O±S so we are forced to address the melt-inclusion data with individual pseudo-ternary systems in the discussion that follows.

H_2O in Augustine Magmas

The abundances of the components H_2O and K_2O, which are relatively incompatible in the phenocrysts and microlites in magmas like these, serve as a useful gauge of the extent of residual melt evolution (Anderson, 1976; Johnston, 1978; Roman and others, 2006). In particular, prior studies have interpreted negative correlations between K_2O and H_2O in silicate melt inclusions to represent the consequences of polybaric, decompression crystallization of fluid-saturated magma during ascent (Roman and others, 2006; Atlas and others, 2006). Therefore, we have plotted the concentrations of H_2O versus K_2O for a set of melt inclusions that were analyzed by FTIR and largely represent prehistoric, 1986, and 2006 high-silica andesitic and dacitic rock samples (fig. 8). Figure 8*A* includes 4 modeled trends that express the influence of (A) fluid-absent crystallization of 20 weight percent plagioclase, pyroxene, Fe-Ti oxides, and apatite (in modal abundances that are compatible with 2006 Augustine rocks), (B) complete degassing of an open magmatic system with no concurrent crystallization, (C) polybaric crystallization of 25 weight percent phenocrysts from this same mineral suite in a magma that also contains 4 weight percent exsolved aqueous fluid, and (D) mixing of magmas that may or may not be fluid saturated. The lengths of the arrows designating these trends are quantitative representations of the influence of these processes.

Trend A (fig. 8*A*) is consistent with the positive correlation involving the three most H_2O-enriched, prehistoric melt inclusions, and hence, may reflect the geochemical evolution of these and potentially other fractions of Augustine melts via fluid-absent fractional crystallization. Trend B is inconsistent with the negative correlation of H_2O versus. K_2O that is exhibited by most of the data. The slope of trend C is consistent with the general orientation of the melt-inclusion data field, but this trend requires 25 weight percent crystallization to generate the requisite increase in K_2O content and this degree of crystallization is problematic. It is too extensive for such felsic melts, because it would reduce the FeO, MgO, and CaO contents of the final residual melt to values near zero. Thus, we interpret these melt inclusions to reflect magma evolution dominated by magma mixing and/or mingling (symbolized by trend D) with associated fractional crystallization of fluid-saturated magmas because they are part of the clustered data of figure 2 best interpreted by linear mixing curves.

It should be noted that other processes influence magmatic systems like these. In a study of plagioclase-hosted, felsic melt inclusions in rocks produced during the April 10, 1980 to March 19, 1982, eruptions of Mount St. Helens, Blundy and Cashman (2005) noted a similar negative correlation involving H_2O and K_2O (fig. 8*B*). They computed temperatures of plagioclase-melt equilibrium and estimated the range in crystallization of the magmas involved. Their

results showed distinct and robust correlations between magmatic temperature, water fugacity, crystallinity, and the compositions of residual fractions of melt in the Mount St. Helens magmas. Blundy and Cashman (2001, 2005) and Blundy and others (2006) concluded that the batches of magma represented by their melt inclusions underwent contemporaneous: (1) decompression crystallization, (2) loss of volatile components to magmatic vapor, and (3) associated release of latent heat within the magma due to phenocryst growth. They also concluded that the latent-heat effects may have increased temperatures in Mount St. Helens magmas locally by as much as 100°C, and that, in general, such latent-heat temperature increases are likely in any magma that decompresses slowly enough to undergo crystallization.

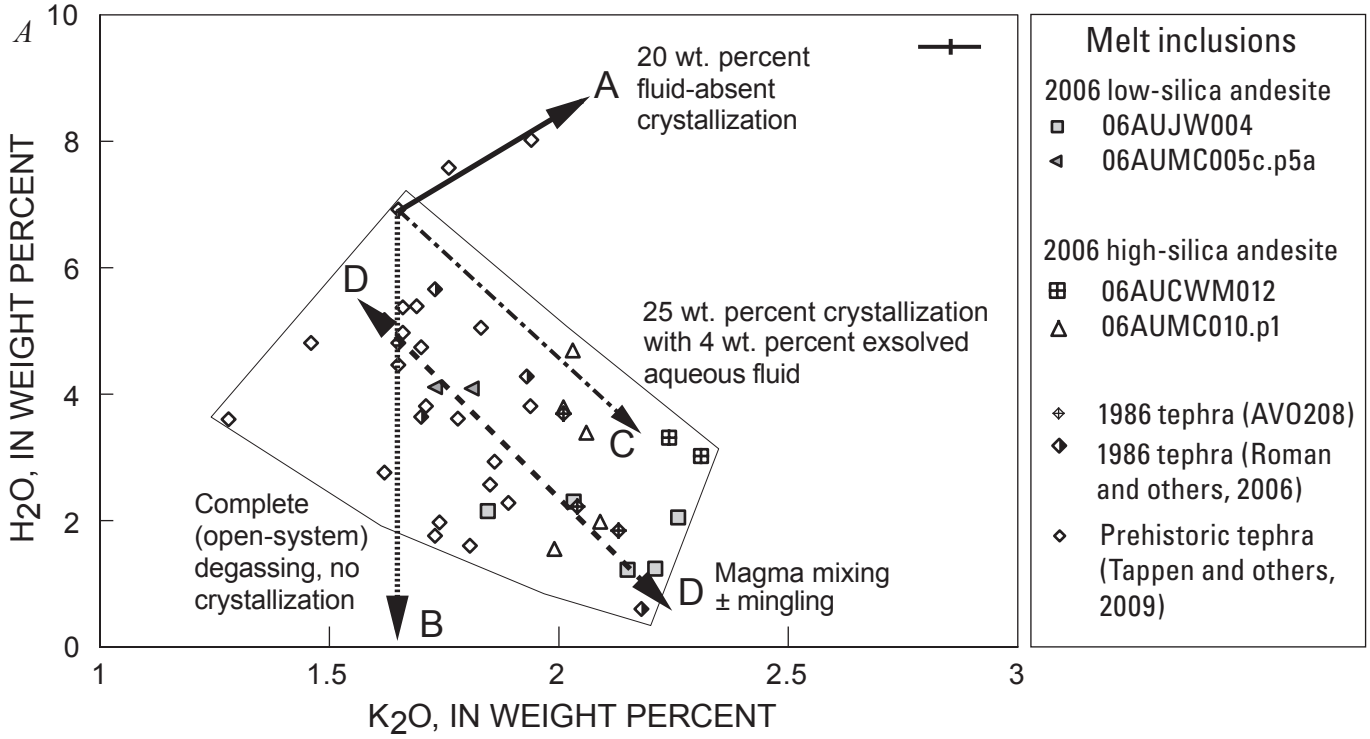

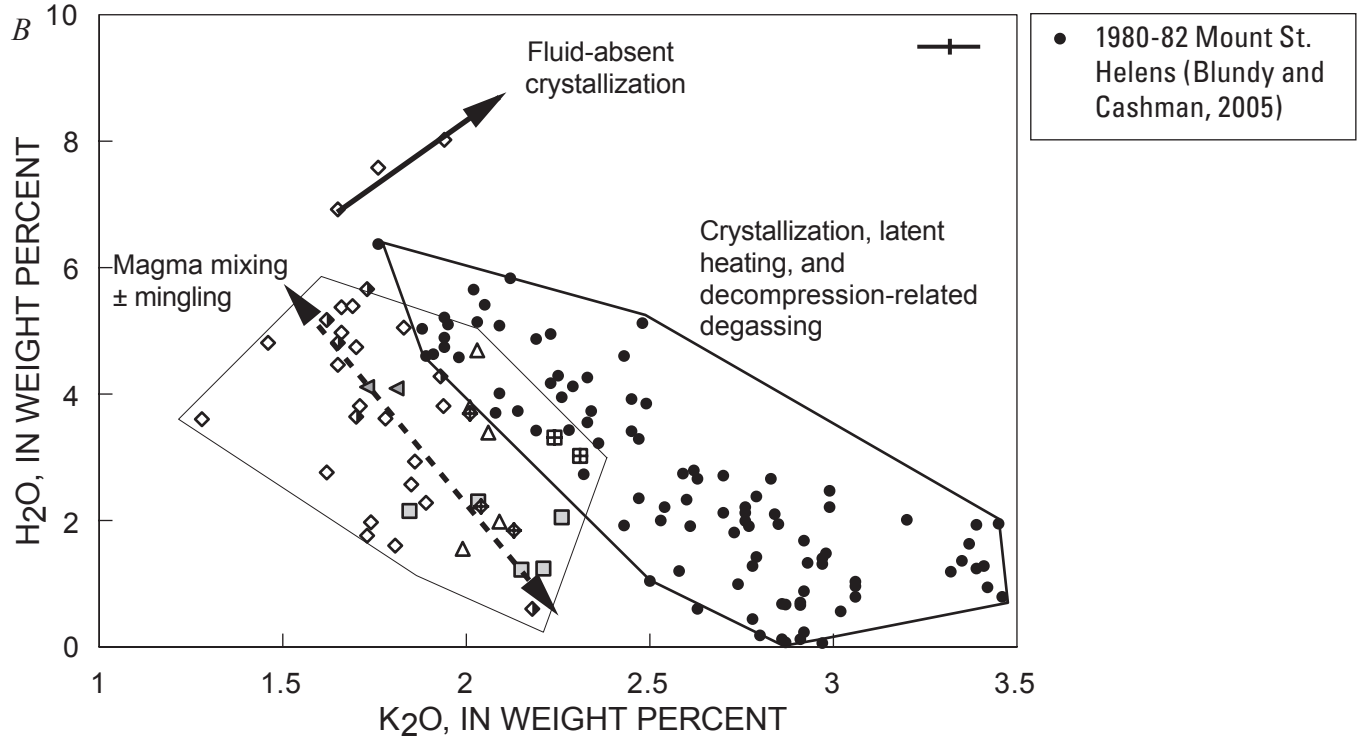

These Mount St. Helens magmas show little textural evidence of magma mixing or mingling which led the authors to note that these processes can account for some common textural features that would otherwise be attributed to preeruptive magma mixing. We conclude that reheating of Augustine magmas, by latent heat release, must also have occurred, but the effects of this process were likely subordinate to reheating caused by magma mixing and/or mingling, given the ample evidence of the latter process.

Sulfur and Chlorine in Augustine Magmas

The S concentrations of most of the rhyodacitic and rhyolitic Augustine melt inclusions are distinctly lower than those of the rehomogenized basaltic-andesite melt inclusions (fig. 3*B*) and the basaltic melt inclusions analyzed by Johnston (1978) and Zimmer and others (2004). These felsic melt inclusions also contain less S than the 0.2 to >0.3 weight percent reported for other subduction-related, calc-alkaline magmas (Anderson, 1982; Wade and others, 2006; Gurenko and others, 2005). The latter concentrations greatly exceed the measured average of 0.02 ± 0.01 weight percent S in all felsic melt inclusions of this study, and these differences indicate that some process of reducing S in the felsic melts occurs in Augustine magmas as they differentiate.

The behavior of S in magmatic systems varies with its oxidation state, and therefore the range in valence states of S in these magmas must be constrained. The 2006 magmas crystallized at f_{O_2} values of approximately NNO+1.5 to NNO+2.5 (fig. 7, table 5; Larsen and others, this volume). This range is similar to the range of circa NNO to NNO+2 reported for prehistoric (Tappen and others, 2009) and 1986 magmas (Roman and others, 2006). At these elevated values of f_{O_2}, the majority of sulfur present would be oxidized to S^{6+} (Carroll and Rutherford, 1988; Mandeville and others, 1998), so the magmatic fluids would contain a mixture of SO_4^{2-}, SO_2, H_2S, and S_2 at shallow crustal pressures (Luhr, 1990; Gerlach and others, 1996; Scaillet and Pichavant, 2003; Jugo and others, 2005; Burgisser and Scaillet, 2007). These theoretical constraints on magmatic $SO_4^{2-}$and SO_2 are compatible with the observation of significant SO_2 concentrations in volcanic vapor of the 2006 eruptive activities (McGee and others, this volume).

Sulfide and sulfate minerals have only rarely been observed at Augustine. For example, Johnston (1978) reported minor sulfides in 1976 rocks, Tappen and others (2009) observed very rare sulfide mineral inclusions in silicate phenocrysts of primitive prehistoric andesites, and anhydrite makes up less than 0.6 volume percent of some 2006 lithologies (Larsen and others, this volume). The presence of these crystalline phases during the early stages of evolution of the relatively primitive magmas, as evidenced by the depletion of S in the less-evolved melt inclusions (fig. 3*B*), would tend to deplete the S abundances of subsequent, residual melts. In fact, if pyrrhotite is included in the fluid-absent crystallization modeling, it would require 1 weight percent sulfide crystallization to generate a rhyolitic melt with only 200 ppm S (that is, a value that is similar to

◀ **Figure 8.** Plots of the relation between H_2O and K_2O in 45 silicate melt inclusions from 2006, 1986, and prehistoric rock samples from Augustine Volcano, Alaska. *A*, The enveloped area (fine, solid polygon) suggests that the K_2O concentrations correlate with H_2O for the data set, but melt inclusions from individual samples may variably reflect a variety of processes. (Trend A) The bold arrow quantitatively defines the influence of polybaric, 20 weight percent crystallization of Augustine felsic melt containing 6.9 and 1.65 wt. percent H_2O and K_2O, respectively, and is consistent with the three most H_2O-enriched melt inclusions that are also inconsistent with the other inclusions. (Trend B) The dotted arrow reflects the consequences of complete, open-system degassing of H_2O with no crystallization. (Trend C) The length of this dot-dash arrow quantitatively reflects the effect of 25 wt. percent crystallization of magma containing 4 wt. percent exsolved aqueous fluid during magma ascent and polybaric decompression. (Trend D) These melt inclusions also reflect consequences of mixing and/or mingling of multiple magmas, and the dashed arrow represents the differentiation of residual rhyolitic melts by mixing of relatively hydrous and Na_2O-, K_2O-, and Cl-deficient magma with relatively anhydrous magma. Mixing apparently occurred during contemporaneous crystallization and fluid exsolution. *B*, The H_2O and K_2O concentrations of silicate melt inclusions (filled circles) from Mount St. Helens eruptions of April, 10, 1980 to March 19, 1982, (Blundy and Cashman, 2005) are included with the Augustine melt inclusion data. Blundy and Cashman (2005) interpret this negative correlation, by the use of associated constraints on melt-plagioclase equilibration temperatures and modeling, to represent the consequences of decompression crystallization of fluid-saturated felsic magmas and the concurrent release of latent heat of crystallization. These Mount St. Helens magmas show little textural evidence of magma mixing or mingling, but they may have undergone loss of H_2O and other volatile components to magmatic vapor as they ascended and decompressed. The extent of crystallization increased, even though these magmas may have been heated by as much as 100°C by latent heating effects, because of the reduction in the fugacities of volatile components as they were sequestered by vapor. Blundy and others (2006) note that these processes can generate textural characteristics similar to those of magma mixing. Given the very similar nature of this relationship to that exhibited by the Augustine melt inclusions, this process may have also played a minor role in the evolution of Augustine magmas. Representative and relative 1-σ precision for glass analyses is shown in upper right corners. See text for discussion.

those of most of the felsic melt inclusions) from the basaltic-andesite melt inclusion compositions which is inconsistent with the lack of sulfide mineral inclusions in other phenocrysts of these rocks.

Mixing of magmas does not appear to be solely responsible for the trends involving S in most of the felsic melt inclusions. The apparent mixing trends expressed by the major constituents CaO, K_2O, and Na_2O (fig. 2) and some minor constituents P_2O_5 and Cl (fig. 3) in these inclusions exhibit strong variability in the abundances of these components as a result of varying degrees of mixing (that is, they show widely varying concentrations along the mixing lines). In contrast, the concentrations of S of the felsic melt inclusions are much more highly focused (that is, much less dispersed) at the average value of 0.01 weight percent, and, hence, they are inconsistent with this process. Mixing must have generated some variability in the mixed products, but other processes were apparently involved as well.

As sulfides are rare and only present in Augustine rocks at abundance levels well below that required to remove significant S from the residual melts and because magma mixing is not solely responsible for the strong reduction in S concentrations with melt evolution, the involvement of a fluid or fluid phases in S sequestration is required. The partition coefficient for S, D_S (weight percent S in fluid/weight percent S in melt) has been determined experimentally to range from approximately 10 to 80, 100 to 300, and 100 to 900 for basaltic (Scaillet and Pichavant, 2003), andesitic (Scaillet and Pichavant, 2003), and rhyodacitic (Botcharnikov and others, 2004) melts, respectively, at pressures of 100 to 300 MPa and temperatures and oxygen fugacities relevant to Augustine magmas (≤1,050°C and f_{O_2} of NNO to NNO+2) (fig. 7; Roman and others, 2006; Tappen and others, 2009). Thus, exsolved aqueous magmatic fluids would be highly efficient in stripping S from melts of the 2006, 1986, and prehistoric Augustine magmas. Importantly, values of D_S increase with reduced pressure (Scaillet and Pichavant, 2003), so the efficiency of this process would increase with the reduction in pressure that accompanies magma ascent. The differentiation of the residual fractions of melt to more felsic compositions would also enhance the efficiency of S sequestration given that D_S is greater for felsic as compared to mafic melts. Moreover, hydrothermal fluids are also capable of dissolving sulfide minerals not trapped as inclusions in other phenocrysts (Reed, 1997); so it is conceivable that any sulfide minerals that may have crystallized relatively early in these magmas were dissolved by fluids during later stages of fluid-saturated magma evolution.

The Cl concentrations of most felsic melt inclusions from the high-silica andesitic to dacitic rocks are variable, and yet, the Cl contents of many of them either equal or exceed those of the more primitive basaltic-andesite melt inclusions (fig. 3*C*). The Cl contents of melt inclusions from low-silica andesites studied are also variable, but in this case most of them are more equivalent to those of the basaltic-andesite melt inclusions (fig. 3*C*). In addition, the Cl concentrations of matrix glasses that we analyzed and those of Wallace and others (this volume) are quite similar to those of the melt inclusions from low-silica andesites. These comparisons indicate that the Cl concentration of some of the felsic melts represented by the melt inclusions from high-silica andesites increased to a limited extent during differentiation, and the trends apparently reflect the varied consequences of magma mixing, fluid(s) exsolution, and fractional crystallization as described below.

The Cl concentrations in the set of melt inclusions that were analyzed by FTIR (and largely represent prehistoric, 1986, and 2006 high-silica andesitic and dacitic rock samples; fig. 9*A*) correlate negatively with H_2O in general, but this is not true for the various subsets of data (distinguished by individual rock samples and stages of eruption) comprising this larger data set. This lack of correlation for melt inclusions from individual samples is the likely result of a variety of magmatic processes, and hence, the larger trend in this figure has been interpreted relative to a series of modeled trends expressing various processes of magma differentiation. For example, some subsets of these data may be consistent with the trend (A) that expresses fluid-absent, isobaric crystallization of 20 weight percent of a rhyolitic melt under closed-system conditions. Alternatively, some of these melt-inclusion data may be consistent with any of several polybaric, closed-system degassing trends that are shown and involve a reduction in pressure of 200 to 50 MPa. These degassing trends include: (B) 20 weight percent crystallization of a rhyolitic melt that is in equilibrium with a fluid containing 2 weight percent Cl (with an average value of D_{Cl} [concentration of Cl in fluid(s)/concentration of Cl in silicate melt] of 10 averaged for changing pressure) or (C) 20 weight percent crystallization of a rhyolitic melt that is in equilibrium with a fluid containing 1 weight percent Cl (with an average value of D_{Cl} of 5 averaged for changing pressure). These values of D_{Cl} are appropriate for this range of felsic melt compositions and this range in pressure (Webster and others, 1999). As magmatic processes do not necessarily occur at equilibrium, figure 9*A* includes a modeled trend (D) for the crystallization and degassing of magma that exsolves a Cl-free aqueous fluid under open-system conditions. Experimental research summarized by Baker and others (2005) demonstrates that H_2O diffuses more quickly than Cl through silicate melts, so (D) addresses magmatic degassing processes in which there is insufficient time for Cl to achieve an equilibrium distribution between melt and fluid(s). Trend D also involves preferential loss of H_2O with no loss of Cl to the fluid, such that the degassing magma has, in effect, a D_{Cl} value of 0, and some of these data appear consistent with this trend. Trend (E) appears more consistent with the larger, integrated data set, and it reflects the consequences of mixing two magmas that contain different H_2O and Cl contents. In summary, given the strong evidence for magma mixing as a dominant process of evolution

of magmas erupted in 2006 and because of the relationships in figures 3C and 8, we suggest that the progressive evolution of late-stage, felsic Augustine melts of the high-silica andesitic magmas involved the mixing and/or mingling of relatively hydrous and K_2O-, Na_2O-, and Cl-deficient rhyolitic melt with relatively anhydrous, K_2O-, Na_2O-, and Cl-enriched rhyolitic melt.

To interpret these processes more fully, it is useful to apply empirically derived and modeled Cl and H_2O solubilities for geologically relevant melt compositions to the melt-inclusion data. Such comparisons provide key constraints on pressures of fluid phase exsolution and on the type of fluid phase(s) that exsolve. The curves in figure 9*B* express the solubilities of H_2O and Cl in rhyolitic melt for 3 pressure conditions, and they represent the exsolution of either a H_2O- ($\pm$ CO_2) bearing vapor phase, a saline liquid, or vapor plus saline liquid as the (Cl/H_2O) ratio of the silicate melt progressively increases. In addition, the 20- and 200-MPa volatile component solubility curves for H_2O-deficient conditions involve a range in Cl concentrations. This range reflects the computed range in maximum Cl solubility for the corresponding range in glass compositions of the melt inclusions (Webster and De Vivo, 2002). It is crucial to account for the range in melt composition because Cl solubility in silicate melts varies strongly with bulk composition (Webster and De Vivo, 2002). These solubility curves also account for the influences of S and pressure on Cl solubility in silicate melts. Specifically, the solubility of Cl in melts that are saturated in S-bearing fluid(s) decreases dramatically with increasing S in the system (Botcharnikov and others, 2004; Webster and others, 2005). Chlorine solubility also decreases with decreasing pressure for silicate melts that are saturated in a saline liquid (Webster and others, 1999).

The compositions of the three, H_2O-enriched prehistoric melt inclusions that contain <0.33 weight percent Cl plot above but near the 200-MPa curve for vapor plus coexisting silicate melt, and hence, they imply pressures of volatile saturation that exceed 200 MPa and that the fluid would have been an aqueous (or potentially aqueous-carbonic) vapor when fluid saturation occurred. Unlike these three, most other melt inclusions are consistent with saturation of Augustine magmas in fluid(s) at lower pressures ranging from 20 to 200 MPa under closed-system conditions, and the latter data are inconsistent with magma storage and evolution at a single pressure (such as within a magma chamber). Interestingly, the compositions of melt inclusions from 2006 samples contain generally lower H_2O concentrations and exhibit larger (Cl/H_2O) ratios than melt inclusions from prehistoric or 1986 tephra. These relationships indicate that (1) the fluid(s) would have exsolved at generally lower pressures than those in the other, older magmas and (2) the compositions of the magmatic fluid phase(s) represented by the melt inclusions from 2006 samples would have been more highly saline. In fact, some aliquots of the fluids at the lower pressures included anhydrous saline liquids.

H_2O and CO_2 in Augustine Magmas

One can derive additional constraints on pressures of melt entrapment, the concentrations of CO_2 and H_2O in magmatic volatile phases, and applicable pressure-composition paths of magma ascent and degassing by comparing the concentrations of H_2O and CO_2 in felsic melt inclusions with experimentally determined and modeled solubilities of H_2O and CO_2 in rhyolite melt (Newman and Lowenstern, 2002; Moore, 2008). However, this procedure does not account for Cl or S species in the fluids. In the following discussion on fluid geochemistry and degassing processes, it must be recognized that the results of comparing the H_2O and CO_2 abundances of melt inclusions with theoretical H_2O and CO_2 solubilities in silicate melts can be interpreted in two ways. One interpretation is that the locations of the melt inclusion data, relative to the isobaric volatile-component solubility curves, determine pressures at which the corresponding aliquots of magma should have saturated in a H_2O- and CO_2-dominated fluid (vapor) phase as magma ascended toward the surface. Alternatively, if independent evidence—that the melt inclusions represent fluid-saturated magma at the time of melt entrapment—is available, then the locations of the melt-inclusion data relative to the isobaric volatile-component solubility curves constrain the pressure of melt inclusion entrapment. Note that the latter approach does not necessarily establish the initial pressures of or the corresponding maximum depths of magmatic volatile-phase exsolution, because the melt represented by a given melt inclusion could have exsolved a volatile phase at depths and pressures greater than those indicated and the melt inclusion simply represents fluid-saturated melt that was trapped in a growing phenocryst at some time well after the stage of initial magmatic fluid exsolution.

To this end, the H_2O and CO_2 abundances of melt inclusions from the 2006 rocks are plotted along with those collected from prehistoric tephra C (AVO 201), G (AVO 205), H (AVO 204), and I (AVO 203) and from several 1986 pumice samples (ours and those of Roman and others, 2006), and the concentrations of these volatile components are compared with the theoretical (Newman and Lowenstern, 2002) isobaric vapor-saturation curves for CO_2- and H_2O-bearing rhyolite melt (figs. 10*A* and 10*B*). This assessment indicates that the aliquots of rhyolite melt represented by most of these melt inclusions would saturate in H_2O- $\pm$ CO_2-bearing fluid(s) at pressures of 20 to 200 MPa. This observation is consistent with that detected previously in plots of H_2O versus Cl in that the Cl, CO_2, and H_2O data are inconsistent with magma storage and evolution at a single pressure (that is, within a magma chamber). It is noteworthy, however, that the compositions of 5 of these melt inclusions imply pressures of fluid phase saturation that exceed 200 MPa and that 1 inclusion indicates pressures that exceed 350 MPa. This is similar to that observed with H_2O versus Cl, and given that the bulk of the melt inclusions from these eruptions of Augustine Volcano provide roughly similar pressure estimates based on plots

A

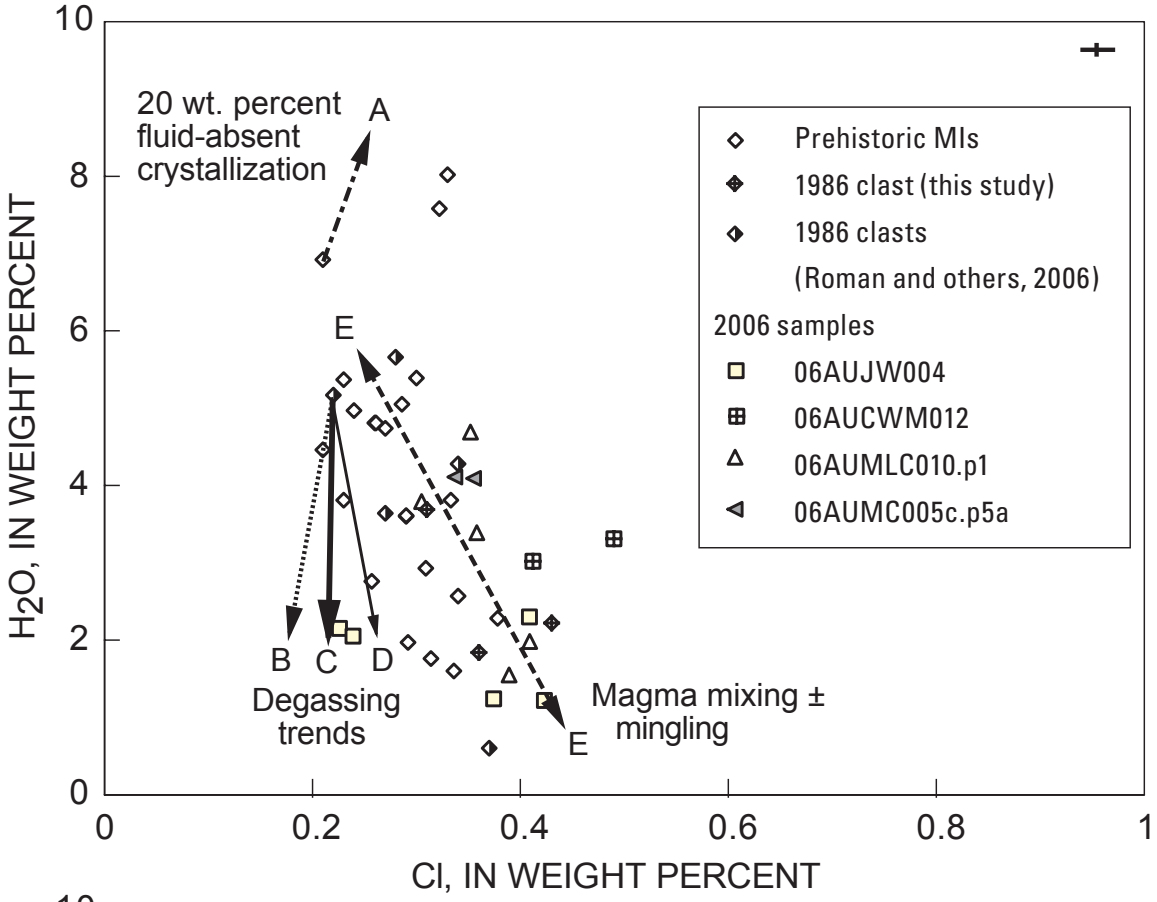
20 wt. percent
fluid-absent
crystallization
A
E
B
C
D
Degassing
trends
Magma mixing ±
mingling
E
Prehistoric MIs
1986 clast (this study)
1986 clasts
(Roman and others, 2006)
2006 samples
06AUJW004
06AUCWM012
06AUMLC010.p1
06AUMC005c.p5a
H2O, IN WEIGHT PERCENT
Cl, IN WEIGHT PERCENT
0
2
4
6
8
10
0
0.2
0.4
0.6
0.8
1

B

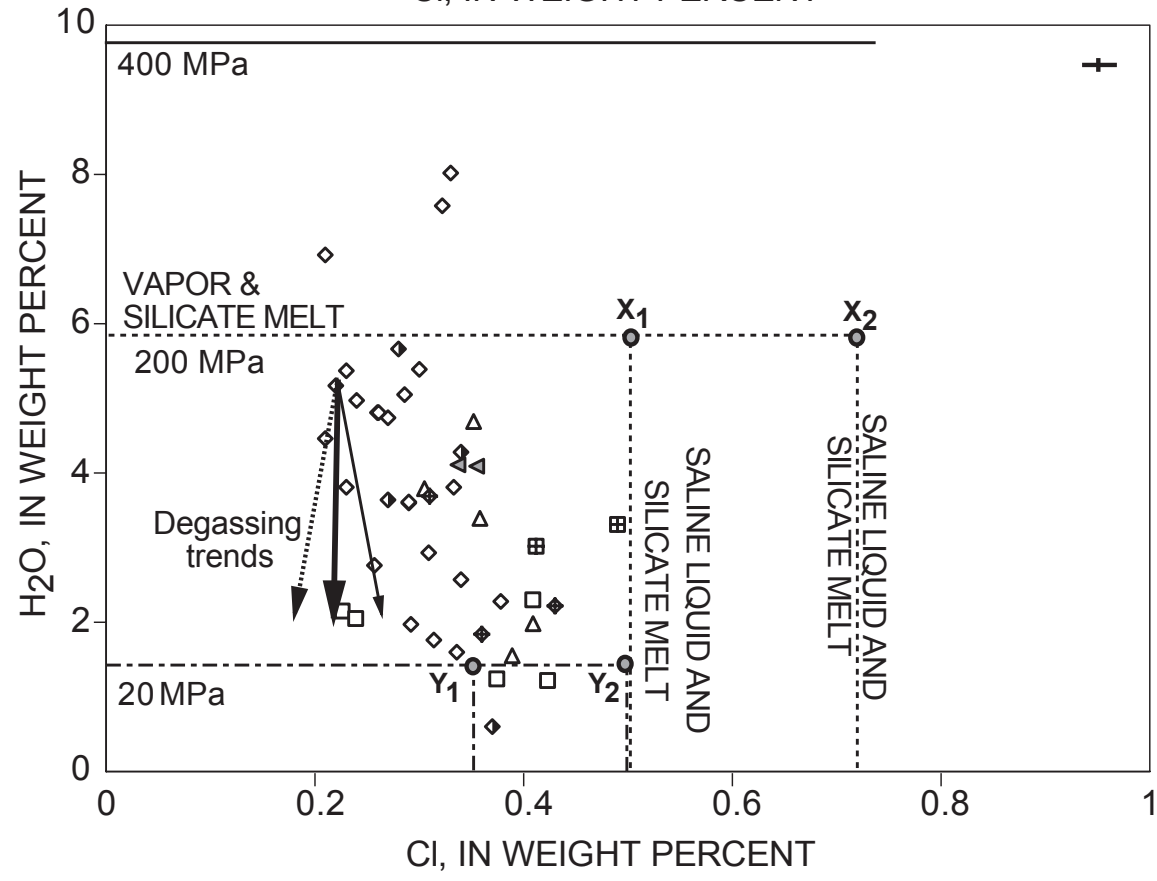
400 MPa
VAPOR &
SILICATE MELT
200 MPa
20 MPa
X1
X2
Y1
Y2
Degassing
trends
SALINE LIQUID AND
SILICATE MELT
SALINE LIQUID AND
SILICATE MELT
H2O, IN WEIGHT PERCENT
Cl, IN WEIGHT PERCENT
0
2
4
6
8
10
0
0.2
0.4
0.6
0.8
1

involving two pseudo-ternary systems, we interpret this agreement to indicate that most of these melt inclusions represent magma that was fluid saturated at the time of entrapment and, therefore, that pre-eruptive saturation of Augustine magmas in fluid(s) was a common process.

The comparison of the melt-inclusion compositions with the volatile solubility curves indicates that many felsic fractions of Augustine magma would have coexisted with volatile phases comparatively enriched in H_2O over CO_2 (fig. 10*A*). In fact, the H_2O content of the fluid(s), not accounting for the influence of Cl and S, was ≥95 mole percent for most aliquots of 2006 and prehistoric magmas and ≥ 85 mole percent for most fractions of 1986 magma.

To establish potential pressure-composition paths of magma ascent and degassing for the recent Augustine magmas, we relate the melt-inclusion data to a series of theoretical curves that express the reduction in H_2O and CO_2 concentrations of residual rhyolitic melt in evolving magmas as they ascend from depths equivalent to pressures of ≥ 350 MPa (fig. 10*B*). The 2006 and prehistoric data are most consistent with the rise of magmas containing 1 weight percent of H_2O-enriched vapor under closed-system conditions. This modeled curve is based on initial conditions involving a fluid-saturated magma at 950°C and approximately 400 MPa; the rhyolitic melt in this magma contains 9.5 weight percent H_2O and 100 ppm CO_2 at the initiation of fluid-saturated ascent and crystallization. Of particular importance is that the pressures estimated from H_2O and CO_2 in melt inclusions in 2006 samples range from 150 to 20 MPa only. This pressure range is consistent with crystallization of 2006 magma from the depths indicated by geodetic measurements (that is, for magma storage at 4 to 6 km) up to depths near the surface (Cervelli and others, this volume). The melt inclusions from 1986 tephra are more compatible with the rise of a fluid-saturated magma that contains 3 weight percent of H_2O-enriched vapor under closed-system conditions; the rhyolitic melt contains 7 weight percent H_2O and 500 ppm CO_2 as it passes through the depth equivalent to 350 MPa. In both cases, the vapor-saturated magmas are assumed to be crystallizing at 950°C while at a depth of 14 km (about 350 MPa).

These magmatic fluids were stable in the presence of melt at pressures ranging from 350 MPa to values <20 MPa. This range of pressure corresponds to depths of magmatic degassing that extend over the range of 14 km to 800 m, and, clearly, degassing must have continued at more shallow conditions (that is, as magma ascended and breached the volcanic edifice). Moreover, the modeling based on relationships involving H_2O and CO_2 is consistent with closed-system magma ascent as polybaric crystallization and degassing progressed, and the computed initial mass of fluids, which ranges from 1 to 3 weight percent and represents minimum fluid quantities, is consistent with prior work on other calc-alkaline, subduction-related magmatic systems (Wallace and Anderson, 2000; Scaillet and Pichavant, 2003; Wallace, 2005).

◀ **Figure 9.** Plots of the relation between H_2O and Cl in 45 silicate melt inclusions from Augustine Volcano samples including prehistoric rocks (open diamonds; Tappen and others, 2009), 1986 tephra sample 86E-63-2 of Roman and others (2006) (diamonds filled on right side), our 1986 tephra (gridded diamonds), low-silica andesitic sample 06AUJW004 (open squares), and high-silica andesitic samples 06AUCWM012 (gridded squares) and 06AUMC010.p1 (upward-pointing triangles). *A,* Melt-inclusion compositions are compared with trends describing: (A, dot-dash arrow) the result of 20 weight percent isobaric crystallization of fluid-absent rhyolitic melt on H_2O and Cl concentrations of residual melt; (B) polybaric, 20 wt. percent crystallization and exsolution of 4 weight percent aqueous fluid (with an average fluid/melt D_{Cl} = 10); (C) polybaric, 20 weight percent crystallization and exsolution of 4 weight percent Cl-bearing aqueous fluid (with average D_{Cl} = 5); (D) 20 weight percent polybaric crystallization and exsolution of 4 weight percent H_2O and no loss of Cl to fluid (i.e., with D_{Cl} = 0); and (trend E) mixing and/or mingling of H_2O-enriched and Na_2O-, K_2O-, and Cl-deficient magma with H_2O-deficient magma. *B,* Melt inclusion data are plotted relative to modeled solubilities of H_2O in H_2O-rich vapor-saturated rhyolite melt at 400 (solid curve), 200 (dashed curve), and 20 (dot-dash curve) MPa and 900°C (after Newman and Lowenstern, 2002), and Cl solubility in rhyolitic melts saturated in Cl-rich, H_2O-poor saline liquid (after Webster and De Vivo, 2002; Webster and others, 1999; 2005). At X_1 and X_2 (200 MPa), and at Y_1 and Y_2 (20 MPa), silicate melt coexists with vapor plus saline liquid. The 20- and 200-MPa volatile component solubility curves for H_2O-deficient conditions involve a range in Cl concentrations. The differences in Cl concentration between X_2-X_1 and Y_2-Y_1 reflect the computed ranges in maximum Cl solubility for the corresponding range in composition for this set of melt inclusions for two pressure conditions (Webster and De Vivo, 2002). The curves also account for the influences of sulfur (Webster and others, 2005; Botcharnikov and others, 2004) and pressure (Webster and others, 1999) on Cl solubility in silicate melts. These data, in conjunction with observations of figure 3B, indicate that at relatively higher pressures >200 MPa the dominant fluid phase coexisting with residual fractions of silicate melt was H_2O- and (potentially CO_2-) enriched vapor; whereas with magma ascent to lower pressures (approaching 20 MPa) the dominant magmatic fluid phase coexisting with evolving silicate melt was saline Cl- (and presumably S-) enriched liquid. Representative and relative 1-σ precision for glass analyses is shown in upper right corners. See text for discussion.

A

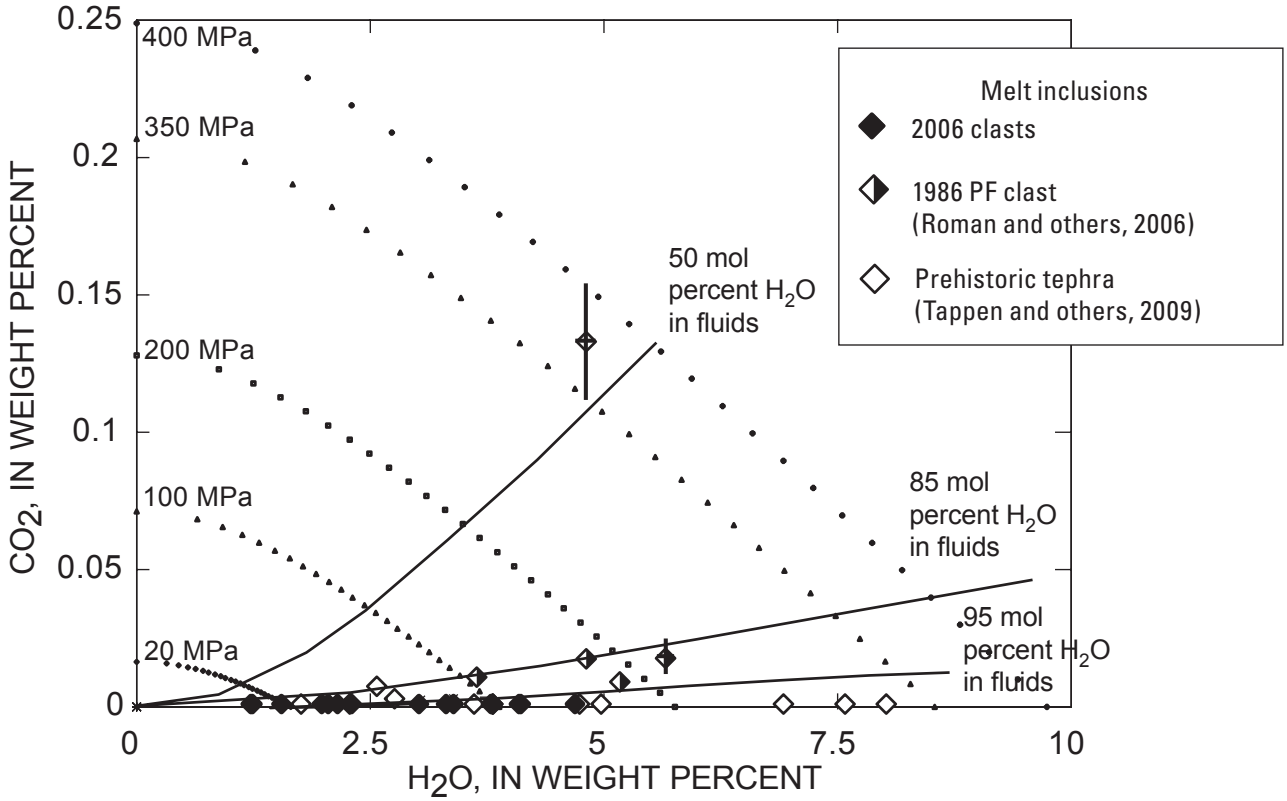
0.25
0.2
0.15
0.1
0.05
0
400 MPa
350 MPa
200 MPa
100 MPa
20 MPa
50 mol percent H_2O in fluids
85 mol percent H_2O in fluids
95 mol percent H_2O in fluids
Melt inclusions
2006 clasts
1986 PF clast (Roman and others, 2006)
Prehistoric tephra (Tappen and others, 2009)
CO_2, IN WEIGHT PERCENT
0
2.5
5
7.5
10
H_2O, IN WEIGHT PERCENT

B

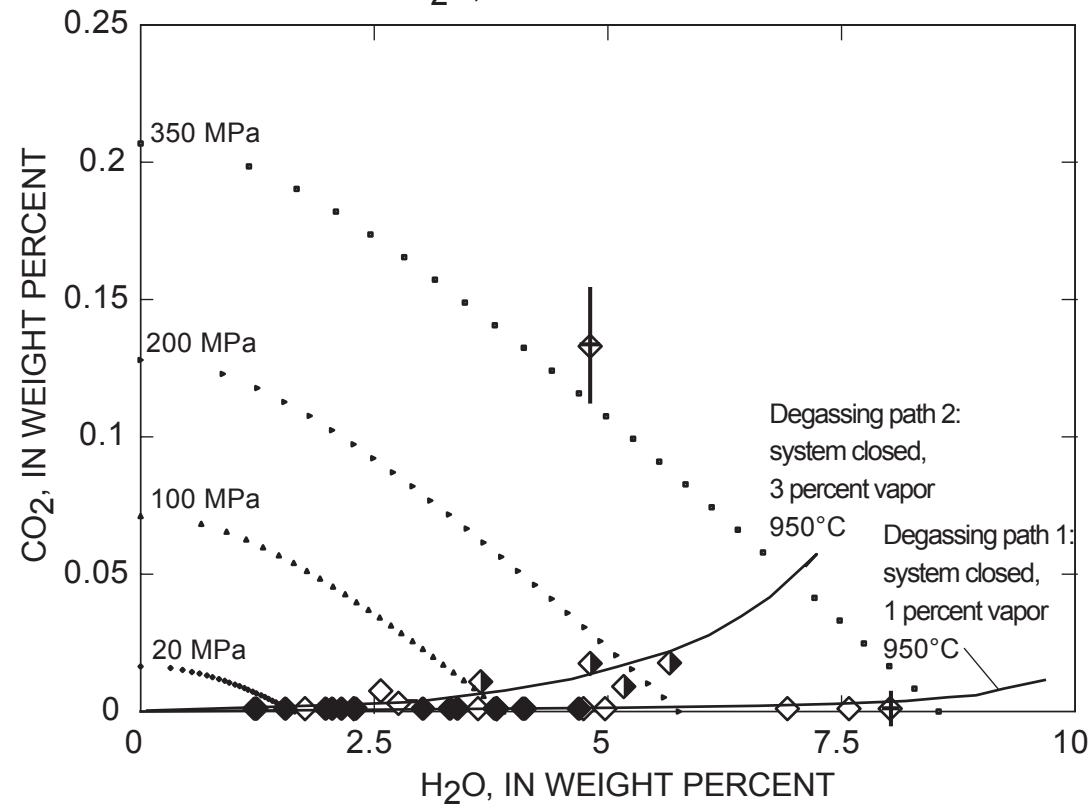
0.25
0.2
0.15
0.1
0.05
0
350 MPa
200 MPa
100 MPa
20 MPa
Degassing path 2: system closed, 3 percent vapor 950°C
Degassing path 1: system closed, 1 percent vapor 950°C
CO_2, IN WEIGHT PERCENT
0
2.5
5
7.5
10
H_2O, IN WEIGHT PERCENT

Developing a Model for the Behavior of Fluid Phase(s) During Magma Ascent and Differentiation

The relationships involving H_2O, CO_2, Cl, and S in the integrated melt-inclusion data reveal that the 2006, 1986, and prehistoric magmas contained one or more fluid phases before eruption, which is consistent with the results of prior research on 1976 (Johnston, 1978) and 1986 (Roman and others, 2006) magmas. These data also indicate that volatile components were sequestered by magmatic fluids as magma mixing ± mingling and fractional crystallization occurred, and that the fluids were stable through an extended pressure range and depth of magma ascent. In this developing model, we focus primarily on shallow-crustal processes influencing magmas after the ascent of hot, volatile-enriched basaltic magma into the crust and after this mafic magma mixed (our mixing event 1) with other more-evolved magma that was residing in the Augustine conduit and reservoir system. This involvement of relatively hot basaltic magma likely represents a potential eruption-triggering mechanism, because of the input of additional thermal energy and volatile components by the basaltic magma (Larsen and others, this volume). Thus, we focus on the potential role of fluids that were present (1) after mixing event 1 (fig. 2) and (2) during and subsequent to mixing event 2 (fig. 2). This treatment is relevant to the 2006 and older eruptions.

The integration of phenocryst and melt-inclusion compositional data demonstrates that these magmas behaved as quasi-closed systems, with regard to volatile component escape, until the magmas reached very shallow crustal depths (that is, ≤800 m). The compositions and rim textures of amphiboles, for example, provide relevant constraints on depths of crystallization and rates of magma ascent, respectively. Comparison of the compositions of 2006 Augustine amphiboles with those grown during hydrothermal experiments on similar bulk compositions at pressure, temperature and f_{O_2} conditions pertinent to Augustine magmas allows us to constrain the more narrow range of magmatic conditions that bear on amphibole crystallization in these magmas. Experimental work on amphibole stability in Mount St. Helens dacite at 850 to 940°C and 70 to 260 MPa (Rutherford and Devine, 2008) indicates that amphiboles contain ≤11 weight percent Al_2O_3 if crystallized below 200 MPa (fig. 11). This is a result of the fact that the Al content of amphiboles is largely dependent on the pressure-sensitive Al-Tschermak [^{M}(Mg,Fe)+ ^{T}Si = ^{M}Al + ^{T}Al], temperature-dependent edenite [^{T}Si +^{A}vacancy = ^{T}Al + ^{A}(Na,K)], and Ti-Tschermak [2^{T}Ti + ^{M}Mn =2^{T}Al +^{M}Ti] substitution mechanisms. In related work, Moore and Carmichael (1998) conducted hydrothermal experiments involving calc-alkaline andesites and basaltic andesites from western Mexico that are strikingly similar in bulk composition and intrinsic f_{O_2} to the 2006 Augustine low-silica and high-silica andesites. Amphiboles generated in experiments on the calc-alkaline andesite at 101 to 285 MPa, 900 to 975°C, and log f_{O_2} of NNO +2 contain ≥10 weight percent Al_2O_3 and ≥15.6 weight percent MgO (fig. 11). In contrast, most Augustine 2006 amphiboles with similar MgO contents contain ≤9.5 weight percent Al_2O_3. In addition, amphibole was not stable in Moore and Carmichael's (1998) calc-alkaline andesite experiments at temperatures >970°C. Amphiboles in Moore and Carmichael's (1998) experiments on the basaltic andesite contain ≥11.9 weight percent Al_2O_3 and >16.0 weight percent MgO at 950° to 1,000°C and 222 to 303 MPa. Interestingly however, most Augustine 2006 amphiboles contain <16 weight percent MgO (as well as Al_2O_3 contents ≤9.5 weight percent; fig. 11), so it is likely that Augustine amphiboles crystallized at pressures <170 MPa, and the rarity of amphiboles also indicates that these magmas passed through the low-pressure portion of the amphibole stability field (~130 to 170 MPa) rapidly. In addition, the lack of decompression-driven reaction rims on many of these amphiboles may indicate rapid magma ascent from depths of 4 to 5 km (Rutherford and Hill, 1993) and/or lack of favorable reaction kinetics for amphibole breakdown (Browne and Gardner, 2006). Interestingly, one of the 2006 amphiboles analyzed (table 6) exhibits an ~ 7-fold increase in F content from core to rim, and Rutherford and Devine (2008) observed similar variations of F concentration in amphiboles from the 2004-2006 dacite of Mount St. Helens. The latter study

◀ **Figure 10.** Plots of the relation between CO_2 and H_2O in 35 silicate melt inclusions from 2006, 1986, and prehistoric Augustine Volcano rock samples; symbols same as in figure 4. *A*, Data are plotted relative to isopleths for compositions of fluids in equilibrium with rhyolitic melts (calculated using model of Newman and Lowenstern, 2002), with fluids ranging from 95 mole percent H_2O (and 5 mole percent CO_2) to 50 mole percent H_2O (and 50 mole percent CO_2). Most melt inclusions are consistent with fluids in 1986 magma(s) containing ≤15 mole percent CO_2 and 85 mole percent H_2O, and many melt inclusions from the 2006 and prehistoric samples indicate that those batches of magma represented by these samples contained only trace CO_2 and so the fluids were CO_2-deficient. *B,* Data are plotted relative to a calculated closed-system degassing paths (using Newman and Lowenstern, 2002). Degassing path 1 applies to rhyolite melt initially saturated with 1 wt. percent vapor containing ≥95 mole percent H_2O at 950°C; this path (and these conditions) are consistent with evolution of fluid-saturated 2006 magmas. Path 2 applies to rhyolite melt initially saturated with 3 weight percent vapor containing approximately 85 mole percent H_2O at 950°C. Estimated values for 1-σ precision for CO_2 and H_2O in glasses are shown as vertical and horizontal lines for two representative high- and low-CO_2 melt inclusions. See text for discussion.

demonstrated that these changes in F content near the rim preceded the formation of reaction rim products, and it attributed this feature to amphiboles that were not within the amphibole stability field during magma ascent.

As part of our working model, we suggest that some of the 2006 and 1986 melt inclusions from high-silica andesites (that is, those of mixing trend 2, fig. 2) represent aliquots of younger felsic magma that interacted with older felsic magma while passing through the volcanic conduit at shallow crustal levels. Indeed, it is clear that some of these melt inclusions reflect shallow pressures of entrapment (due to their low volatile component abundances) while also showing other geochemical differences that reflect varying stages of evolution resulting from mixing and fractional crystallization. Thus, some of these mixing/mingling processes occurred within the conduit system. This interpretation is consistent with the conclusion of Roman and others (2006) that some 1986 magma formed via differentiation within the dike network that comprises the volcanic conduit and not within a magma chamber. It is also compatible with the bulk geochemistry of the two felsic end-member type magmas that are consistent with mixing trend 2 (fig. 2).

Given these constraints on magma composition, what can one establish about the compositions of the dominant fluids involved? It has been demonstrated that some fractions of the 2006, 1986, 1976, and prehistoric magmas contained a Cl-bearing aqueous vapor and other fractions contained Cl-rich saline liquid. In this regard, the results of prior experimental and theoretical research indicate that Cl-bearing magmas, and Cl-enriched magmas in particular, may also contain two fluids (Cl-bearing aqueous or aqueous-carbonic vapor plus saline liquid) at the shallow crustal pressures and magmatic temperatures characterizing volcanic conduits (Shinohara, 1994; Webster and Mandeville, 2007). In such systems, HCl is the dominant chloride species in volcanic vapors at surface or near-surface pressures (Giggenbach, 1996; 1997; Edmonds and others, 2002), which is consistent with prior study of Augustine's volcanic emanations indicating that it releases H_2O-dominated vapors containing significant HCl (Symonds and others, 1990). Conversely, alkali chlorides and alkaline earth chlorides are the dominant Cl-bearing species in coexisting magmatic saline liquids (Giggenbach, 1995). It follows that magmatic vapor and saline liquid should tend to separate from one another because of their strongly differing densities. The vapor will tend to

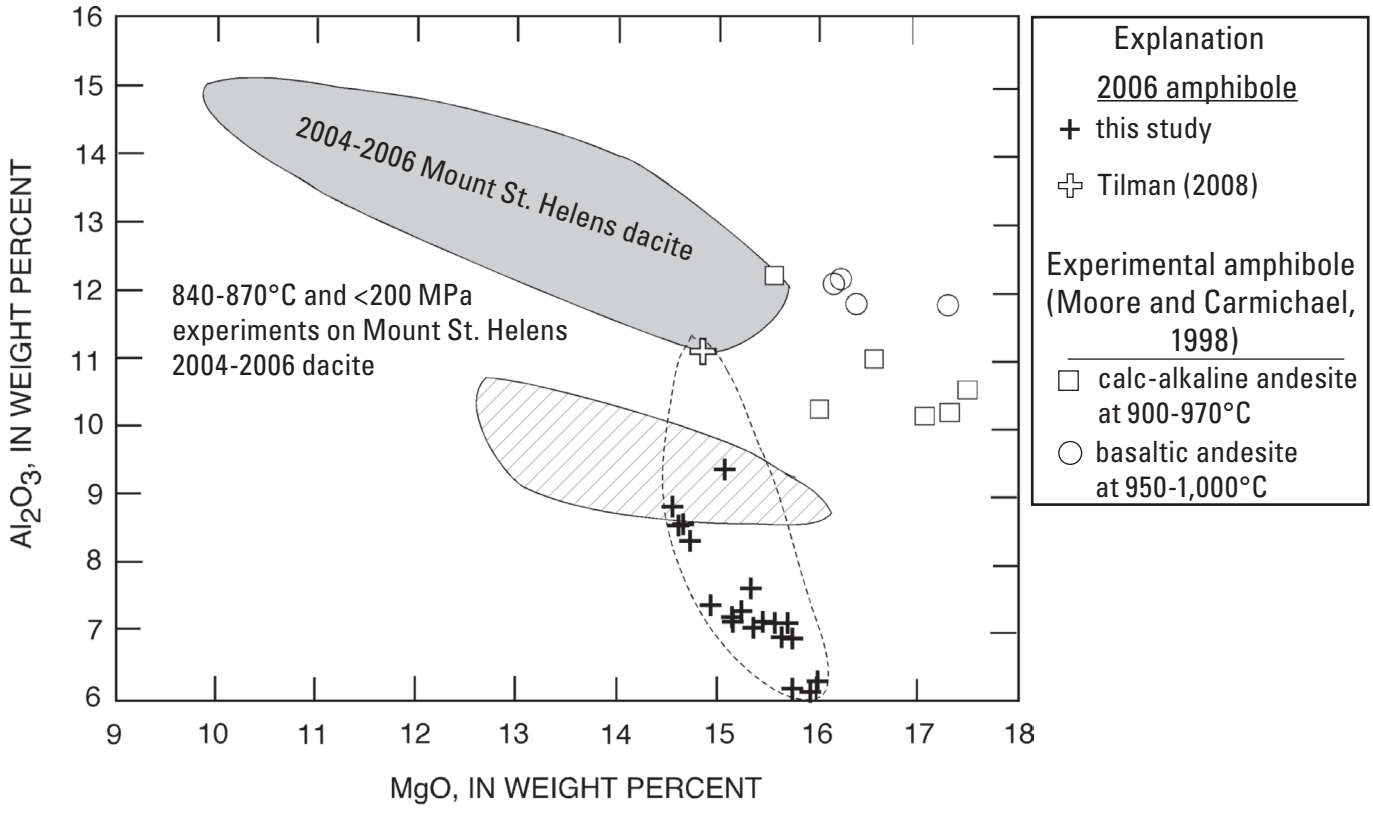

Figure 11. Plot of the relation between the concentrations of Al_2O_3 and MgO in amphiboles of Augustine Volcano rock samples compared to other natural and experimental amphibole compositions. Natural and experimental amphibole compositions from Mount St. Helens 2004–6 dacite from Rutherford and Devine (2008). Data from relatively rare Augustine 2006 amphiboles indicate they crystallized in the lower-pressure region of the amphibole stability field (~130 to 170 MPa).

ascend more rapidly through magma, and the saline liquid may either collect within a stratified "dryout" zone or horizon (Henley and McNabb, 1978) in the conduit (Hardee, 1982; Shmulovich and Churakov, 1998) or it may slowly ascend through the magma because its density is roughly half that of the encompassing silicate melt. In this regard, molten salt was observed flowing from fissures in the Vesuvius crater in the first decade following the 1944 eruption (Chiodini and others, 2001). Moreover, recent experimental studies have determined high solubilities of SO_4^{2-} in alkali chloride-enriched hydrothermal fluids at the pressures relevant to volcanism (Newton and Manning, 2005; Webster and others, 2007). Thus, the relatively oxidizing magmatic fluids at Augustine likely included H_2O-enriched and HCl-, H_2S-, S_2-, and SO_2- ± CO_2-bearing vapors; hydrosaline aqueous liquids largely enriched in Cl^-, SO_4^{2-}, alkalis, and H_2O; to moderately saline, H_2O-poor liquids containing Cl^-, SO_4^{2-}, and alkali elements.

The fluids at Augustine may also have played a significant role in the differentiation of evolved magma passing through shallowly located dikes. For example, one mechanism of forming a partially degassed and relatively anhydrous end-member melt composition that retains relatively high Cl contents during differentiation, that is, one similar to that involved in mixing/mingling at Augustine, involves the exsolution and loss of a saline liquid from felsic magma at low pressures. This is supported by close inspection of the volatile-component solubility relationships for H_2O and Cl that demonstrate that some fractions of felsic Augustine melt, represented by the most Cl-rich and H_2O-deficient melt inclusions, could exsolve a highly saline liquid (with or without coexisting vapor) and still contain moderate concentrations of H_2O at 20 MPa (at or near Y_1 and Y_2 in fig. 9*B*). This observation is a consequence of the strong deviations from ideal mixing behavior that occur in NaCl- and H_2O-bearing systems containing a saline liquid with or without vapor (Webster, 1992; Shinohara, 1994; Botcharnikov and others, 2004), and it is consistent with the modeled results of degassing trends B and C (fig. 9*A*). Even though the saline liquid is enriched in Cl, the exsolution of this phase does not reduce the Cl content of the melt significantly, because the activities of H_2O and chloride species are buffered at constant values in all phases present at equilibrium in a closed system (Shinohara, 1994; Webster and Mandeville, 2007). Thus, the subsequent separation and escape of a saline liquid from melt reduces the H_2O concentrations of the residual silicate melt, while maintaining elevated Cl levels in the melt.

Determining the origin of the low-K_2O end-member melt composition involved in mixing trend 2 is more of a challenge. It is difficult to envision how fractional crystallization could generate felsic melt compositions with such low K_2O concentrations like these without crystallizing alkali feldspar, which these rocks do not contain. This K_2O-enriched phase would have to have fractionated in significant quantities to generate the low K_2O values. Larsen and others (this volume) suggest that the low-K_2O matrix glasses may have formed by melting of low-K_2O, fine-grained gabbroic cumulate material, which follows the interpretation of Harris (1994) that mafic magma of the 1986 eruption mixed with magma residual from the 1976 eruption and also with low-K_2O, partially crystallized chamber residua. We suggest that the comparatively low concentrations of K, Na, Fe, S, and Cl in the melt inclusions representing this end-member composition are consistent with their mobilization in a fluid phase. Moreover, the elevated H_2O concentrations of this second "type" melt require that this style of fluid exsolution must have occurred at pressures greater than those bearing on the formation of the other end-member melt (for example, 100 to 200 MPa) because of the strong, positive relationship between pressure and water solubility in silicate melts. Experiments have demonstrated that the interaction of silicate melt with an HCl-bearing aqueous vapor tends to strip alkalis and Cl from the melt; in fact, some experiments have generated peraluminous melt compositions through the interaction of HCl-enriched vapors with melts that were initially subaluminous to metaluminous (Webster and Holloway, 1988; Williams and others, 1997; Frank and others, 2003). As discussed, the components in the vapor exsolved from Augustine magmas included HCl. Thus, it is plausible that the interaction of rhyolitic melt with HCl-bearing aqueous vapor at pressures of 100 to 200 MPa could have generated the observed geochemical characteristics of this second magma-mixing end member.

Relationships Involving Volatile Components, Fluids, and Eruptive Processes

Magma differentiation strongly influences volcanic activity, because the rate and style of eruptions vary directly with magma rheology, melt viscosity, and the concentrations of volatile components in late-stage magma as well as with temperature and pressure. Most melt inclusions chosen for this study represent silica-enriched residual melts with widely varying H_2O and Cl concentrations, and these parameters variably influence the viscosity of differentiated and fluid-saturated residual melts. We suggest that as the aliquots of younger and more hydrous felsic magma, which were variably depleted in Cl, Na_2O, K_2O, and FeO, ascended through the conduit system, they interacted at shallow depths with older and less hydrous felsic magma that had previously lost H_2O via degassing. The latter magma contained elevated concentrations of Cl, Na_2O, K_2O, and FeO that are more typical of evolved rhyolitic melts. The interaction of these magmas involved the exchange of heat as well as volatile components which played a critical role in subsequent eruptive processes.

Relationships involving H_2O, Cl, and CO_2 in some felsic melt inclusions, interpreted through experimental data from the corresponding melt-H_2O-CO_2 and melt-H_2O-Cl pseudoternaries provide independent indications (1) that the exsolution of fluid(s) from residual melt occurred at depths ≤14 km (that is, equivalent to approximately 350 MPa), (2) of the entrapment of fluid(s)-saturated melt at pressures as low as 20 MPa, and hence (3) that Augustine's magmatic volatile phase(s) remained in equilibrium with the rhyolitic melts to depths of ≤800 m (that is, that closed-system behavior was

maintained to quite shallow depths). Combination of these constraints with the observed lack of rimming or alteration of some amphibole phenocrysts (that crystallized in the 170 to 130 MPa range) suggests that the final ascent of amphibole-bearing magmas was also rapid.

It is noteworthy that before the 2006 eruption, precursory unrest in the form of increased seismicity, inflation, and pressurization at sea level began in mid-2005 (Cervelli and others, 2006; Power and Lalla, this volume). Similarly, seismic hypocenters preceding the 1986 eruption began to ascend from depths of 600 m to the crater just nine months before that eruptive phase began (Power, 1988; Roman, 2001; Power and Lalla, this volume), and similar seismic behavior was also observed before the 1976 eruption (Kienle, 1987). These seismic activities have been interpreted to signal hydraulic fracturing of overlying rock as magma (that is, fluid) pressure increased (Roman, 2001). This interpretation is consistent with observations from a similar study in which magmatic gas movement at Redoubt Volcano was called on as the source of some of its shallow seismic activity (Wolf and Eichelberger, 1997). We suggest these signals may also indicate that the fluid overpressures in Augustine magmas (with apparent fluid abundances of 1 to 3 weight percent) exceeded the confining rock strength and that they are indications of the separation of fluid(s) from magma at depths of 800 m or less. Augustine's crater rim is approximately 1.2 km in elevation, which means that some fluid-melt separation took place above sea level and well within the edifice. Interestingly, related modeling of the 2006 events by Coombs and others (this volume), based on average volumes of erupted material per explosion and the estimated conduit dimensions, determines that each Vulcanian explosion involved evacuation of the conduit to a depth of 1.9 km below the summit. In addition, they estimate an average evacuation depth, during eruptions, of 1 km. Thus, it is well supported that the separation and ascent of magmatic fluid at these quite shallow depths may have generated some of the recorded seismic behavior, while opening pathways for subsequent magma ascent.

Acknowledgments

We sincerely thank the staff of the Alaska Volcano Observatory for their considerable support and assistance during fieldwork on Augustine Island, and for subsequent collaborative assistance. We thank Dr. Richard B. Waitt of the USGS for providing the basalt sample (RBW-91A-137) and Dr. Chris Nye of the Alaska Division of Geological and Geophysical Surveys for sharing trace-element data for 6 Augustine basalt samples. Dr. George Harlow kindly shared his mineral recalculation program PRBDATNT. We thank Professor Jessica Larsen and Mariah Tilman of the University of Alaska at Fairbanks for providing data on amphiboles of 2006 rock samples. John Pallister, John Power, and Bruno Scaillet kindly provided detailed and thoughtful reviews of the manuscript. This research was supported by National Science Foundation award EAR-0308866 to J.D. Webster.

References Cited

Anderson, A.T., Jr., 1976, Magma mixing—petrological process and volcanological tool: Journal of Volcanology and Geothermal Research, v. 1, p. 3–33.

Anderson, A.T., Jr., 1982, Parental basalts in subduction zones—implications for continental evolution: Journal of Volcanology and Geothermal Research, v. 87, p. 7047–7060.

Anderson, A.T., Jr., 2003, An introduction to melt (glass ± crystals) inclusions, chap. 14 *in* Samson, I., Anderson, A., and Marshall, D., eds., Fluid inclusions—analysis and interpretation: Mineralogical Association of Canada, v. 32, p. 353–364.

Andersen, D.J., Lindsley, D.H., and Davidson, P.M., 1993, QUILF—A program to assess equilibria among Fe-Mg-Ti oxides, pyroxenes, olivine, and quartz: Computers and Geosciences, v. 19, p. 1333–1350.

Atlas, Z.D., Dixon, J.E., Sen, G., Finny, M., Pozzo, A.L.M.-D., 2006, Melt inclusions from Volcán Popocatépetl and Volcán de Colima, Mexico—Melt evolution due to vapor-saturated crystallization during ascent: Journal of Volcanology and Geothermal Research, v. 153, p. 221–240.

Bacon, C.R., and Hirshmann, M.M., 1988, Mg/Mn partitioning as a test for equilibrium between coexisting Fe-Ti oxides: American Mineralogist, v. 73, p. 57–61.

Bacon, C.R., Newman, S., and Stolper, D., 1992, Water, CO_2, Cl, and F in melt inclusions in phenocrysts from three Holocene explosive eruptions, Crater Lake, Oregon: American Mineralogist, v. 77, p. 1021–1030.

Baker, D.R., Freda, C., Brooker, R.A., and Scarlato, P., 2005, Volatile diffusion in silicate melts and its effects on melt inclusions: Annals of Geophysics, v. 48, p. 699–717.

Blundy, J., and Cashman, K., 2001, Ascent-driven crystallization of dacite magmas at Mount St. Helens, 1980-1986: Contributions to Mineralogy and Petrology, v. 140, p. 631–650.

Blundy, J., and Cashman, K., 2005, Rapid decompression-driven crystallization recorded by melt inclusions from Mount St. Helens volcano: Geology, v. 33, p. 793–796.

Blundy, J., Cashman, K., and Humphreys, M., 2006, Magma heating by decompression-driven crystallization beneath andesitic volcanoes: Nature, v. 443, p. 76–809.

Bodnar, R.J., and Student, J.J., 2006, Melt inclusions in plutonic rocks: petrography and microthermometry. chap. 1 *in* Webster, J., ed., Melt inclusions in plutonic rocks: Mineralogical Association of Canada v. 36, p. 165–188.

Botcharnikov, R.E., Behrens, H., Holtz, F., Koepke, J., and Sato, H., 2004, Sulfur and chlorine solubility in Mt. Unzen rhyodacitic melt at 850°C and 200 MPa: Chemical Geology, v. 213, p. 207–225.

Browne, B.L., and Gardner, J.E., 2006, The influence of magma ascent path on the texture, mineralogy, and formation of hornblende reaction rims: Earth and Planetary Science Letters, v. 246, p. 161–176.

Browne, B.L., Eichelberger, J.C., Patino, L.C., Vogel, T.A., Uto, K., and Hoshizumi, H., 2006, Magma mingling as indicated by texture and Sr/Ba ratios of plagioclase phenocrysts from Unzen volcano, SW Japan: Journal of Volcanology and Geothermal Research, v. 154, p. 103–116.

Burgisser, A., and Scaillet, B., 2007, Redox evolution of a degassing magma rising to the surface: Nature, v. 445, p. 194–197.

Carmichael, I.S., Turner, I., and Verhoogen, J., 1974. Igneous Petrology: McGraw-Hill, 739 p.

Carroll, M.R., and Rutherford, M.J., 1988, Sulfur speciation in hydrous experimental glasses of varying oxygen state—results from measured wavelength shifts of sulfur X-rays. American Mineralogist, v. 73, p. 845–849.

Cervelli, P.F., Fournier, T.J., Freymueller, J., and Power, J.A., 2006, Ground deformation associated with the precursory unrest and early phases of the January 2006 eruption of Augustine Volcano, Alaska: Geophysical Research Letters, v. 33, 5 p., doi: 10.1029/2006GL027219.

Cervelli, P.F., Fournier, T.J., Freymueller, J.T., Power, J.A., Lisowski, M., and Pauk, B.A., 2010, Geodetic constraints on magma movement and withdrawal during the 2006 eruption of Augustine Volcano, *in* Power, J.A., Coombs, M.L., and Freymueller, J.T., eds., The 2006 eruption of Augustine Volcano, Alaska: U.S. Geological Survey Professional Paper 1769 (this volume).

Chiodini, G., Marini, L., and Russo, M., 2001, Geochemical evidences of high-temperature hydrothermal brines at Vesuvio Volcano (Italy): Geochimica et Cosmochimica Acta, v. 65, p. 2129–2147.

Chou, I.-M., 1978, Calibration of oxygen buffers at elevated P and T using the hydrogen fugacity sensor: American Mineralogist, v. 63, p. 690–703.

Coombs, M.L., Bull, K.F., Vallance, J.W., Schneider, D.J., Thoms, E.E., Wessels, R.L., and McGimsey, R.G., 2010, Timing, distribution, and volume of proximal products of the 2006 eruption of Augustine Volcano, *in* Power, J.A., Coombs, M.L., and Freymueller, J.T., eds., The 2006 eruption of Augustine Volcano, Alaska: U.S. Geological Survey Professional Paper 1769 (this volume).

Daley, E.E., 1986. Petrology, geochemistry, and the evolution of magmas from Mt. St. Augustine volcano, Alaska: unpublished M.S. thesis, University of Alaska, Fairbanks, 106 p.

Danyushevsky, L.V., Della-Pasqua, F.N., and Sokolov, S., 2000, Re-equilibration of melt inclusions trapped by magnesian olivine phenocrysts from subduction-related magmas—petrological implications: Contributions to Mineralogy and Petrology, v. 138, p. 68–83.

Edmonds, M., Pyle, D., and Oppenheimer, C., 2002, HCl emissions at Soufriére Hills Volcano, Montserrat, West Indies, during a second phase of dome building: November 1999 to October 2000: Bulletin of Volcanology, v. 64, p. 21–30.

Evans, B.W., Scaillet, B., and Kuehner, S.M., 2006, Experimental determination of coexisting iron–titanium oxides in the systems FeTiAlO, FeTiAlMgO, FeTiAlMnO, and FeTiAlMgMnO at 800 and 900° C, 1–4 kbar, and relatively high oxygen fugacity: Contributions to Mineralogy and Petrology, v. 152, p. 149–167.

Frank, M.R., Candela, P.A., and Piccoli, P.M., 2003, Alkali exchange equilibria between a silicate melt and coexisting magmatic volatile phase—an experimental study at 800ºC and 100 MPa. Geochimica et Cosmochimica Acta, v. 67, p. 1415–1427.

Gerlach, T.M., Westrich, H.R., and Symonds, R.B., 1996, Preeruption vapor in magma of the climactic Mount Pinatubo eruption—source of the giant stratospheric sulfur dioxide cloud, *in* Newhall, C.G., and Punongbayan, R.S., eds., Fire and mud—eruptions and lahars of Mount Pinatubo, Philippines: PHIVOLCS and University of Washington Press, p. 415–433.

Giggenbach, W.R., 1997, The origin and evolution of fluids in magmatic-hydrothermal systems, chap. 15 *in* Barnes, H.L., ed., Geochemistry of hydrothermal ore deposits 3rd ed.: John Wiley and Sons Inc. New York, p. 737–796.

Giggenbach, W.R., 1996, Chemical composition of volcanic gases, *in* Scarpa, R., and Tilling, R., eds., Monitoring and mitigation of volcano hazards: Springer Berlin, p. 221–256

Giggenbach, W.R., 1995, Composition of magmatic components in hydrothermal fluids, chap. 11 *in* Thompson, J.F.H., ed., Magmas, fluids, and ore deposits, vol. 23: Mineralogical Association of Canada, p. 247–261.

Gurenko, A.A., Belousov, A.B., Trumbull, R.B., Sobolev, A.V., 2005, Explosive basaltic volcanism of the Chikurachki volcano (Kurile arc, Russia)—insights on pre-eruptive magmatic conditions and volatile budget revealed from phenocryst-hosted melt inclusions and groundmass glasses: Journal of Volcanology and Geothermal Research, v. 147, p. 203–232.

Hardee, H.C., 1982, Permeable convection above magma bodies: Tectonophysics, v. 84, p. 179–195.

Harlow, G.E., Murphy, A.R., Hozjan, D.J., de Mille, C.N., and Levinson, A.A., 2006, Pre-Columbian jadeite axes from Antigua, West Indies—description and possible sources: Canadian Mineralogist, v. 44, p. 305–321.

Harris, G., 1994. The petrology and petrography of lava from the 1986 eruption of Augustine volcano: University of Alaska, Fairbanks, unpub. M.S. thesis, 131 p.

Hawthorne, F.C., and Oberti, R., 2007, Classification of amphiboles: Reviews in Mineralogy and Geochemistry, v. 67, p. 55–88.

Henley, R.W., and McNabb, A., 1978, Magmatic vapor plumes and ground-water interaction in porphyry copper emplacement: Economic Geology, v. 73, p. 1–20.

Huebner, J.S., and Sato, M., 1970, The oxygen fugacity-temperature relationships of manganese oxide and nickel oxide buffers: American Mineralogist, v. 55, p. 934–952.

Izbekov, P., Wallace, K., Larsen, J., Nye, C., and Eichelberger, J., 2006, Variations of glass composition at the start of the 2006 eruption, Augustine Volcano, Alaska [abs.]: Geological Society of America Abstracts with Programs, v. 38, no. 5, p. 76–77.

Johnson, K.E., 1986, Isotope geochemistry of Augustine volcano, Alaska: Southern Methodist University, unpub. M.S. thesis, 144 p.

Johnson, K.E., Harmon, R.S., Richardson, J.M., Moorbath, S., and Strong, D.F., 1996, Isotope and trace-element geochemistry of Mt. St. Augustine volcano, Alaska—implications for magmatic evolution: Journal of Petrology, v. 37, p. 95–115.

Johnson, M.C., and Rutherford, M.J., 1989, Experimental calibration of the aluminum-in-magnesio-hornblende geobarometer with application to Long Valley caldera (California) volcanic rocks: Geology, v. 17, p. 837–841.

Johnston, D.A., 1978, Volatiles, magma mixing, and the mechanism of eruption of Mt. St. Augustine Volcano, Alaska: Seattle, Washington, University of Washington, unpub. Ph.D. dissertation, 177 p.

Johnston, D.A., 1979, Onset of volcanism at Mt. St. Augustine Volcano, Lower Cook Inlet: U.S. Geological Survey Circular 804-B, 78–80.

Jugo, P.J., Luth, R.W., and Richards, J.P., 2005, An experimental study of the sulfur content in basaltic melts saturated with immiscible sulfide or sulfate liquids at 1300°C and 1.0 GPa: Journal of Petrology, v. 46, p.783–798.

Kienle, J., 1987, Mt. St. Augustine works, but how?: Proceedings, Hawaii Symposium on How Volcanoes Work, p. 139.

Kienle, J., and Forbes, R.B., 1976, Augustine—evolution of a volcano: Geophysics Institute, University of Alaska Fairbanks, Annual Report 1975/76, p. 26–48.

Kienle, J., and Swanson, S.E., 1980, Volcanic hazards from future eruptions of Mt. St. Augustine volcano, Alaska: Geophysics Institute, University of Alaska, Fairbanks, Report UAG R-275, 122 p.

Larsen, J.F., Nye, C.J., Coombs, M.L., Tilman, M., Izbekov, P., and Cameron, C., 2010, Petrology and geochemistry of the 2006 eruption of Augustine Volcano, *in* Power, J.A., Coombs, M.L., and Freymueller, J.T., eds., The 2006 eruption of Augustine Volcano, Alaska: U.S. Geological Survey Professional Paper 1769 (this volume).

Lattard, D., Sauerzapf, U., and Kasemann, M., 2005, New calibration data for the Fe-Ti oxide thermo-oxybarometers from experiments in the Fe-Ti-O system at 1 bar, 1,000–1,300ºC and a large range of oxygen fugacities: Contributions to Mineralogy and Petrology, v. 149, p. 735–754.

Leake, B.E., 1997, Nomenclature of amphiboles; Report of the Subcommittee on Amphiboles of the International Mineralogical Association Commission on New Minerals and Mineral Names: American Mineralogist, v. 82, p. 1019–1037.

Le Bas, M.J., Le Maitre, R.W., Streckeisen, A., and Zanettin, B., 1986, A chemical classification of volcanic rocks based on the total alkali-silica diagram: Journal of Petrology, v. 27, p. 745–750.

Lowenstern, J.B., 1995, Applications of silicate-melt inclusions to the study of magmatic volatiles. chap. 4 *in* Thompson, J.F.H., ed., Magmas, fluids, and ore deposits: Mineralogical Association of Canada, v. 23, p. 71–99.

Luhr, J.F., 1990, Experimental phase relations of water-and sulfur-saturated arc magmas and the 1982 eruptions of El Chichon Volcano: Journal of Petrology, v. 31, p. 1071–1114.

Mandeville, C.W., A. Sasaki, G. Saito, K. Faure, R. King and E. Hauri, 1998, Open-system degassing of sulfur from Krakatau 1883 magma: Earth and Planetary Science Letter*s*, v. 160, no. 3/4, p. 709–722.

Mandeville, C.W., Webster, J.D., Rutherford, M.J., Taylor, B.E., Timbal, A., and Faure, K., 2002, Determination of molar absorptivities for infrared absorption bands of H_2O in andesitic glasses: American Mineralogist, v. 87, p. 813–821.

Massare, D., Métrich, N., Clocchiatti, R., 2002, High-temperature experiments on silicate melt inclusions in olivine at 1 atm—inference on temperatures of homogenization and H_2O concentrations: Chemical Geology, v. 183, p. 87–98.

McGee, K.A., Doukas, M.P., McGimsey, R.G., Neal, C.A., and Wessels, R.L., 2010, Emission of SO_2, CO_2, and H_2S from Augustine Volcano, 2002–2008, *in* Power, J.A., Coombs, M.L., and Freymueller, J.T., eds., The 2006 eruption of Augustine Volcano, Alaska: U.S. Geological Survey Professional Paper 1769 (this volume).

Moore, G., 2008, Interpreting H_2O and CO_2 contents in melt inclusions—constraints from solubility experiments and modeling, chap. 9 *in* Putirka, K.D, and Tepley III, F.J., eds., Minerals, inclusions,, and volcanic processes: Reviews in Mineralogy and Geochemistry, v. 69, p. 333–361.

Moore, G., and Carmichael, I.S.E., 1998, The hydrous phase equilibria (to 3 kbar) of an andesite and basaltic andesite from western Mexico—constraints on water content and conditions of phenocryst growth: Contributions to Mineralogy and Petrology, v. 130, p. 304–319.

Newman, S., and Lowenstern, J.B., 2002, VOLATILECALC—a silicate melt-H_2O-CO_2 solution model written in

Visual Basic for excel: Computers and Geosciences, v. 28, p. 597–604.

Newman, S., Bacon, C.R., and Stolper, E., 1986, Measurement of water in rhyolitic glass—calibration of an infrared spectroscopic technique: American Mineralogist, v. 71, p. 1527–1541.

Newton, R.C., and Manning, C.E., 2005, Solubility of anhydrite, $CaSO_4$, in NaCl-H_2O solutions at high pressures and temperatures: Journal of Petrology, v. 46, p. 701–716.

Nye, C.J., 2006, The 2006 eruption of Augustine Volcano—overview [abs.]: Geological Society of America Abstracts with Programs, v.38, no. 5, p. 28.

Power, J.A., 1988, Seismicity associated with the 1986 eruption of Augustine Volcano, Alaska: University of Alaska, Fairbanks, unpub. Ph.D. dissertation, 142 p.

Power, J.A., Nye, C.J., Coombs, M.L., Wessels, R.L., Cervelli, P.F., Dehn, J., Wallace, K.L., Freymueller, J.T., and Doukas, M.P., 2006, The reawakening of Alaska's Augustine Volcano: Eos (American Geophysical Union Transactions), v. 87, no. 37, p. 373–377.

Power, J.A., and Lalla, D.J., 2010, Seismic observations of Augustine Volcano, 1970–2007, *in* Power, J.A., Coombs, M.L., and Freymueller, J.T., eds., The 2006 eruption of Augustine Volcano, Alaska: U.S. Geological Survey Professional Paper 1769 (this volume).

Reed, M.H., 1997, Hydrothermal alteration and its relationship to ore fluid composition. chap. 7 *in* Barnes, H.L., ed., Geochemistry of hydrothermal ore deposits, 3rd ed: John Wiley and Sons, p. 303–365.

Roedder, E., 1984, Fluid inclusions: Reviews in Mineralogy and Geochemistry, v. 12, 644 p.

Roman, D.C., 2001, The 1986 eruption of Mt. St. Augustine Volcano, Alaska—magma storage and ascent. The University of Oregon unpub. Ph.D. dissertation, 129 p.

Roman, D.C., Cashman, K.V., Gardner, C.A., Wallace, P.J., and Donovan, J.J., 2006, Storage and interaction of compositionally heterogeneous magmas from the 1986 eruption of Mt. St. Augustine Volcano, Alaska: Bulletin of Volcanology, v. 68, p. 240–254.

Rutherford, M.J., and Devine, J.D., III, 1996, Preeruption pressure-temperature conditions and volatiles in the 1991 dacitic magma of Mount Pinatubo, *in* Newhall, C.G., and Punongbayan, R.S., eds., Fire and Mud—Eruptions and lahars of Mount Pinatubo, Philippines: Seattle, University of Washington Press, p. 751–766.

Rutherford, M.J., and Devine, J.D., III, 2008, Magmatic conditions and processes in the storage zone of the 2004-2006 Mount St. Helens dacite, chap. 31 *in* Sherrod, D.R., Scott, W.E., and Stauffer, P.H., eds., A volcano rekindled—the renewed eruption of Mount St. Helens, 2004–2006: U.S. Geological Survey Professional Paper 1750.

Rutherford, M.J., and Hill, P.M., 1993, Magma ascent rates from amphibole breakdown—an experimental study applied to the 1980–1986 Mt. St. Helens eruptions: Journal of Geophysical Research, v. 93, p. 19,667–19,685.

Scaillet, B., and Pichavant, M., 2003, Experimental constraints on volatile abundances in arc magmas and their implications for degassing processes, chap. 2, *in* Oppenheimer, C., Pyle, D.M., and Barclay, J., eds., Volcanic degassing: Geological Society of London Special Publication, v. 213, p. 23–52.

Shinohara, H., 1994, Exsolution of immiscible vapor and liquid phases from a crystallizing silicate melt—implications for chlorine and metal transport: Geochimica et Cosmochimica Acta, v. 58, p. 5215–5221.

Shmulovich, K.I., and Churakov, S.V., 1998, Natural fluid phases at high temperatures and low pressures: Journal of Geochemical Exploration, v. 62, p. 183–191.

Stormer, J.C., 1983, The effects of recalculation on estimates of temperature and oxygen fugacity from analyses of multicomponent iron-titanium oxides: American Mineralogist, v. 68, p. 586–594.

Straub, S.M., and Layne, G.D., 2003, The systematics of chlorine, fluorine, and water in Izu arc front volcanic rocks—implications for volatile recycling in subduction zones: Geochimica et Cosmochimica Acta, v. 67, no. 21, p. 4179–4203.

Sun, S.-S., and McDonough, W.F., 1995, The composition of the Earth: Chemical Geology, v. 120, p. 223–253.

Symonds, R.B., Rose, W.I., Gerlach, T.M., Briggs, P.H., and Harmon, R.S., 1990, Evaluation of gases, condensates, and SO_2 emissions from Augustine volcano, Alaska—the degassing of a Cl-rich volcanic system: Bulletin of Volcanology, v. 52, p. 355–374.

Tappen, C., Webster, J.D., Mandeville, C.W., and Roderick, D., 2009, Petrology and geochemistry of ca. 2100–1000 a.B.P. magmas of Augustine Volcano, Alaska, based on analysis of prehistoric pumiceous tephra: Journal of Volcanology and Geothermal Research, v. 183, p. 42–62.

Tilman, M.R., 2008, An investigation of symplectite-rimmed olivine and magmatic processes during the 2006 eruption of Augustine Volcano, Alaska: University of Alaska, Fairbanks, unpub. M.S. thesis, 166 p.

Vallance, J.W., Bull, K.F., and Coombs, M.L., 2010, Pyroclastic flows, lahars, and mixed avalanches generated during the 2006 eruption of Augustine Volcano, *in* Power, J.A., Coombs, M.L., and Freymueller, J.T., eds., The 2006 eruption of Augustine Volcano, Alaska: U.S. Geological Survey Professional Paper 1769 (this volume).

Wade, J.A., Boudon, G., Nougrigat, S., Poteaux, S., and Michel, A., 2006, The volatile content of magmas from Arenal volcano, Costa Rica: Journal of Volcanology and Geothermal Research, v. 157, p. 94–120.

Waitt, R.B., and Begét, J.E., 2009, Volcanic processes and geology of Augustine Volcano, Alaska. USGS Professional Paper 1762, 78 p., 2 map plates [http://pubs.usgs.gov/pp/1762/].

Wallace, K.L., Neal, C.A., and McGimsey, R.G., 2010, Timing, distribution, and character of tephra fall from the 2005–2006 eruption of Augustine Volcano, *in* Power, J.A., Coombs, M.L., and Freymueller, J.T., eds., The 2006 eruption of Augustine Volcano, Alaska: U.S. Geological Survey Professional Paper 1769 (this volume).

Wallace, P.J., 2005, Volatiles in subduction zone magmas—concentrations and fluxes based on melt inclusion and volcanic gas data: Journal of Volcanology and Geothermal Research, v. 140, p. 217–240.

Wallace, P.J., and Anderson, A.T., Jr., 2000, Volatiles in magma, *in* Sigurdsson, H., ed., Encyclopedia of volcanoes: Academic Press, San Diego, p. 149–170.

Waythomas, C.F., and Waitt, R.B., 1998, Preliminary volcano-hazard assessment for Augustine volcano, Alaska: U.S. Geological Survey Open-File Report 98-106, 39 p.

Webster, J.D., 1992, Fluid-melt interactions involving Cl-rich granites—experimental study from 2 to 8 kbar: Geochimica et Cosmochimica Acta, v. 56, p. 679–687.

Webster, J.D., and DeVivo, B., 2002, Experimental and modeled solubilities of chlorine in aluminosilicate melts, consequences of magma evolution, and implications for exsolution of hydrous chloride melt at Mt. Somma-Vesuvius: American Mineralogist, v. 87, p. 1046–1061.

Webster, J.D., and Holloway, J.R., 1988, Experimental constraints on the partitioning of Cl between topaz rhyolite melt and H_2O and $H_2O + CO_2$ fluids—new implications for granitic differentiation and ore deposition: Geochimica et Cosmochimica Acta, v. 52, p. 2091–2105.

Webster, J.D., and Mandeville, C.W., 2007, Fluid immiscibility in volcanic environments, chap. 10 *in* Leibscher, A., Heinrich, C., eds., Fluid-fluid equilibria in the crust: Reviews in Mineralogy and Geochemistry, v. 65, p. 313–362.

Webster, J.D., Kinzler, R.J., and Mathez, E.A., 1999, Chloride and water solubility in basalt and andesite liquids and implications for magmatic degassing: Geochimica et Cosmochimica Acta, v. 63, p. 729–738.

Webster, J.D., Sintoni, M.F., and De Vivo, B., 2005, The role of sulfur in promoting magmatic degassing and volcanic eruption at Mt. Somma-Vesuvius, *in* De Vivo, B., ed., Volcanism in the Campania Plain—Vesuvius, Campi Flegrei and Ignimbrites: Elsevier, Developments in Volcanology, v. 9, p. 221–236.

Webster, J.D., Sintoni, M.F., De Vivo, B., Lima, A., 2007, Volatile solubilities in Mt. Somma-Vesuvius phonolite melt and new insights on degassing of sulfur, chlorine, and water [abs.]: Eos (American Geophysical Union Transactions), v. 88, V42B-03.

Webster, J.D., Mandeville, C.W., Gerard, T., Goldoff, B., and Coombs, M.L., 2006. Volatile abundances and magma geochemistry of recent (2006) through ancient eruptions (< 2100 a BP) of Augustine Volcano, Alaska [abs.]: Eos (American Geophysical Union Transactions), v. 87, V42B-05.

Williams, T.J., Candela, P.A., and Piccoli, P.M., 1997, Hydrogen-alkali exchange between silicate melts and two-phase aqueous mixtures—an experimental investigation: Contributions to Mineralogy and Petrology, v. 128, p. 114–126.

Wolf, K.J., and Eichelberger, J.C., 1997, Syneruptive mixing, degassing and crystallization at Redoubt Volcano, eruption of December, 1989 to May 1990: Journal of Volcanology and Geothermal Research, v. 75, p. 19–37.

Zimmer, M.M., Plank, T., Hauri, E.H., Faust Larsen, J., and Kelemen, P.B., 2004, Volatile contents in mafic magmas from two Aleutian volcanoes—Mts. St. Augustine and Makushin [abs.]: Eos (American Geophysical Union Transactions), v. 85 no. 46, V34A-01.

Appendix 1. Sample Descriptions

2006 Samples

06AUMC005C.p5a Low-silica andesite scoria. Petrographic description: the sample is a vesicular, porphyritic andesite with brownish felty matrix contains areas of trace glass and many microlites. Plagioclase shows remelting/reequilibration growth zones containing orthopyroxene needles and melt inclusions. Melt inclusions are pink to dark brown in color. Plagioclase phenocrysts show complex and variable growth zoning; some contain growth zones with dusty dark groundmass material entrained. Orthopyroxene and clinopyroxene phenocrysts are subequal in abundance. Pyroxenes do not appear, in general, to be as zoned as the plagioclase phenocrysts do but pyroxenes do show more incipient oxidation/alteration. Some glomerocrystic clots contain plagioclase, pyroxenes, and iron-titanium oxides. Minor embayed and altered olivine phenocrysts. Coexisting oxides (ilmenite and magnetite) occur in matrix and phenocrysts; ilmenite is typically rimmed by magnetite with no visible exsolution textures; 0.025 to 0.6 mm diameter for coexisting oxides. No amphibole or quartz observed. No anhydrite observed.

06AUMC008b.p1A Low-silica andesite scoria. Petrographic description: the sample is a porphyritic andesite with a plagioclase- and oxide-microlite-rich, brownish, felty groundmass. Plagioclase is dominant phenocryst; some show oscillatory zoning. Others have sieve-textured cores and others show dusty groundmass material in growth zones. Melt inclusions occur in some plagioclase remelting/reequilibration/growth zones; melt inclusions somewhat less abundant than in other 2006 samples. Plagioclase phenocrysts are as much as 2. 5 mm in length. Clinopyroxene phenocrysts more abundant than orthopyroxene phenocrysts. Orthopyroxene phenocrysts up to 1.2 mm in length. Some orthopyroxene rimmed by clinopyroxene. Some complex glomeroporphyritic clots have oxides, plagioclase, and pyroxenes. Several volume percent euhedral, some unaltered olivine phenocrysts (up to 2 mm in diameter). Olivine also present as microlites in groundmass. Minor amphibole; some unaltered but others show alteration. Coexisting oxides (ilmenite and magnetite) occur in matrix and phenocrysts; ilmenite is typically rimmed by magnetite with no visible exsolution textures; 0.025 to 0.6 mm diameter for coexisting oxides. No quartz observed.

06AUMC010p1 High-silica andesite. Petrographic description: the sample is a porphyritic andesite that contains plagioclase as dominant phenocryst. Many plagioclase phenocrysts appear skeletal with other mineral inclusions partially entrained in the skeletal plagioclase. Smaller plagioclase laths and glass shards appear aligned. Plagioclase phenocrysts show complex zoning and growth history; oscillatory zoning, remelting/re-equilibration/growth zones with melt inclusions. Other plagioclase phenocrysts appear quite clean of inclusions. Plagioclase phenocrysts up to 4.5 mm in length. Melt inclusions in plagioclase are relatively abundant and pink to brown in color. Orthopyroxene phenocrysts less abundant than clinopyroxene phenocrysts; some orthopyroxene appears replaced by clinopyroxene. Pyroxenes show less zoning than plagioclase, but some pyroxenes show oxidation. Orthopyroxene and clinopyroxene phenocrysts up to 1 mm in length. Minor olivine phenocrysts present. Coexisting oxides (ilmenite and magnetite) occur in matrix and phenocrysts; ilmenite is typically rimmed by magnetite with no visible exsolution textures; 0.025 to 0.15 mm diameter for coexisting oxides. We observed no amphibole. No quartz observed.

06AUCWM007 Low-silica andesite scoria. Petrographic description: porphyritic andesite with phenocryst abundances listed in order of decreasing modal abundance. Plagioclase is subhedral to euhedral and occurs as crystals 0.2 to 1.7 mm in diameter and also as glomeroporphyritic crystal clots in association with orthopyroxene, clinopyroxene, and Fe-Ti oxides. Some plagioclase phenocrysts contain melt inclusions in remelting/reequilibration growth zones and many other plagioclase phenocrysts contain dusty matrix-enriched growth zones. Orthopyroxene occurs as subhedral to euhedral phenocrysts from 0.1 to 0.6 mm in diameter and as part of glomeroporphyritic crystal clots in association with plagioclase, clinopyroxene, and Fe-Ti oxides. Orthopyroxene is more abundant than clinopyroxene phenocrysts by an approximate ratio of 2:1, and is also present in the groundmass glass as fine needles. Clinopyroxene occurs as phenocrysts from 0.1 to 0.3 mm in diam. and also as glomerocrysts in glomeroporphyritic crystal clots in association with plagioclase, orthopyroxene, and Fe-Ti oxides. Some orthopyroxene undergoing replacement by clinopyroxene. Titanomagnetite and ilmenite occur as phenocrysts ranging from 0.03 to 0.2 mm and present also in glomeroporphyritic crystal clots. There are touching oxide pairs in contact with matrix glass that exhibit no exsolution lamellae and these should be good for preeruptive temperature- f_{O_2} estimates. One very rare pyroxene-rimmed olivine grain was observed.

Groundmass glass is clear in color with abundant microlites of clinopyroxene, orthopyroxene, plagioclase, and oxides. Rough volumetric proportion of vesicularity 45 to 50 percent based on blue epoxy. Note no amphibole observed in thin section, however, 1 amphibole was handpicked from crushed rock crystal concentrate. No visible quartz.

06AUCWM012 High-silica andesite. Petrographic description: Porphyritic andesite with phenocrysts in order of decreasing abundance: plagioclase occurs as large subhedral to euhedral crystals from 0.2 to 2.0 mm. Plagioclase also present as glomerocrysts. Many contain good glassy melt inclusions in plagioclase. Some plagioclase phenocrysts contain melt inclusions in remelting/ reequilibration growth zones and many other plagioclase phenocrysts contain dusty matrix-enriched growth zones. Orthopyroxene occurs as subhedral to euhedral crystals up to 1.0 mm and as part of glomeroporphyritic crystal clots. Orthopyroxene is more abundant than clinopyroxene by less than 2:1 (maybe 60/40). Orthopyroxene also contains good melt inclusions. Clinopyroxene occurs as subhedral to euhedral crystals from 0.2 to 0.7 mm and also in glomeroporphyritic clots associated with orthopyroxene, plagioclase, and Fe-Ti oxides. Pyroxenes show less zoning than plagioclase. Titanomagnetite and ilmenite occur as phenocrysts from 0.05 to 0.2 mm in diameter. Many touching oxide pairs in contact with glass with no exsolution lamellae that are good for temperature and oxygen fugacity estimation. Three amphibole grains were found in two thin sections and have the following occurrences: one small subhedral-embayed grain that has no reaction rim and is clean up to contact with matrix glass; one large 0.7 mm grain rimmed by pyroxene; one small amphibole inclusion in plagioclase. Groundmass glass is clear (rhyolitic) and in many areas is microlite-free and forms either thin stringers and wisps to more massive-texured glass near phenocryst clots. Despite high phenocryst abundance, matrix glass is highly vesiculated. No visible quartz.

06AUCWM014 Dense low-silica andesite. Petrographic description: Porphyritic andesite with phenocrysts in order of decreasing abundance: plagioclase occurs as large subhedral to euhedral crystals from 0.2 to 1.8 mm, some with partly resorbed/ spongy cores and as part of glomeroporphyritic crystal clots in association with orthopyroxene, clinopyroxene, Fe-Ti oxides. Some plagioclase phenocrysts contain melt inclusions in remelting/reequilibration growth zones and many other plagioclase phenocrysts contain dusty matrix-enriched growth zones. Orthopyroxene occurs as large subhedral to euhedral crystals from 0.2 to 1.2 mm in diameter and is also present as part of glomeroporphyritic crystal clots associated with plagioclase, clinopyroxene, and oxides. Abundance of orthopyroxene is equivalent to that of clinopyroxene. Clinopyroxene occurs as subhedral to euhedral crystals ranging from 0.1 to 1.0 mm in diameter, and in glomeroporphyritic crystal clots. Some clinopyroxene replaces orthopyroxene. Olivine is common and occurs as isolated phenocrysts as much as 0.6 mm in diameter but it is always completely rimmed by orthopyroxene± clinopyroxene. All olivine phenocrysts contain small brown spinel inclusions. Groundmass glass is brown in color and has a felty texture as it is enriched in clinopyroxene, orthopyroxene, plagioclase, and Fe-Ti oxide microlites. Titanomagnetite and ilmenite occur as rare phenocrysts up to 0.2 mm in size, with most crystals < 0.05 mm. Titanomagnetite and ilmenite exhibit extensive exsolution lamellae, so won't be good for temperature and oxygen fugacity estimation. Groundmass vesicularity ~ 35 to 40 percent. No amphibole crystals or amphibole pseudomorphs were observed. No visible quartz.

06AUJW001 Oxidized dense low-silica andesite. Petrographic description: Sample is a vesicular and somewhat inflated rx; matrix contains large areas of apparently good glass undergoing spherulitic devitrification with numerous oxides and some (minor) microlites. Porphyritic andesite with phenocrysts in order of decreasing abundance: plagioclase-dominated rock with some in plagioclase as part of glomeroporphyritic crystal clots in association with orthopyroxene, clinopyroxene, and Fe-Ti oxides Some plagioclase contains melt inclusions in remelting/re-equilibration growth zones and other plagioclase phenos contain dusty matrix growth zones; also the plagioclase-hosted melt inclusions tend to be more crystallized than those in other samples. Plagioclase phenocrysts are 0.05 to 3.5 mm in length; some larger plagioclase phenocrysts show complex and variable growth histories in their patterns of zonation. Orthopyroxene phenocrysts 0.05 to 1 mm, and clinopyroxene phenocrysts are 0.1 to 2 mm in length; some orthopyroxene undergoing replacement by clinopyroxene. The pyroxenes do not appear, in general, to be as zoned as the plagioclase phenocrysts. Sample contains significant but small amphibole phenocrysts with strong red-brown color; their margins do not show typical reaction rims but some show embayment and/or filling or replacement by plagioclase. Minor altered/embayed olivine phenocrysts are as much as 0.6 mm in diameter. Coexisting oxides (ilmenite and magnetite) occur in matrix and phenocrysts; ilmenite is typically rimmed by magnetite; significant exsolution features present; 0.03 to 0.3 mm diameter for coexisting oxides. There are far fewer melt inclusions in this sample than in other samples, and many of the largest plagioclase phenocrysts and as part of glomerocrysts contain few to no melt inclusions. No visible quartz.

06AUJW004 Dense low-silica andesite. Petrographic description: porous, porphyritic andesite containing brownish microlite-rich felty groundmass that still contains minor glass. Phenocrysts in order of decreasing abundance, plagioclase is 0.05 to 3.4 mm

in length. Most plagioclase phenocrysts are relatively clean of matrix or oxides, but many very large plagioclase phenocrysts or in glomerocrystic clots show extensive and complex zoning. Some plagioclase contains melt inclusions in remelting/reequilibration growth zones and sieve textured cores. The plagioclase phenocrysts tend to contain clear to generally brownish melt inclusions, but many of the largest unbroken plagiocase phenocrysts and glomerocrysts contain few to no melt inclusions. Pyroxenes are subequal in abundance with orthopyroxene phenocryst 0.05 to 1.8 mm in length, and clinopyroxene phenocrysts are 0.05 to 1 mm in length. Some evidence of plagioclase replacing pyroxene. Rare embayed and altered olivine phenocrysts are as much as 0.5 mm in diameter. Also contains amphibole phenocrysts which are rare and some appear to be undergoing replacement by pyroxene. Coexisting oxides (ilmenite and magnetite) occur in matrix and phenocrysts; ilmenite is typically rimmed by magnetite. Most oxides show no exsolution features; 0.025 to 0.5 mm diameter for coexisting oxides. No visible quartz.

06AUJW010 Dense low-silica andesite. Petrographic description: porphyritic rock containing brownish microlite-rich felty groundmass enriched in plagioclase and iron-titanium oxides. Plagioclase is the dominant phenocryst, phenocrysts are 0.05 to 4.8 mm in length; and it occurs as part of glomerocrystic clots containing pyroxenes and oxides. Approximately 20 to 25 percent of plagioclase phenocrysts contain sieve-textured cores, contain pyroxene inclusions, exhibit reheated growth zones that contain melt inclusions, and/or dusty growth zones that appear to have incorporated devitrified groundmass during late-stage plagioclase growth. Plagioclase phenocrysts contain clear to generally brownish melt inclusions, but the number of melt inclusions is not large. Zoning patterns in plagioclase show evidence of complex and variable growth histories. Orthopyroxene is more abundant than clinopyroxene. Orthopyroxene phenocrysts are 0.05 to 1.8 mm, and clinopyroxene phenocrysts are 0.05 to 0.8 mm in length; pyroxene phenocrysts show little optical evidence of zoning. Some pyroxene replaced by plagioclase. Minor altered (oxidized) and embayed olivine phenocrysts are as much as 0.4 mm in diameter. Coexisting oxides (ilmenite and magnetite) occur in matrix and phenocrysts; ilmenite is typically rimmed by magnetite. Significant exsolution features present; 0.025 to 0.4 mm diameter for coexisting oxides. No amphibole phenocrysts observed. No visible quartz.

Other samples

RBW-91A-137A Vesicular porphyritic olivine basalt. Petrographic description: porphyritic rock containing (in decreasing modal abundance) clinopyroxene, plagioclase, olivine, amphibole, and trace orthopyroxene. Clinopyroxene phenocrysts are oscillatory zoned and are as much as 3.5 mm in length; some show sieve-textured cores. Clinopyroxene phenocrysts are either euhedral or rounded (appearing partially resorbed); some clinopyroxene makes up most of glomeroporphyritic clots. Plagioclase phenocrysts are euhedral and are as much as 2.5 mm in length. Olivine phenocrysts are rounded, partially embayed, and bordered and apparently replaced by pyroxene. Olivine phenocrysts are as much as 1.5 mm in diameter. Groundmass is highly vesicular and holocrystalline, and contains pyroxene and tabular plagioclase microlites. Melt inclusions occur in olivine, pyroxene, and plagioclase; most inclusions are partially to fully crystallized but minor glassy inclusions are present.

AVO 208 Porphyritic pumiceous andesite. Petrographic description: porphyritic rock containing clear, highly vesicular, glassy groundmass containing few microlites of plagioclase, pyroxene, and iron-titanium oxides. Plagioclase is the dominant phenocryst and is as much as 2.5 mm in length. Plagioclase occurs as part of glomerocrystic clots containing pyroxenes and oxides. Some plagioclase phenocrysts contain clear to pinkish melt inclusions in remelting/re-equilibration growth zones, but unlike other samples few plagioclase phenocrysts contain dusty groundmass-bearing growth zones. Many oscillatory zoned plagioclase phenocrysts present. Orthopyroxene phenocrysts and clinopyroxene phenocrysts are subequal and far less abundant than plagioclase; pyroxene phenocrysts <1 mm in diameter. Pyroxene phenocrysts are not as strongly zoned as plagioclase. Trace olivine phenocrysts (<0.5 mm in diameter) appear resorbed, embayed, and replaced by pyroxene. Trace of amphibole observed. Melt inclusions are pink to clear to heavily crystallized and dark. Coexisting oxides (ilmenite and magnetite) occur in matrix and phenocrysts; ilmenite is typically rimmed by magnetite, with 0.025 to 0.4 mm diameter for coexisting oxides. No quartz observed.